ON THE PHYSICAL PROCESSES RESPONSIBLE FOR TROPICAL CYCLONE MOTION

By

Johnny C. L. Chan

Atmospheric Science Department

Colorado State University

Fort Collins, Colorado

November, 1982

Atmospheric Science Paper No. 358

ABSTRACT

This paper investigates the possible physical processes involved in tropical cyclone motion. The first part analyzes the relation between the synoptic-scale flow around tropical cyclones and cyclone movement. It was found that, in most cases, tropical cyclones in the Northern (Southern) Hemisphere move to the left (right) of and faster than their environmental flow. However, westward- and eastward-moving cyclones tend to differ in their relations with the environmental flow.

To understand these observations, an analytical study using a simplified form of the divergent barotropic vorticity equation was performed. The results show the importance of the change in the Coriolis parameter across the cyclone in determining cyclone motion. The environmental flow was found to advect vorticity to the front of the cyclone. These two factors, combined with the coupling between the total divergence and the earth's vorticity, produce maximum local changes of relative vorticity at locations that can be interpreted to correspond to the observational results.

The interaction between the vortex and the environmental flows was further investigated by analyzing the radial equation of motion. Results from a simple model and observations both indicate the presence of radial accelerations which can be explained in terms of parcel trajectories. The difference of radial accelerations between the right and left sides of the cyclone (with respect to cyclone direction) was

found to be proportional to the speed of the cyclone. Differences in radial accelerations between the front and the back of a cyclone appear to be related to a change in cyclone direction.

Vorticity budgets for cyclones with different speeds and turning directions were then analyzed. The horizontal advection of absolute vorticity and the divergence terms in the vorticity equation were found to be predominant. The tilting and vertical advection terms are much smaller in magnitude. The sum of all the terms gives a very good estimate of the local change of relative vorticity in the mid-troposphere. These results are consistent with those from the analytical study of the vorticity equation described above.

Combining the theoretical and observational results, a hypothesis is proposed to describe the possible physical processes involved in tropical cyclone motion. Interaction of the vortex and environmental flows brings about a vorticity increase to the front of the cyclone. This increase in relative vorticity forces a mass adjustment through subsidence, producing a net tropospheric warming and eventually a new center of vortex circulation. The movement of a tropical cyclone is therefore one of "propagation", with eye wall clouds continually reforming around the new "eye" and dissipating around the old center. Observational evidence of this hypothesis is presented using data around cyclones which underwent a change in direction.

TABLE OF CONTENTS

TABLE OF CONTENTS (cont'd)

TABLE OF CONTENTS (cont'd)

LIST OF SYMBOLS

a	tangent of the inflow angle
b	L_s/L_v
B	used as a subscript to denote the back side of a cyclone (with respect to cyclone direction)
c	(1) speed of environmental flow (2) denotes 'of the environmental flow' when used as a subscript
C	instantaneous velocity of the center of a symmetric vortex
d/dt	individual derivative following an air parcel
DD	Directional Difference between direction of cyclone movement and that of environmental wind
f	Coriolis parameter
f_o	Value of f at the center of a cyclone
F	(1) poleward force (per unit height) acting on a symmetric vortex (2) denotes the front side of a cyclone (with respect to cyclone direction) when used as a subscript
g	acceleration due to gravity
G	function relating to σ, τ and λ
H	mean depth of a fluid
I	net wind-pressure imbalance between the left and right side of a cyclone
I_{FB}	net wind-pressure imbalance between the front and back of a cyclone
I_N	normalized value of I
k	regression constant

LIST OF SYMBOLS (cont'd)

$\mathbb{k}$	unit vector in the vertical
K	characteristic constant of vortex
L	(1) length scale (2) denotes the left hand side when used as a subscript
L_s	length scale of environmental flow
L_v	length scale of vortex
p	pressure
$\mathbb{Q}$	coupling term between two levels in a baroclinic model
r	radial distance from center of a cyclone
r_E	effective radius
r_m	radius of maximum wind
R	(1) radial outer boundary of vortex (2) denotes the right hand side of a cyclone (with respect to cyclone direction) when used as a subscript
R_E	radius of the earth
R_o	Rossby number
S	scatter of values of a parameter among different data sets
t	time
u	radial wind
$\bar{u}$	radial wind of the Rankin-combined vortex used in Chapter 4
u'	radial component of environmental flow
U	(1) velocity scale (2) X-component of environmental flow
U_o	constant part of U
U_1	amplitude of spatially-varying part of U

v	(1) tangential wind (2) denotes 'of the vortex' when used as a subscript
$\bar{v}$	tangential wind of the Rankin-combined vortex used in Chapter 4
v_o	vortex constant
v_m	maximum tangential wind
v'	tangential component of environmental flow
V	Y-component of environmental flow
V_o	constant part of V
V_1	amplitude of spatially-varying part of V
V_c	cyclone speed
V_N	component of wind normal to the direction of cyclone movement
V_P	component of wind parallel to the direction of cyclone movement
V_{PM}	magnitude of V_p relative to cyclone
$\mathbf{V}$	vector wind velocity
$\tilde{\mathbf{V}}_o$	vector velocity of the environmental fow at the center of a cyclone
x	(1) longitudinal distance (2) exponent of r in the equation of the tangential wind profile
X	distance from the center of a cyclone along a direction normal to the Y-direction
y	latitudinal distance
Y	distance from the center of a cyclone along the direction of basic environmental flow
z	vertical coordinate
Z	frictional effects in the vorticity equation

LIST OF SYMBOLS (cont'd)

α	geographic azimuth of X-axis
β	variation of Coriolis parameter with latitude
Γ	relative potential vorticity
δ	meridional distance from the cyclone center
λ	$f_o / \sqrt{gH}$
$\bar{\eta}_o$	absolute vorticity of the environmental fow at the center of a cyclone
ω	vertical p-velocity
Ω	angular velocity of earth's rotation
ϕ	inflow angle
ϕ_o	latitude of cyclone center
ψ	streamfunction of a vortex
ρ	density of air
σ, τ	parameters relating to the potential vorticity of a vortex
θ	azimuthal coordinate relative to Y-direction
θ_m	value of θ at which the local change of relative vorticity is a maximum
ζ	relative vorticity
$\bar{(\ )}$	azimuthal average
∇	horizontal gradient operator

CHAPTER 1 - INTRODUCTION

1.1 Background

The movement of tropical cyclones is one of the most important forecasting problems in tropical meteorology. Since the 1940's, a number of cyclone track forecast schemes have been developed based on past observations. With the advance of computer technology, numerical methods have also been designed to predict tropical cyclone motion. With the exception of a few theoretical studies in the 1950's and early 1960's, very little research has been devoted to the understanding of the physical processes responsible for tropical cyclone motion. This is partly due to the mathematical complexity of the problem which involves the interaction of a vortex with its surrounding flow. From the observational perspective, data are usually too sparse around tropical cyclones to perform meaningful calculations of dynamic and thermodynamic quantities that might reveal the physical processes involved. Finally, those who are naturally most interested in tropical cyclone motion are hurricane/typhoon forecasters whose main objective is to make a better track forecast by whatever means possible. The physics of the motion process does not necessarily have to be considered.

What appears to be generally overlooked, however, is a perception that a better understanding of the physics of cyclone motion might lead to better track forecasts. This is because the proper physics of cyclone motion could then be incorporated into empirical and numerical models. Special efforts could also be made to measure the parameters

most relevant to cyclone motion. Furthermore, from a scientific point of view, a physical theory is needed to explain the various observed characteristics of tropical cyclone motion.

All observational studies on tropical cyclone motion in the past dealt with the synoptic-scale flow (~ 500 - 1000 km) around the cyclone. This is not merely due to the lack of data around the center of a cyclone. More importantly, it is because most studies demonstrate a highly significant relation between tropical cyclone motion and its surrounding flow on such a scale. In other words, the movement of a tropical cyclone can be described approximately by the direction and speed of the flow at ~ 500 - 1000 km from the center of the cyclone. This has been referred to as the steering flow concept. The pressure level at which the speed and direction of the surrounding winds (or equivalently, the pressure or height gradients across the cyclone) best correlate with those of the cyclone is called the steering level.

Based on the steering concept, a number of tropical cyclone track forecasting schemes have been developed to relate statistically or dynamically cyclone motion to the surrounding flow field. See for example, Riehl and Shafer (1944), Miller and Moore (1960), Tse (1966) and Renard _et al_. (1973). For a detailed description of these methods, the reader is referred to the WMO Tropical Cyclone Project Report Number WMO-528 (World Meteorological Organization, 1979). Although different forecast schemes employ different steering levels, it is generally accepted that the mid-tropospheric levels (700 mb and 500 mb) are the best in predicting tropical cyclone movement. Attempts to use winds and heights at upper tropospheric levels (see for example, E. Jordan, 1952; Miller, 1958) have not been as successful. No unified conclusion can be

reached from all these schemes as to the location (relative to the cyclone center) at which one should measure the surrounding winds or height gradients to get the best description of cyclone movement for all classes of cyclones. This diversity exists because the data samples used in these studies have in general not been large and the variety of cyclone types has not been extensive.

However, with the accumulation of rawinsonde data over the last twenty years, it is now possible to document more thoroughly the relation between tropical cyclone motion and its surrounding flow through various compositing techniques. In addition, research flights into tropical cyclones have collected vast amounts of data near the cyclone center. These two types of data provide a new opportunity to study the interaction between a tropical cyclone and its environment. Therefore, the present study was undertaken to re-examine the whole problem of tropical cyclone motion. Note, however, that this paper will only address the basic physical processes involved in tropical cyclone motion. The problem of track forecasting is not specifically dealt with.

1.2 Objectives and Approach

As mentioned in the last section, observational results in the past have not been able to document conclusively the relation between tropical cyclone motion and its surrounding flow. The first part of this study is therefore devoted to a more comprehensive analysis on the steering flow problem in order to determine:

1) which level(s) is(are) the best steering level(s);
2) how far from the center of the cyclone the surrounding flow best correlates with the movement of the cyclone; and

3) if the correlation in (2) varies among cyclones in different oceans, with different directions and speeds of movement, at different latitudes, of different intensities, intensity changes and sizes, etc.

After this observational information is established, the main objective is to investigate the possible physical processes that cause a cyclone to move. Such processes will be used to explain the observational results. To study the physics of cyclone motion, two different approaches will be used. The first one involves an analytical study of a simplified form of the divergent, barotropic vorticity equation. Although previous studies using this type of model have been performed (see Chapter 3 for a review of these studies), the approach used here is more applicable in explaining some of the observations made in the first part of this paper.

The second approach is an analysis of the dynamic parameters (wind-pressure balance, divergence, vorticity, vertical motion, terms in the vorticity equation, etc.) computed from observations made around tropical cyclones. These include not only rawinsonde data but also those obtained from research aircrafts. This latter type of data, which describes the flow near the center of a cyclone, has not yet been used in the study of tropical cyclone motion. A combination of aircraft and conventional rawinsonde data (the latter being virtually non-existent within ~ 100 km from the cyclone center) will give a continuous description of the flow field around the cyclone. The vorticity budget and related parameters were then analyzed for cyclones with different characteristics. The results appear to be able to explain the

observations made in the first part of this paper and also those by Chan et. al. (1980) in a study of turning motion of tropical cyclones.

A conceptual model of tropical cyclone motion is then developed from the results obtained using these two approaches. This model offers a hypothesis of the possible physical processes responsible for tropical cyclone motion. Observational evidence supporting this hypothesis is found in the turning motion data set used by Chan et al. (1980).

1.3 Structure of the Paper

The layout of the paper follows closely the development of the objectives described in the last section. Chapter 2 presents observational results of the relation between the movement of tropical cyclones and their surrounding synoptic-scale flow. Rawinsonde data composited around tropical cyclones in three ocean basins (west Atlantic, northwest Pacific and Australia- South Pacific) were used. These cyclones were composited (by other researchers at Colorado State University) according to specified characteristics such as latitude, direction, speed, intensity, intensity change and sizes. Relationships between the direction and speed of the synoptic-scale surrounding flow and those of cyclone movement for the composites were established.

In Chapter 3, a review of previous theoretical studies on tropical cyclone motion is presented. This provides some background information on the different hypotheses that have been advanced to explain tropical cyclone motion. An analytical study using a simplified form of the divergent barotropic vorticity equation is then discussed in Chapter 4. After the general theory has been established, several simple cases that have close resemblance to real situations were investigated. Results

from these cases can be used to explain some of the observations made in Chapter 2.

An investigation of the balance between the centrifugal force, the Coriolis acceleration and the height gradient terms in the radial equation of motion in cylindrical coordinates is described in Chapter 5. A simple theoretical analysis was first performed to study the type of imbalance that is possible when an environmental circulation is superimposed onto a vortex circulation. To study the validity of the theoretical analysis, three types of data were analyzed. First, data collected from research aircrafts of the National Hurricane Research Project (for Atlantic cyclones occurring during the period 1957-1967 and in 1969) were used. These provide information near the cyclone center. The other data sets studied are those in Chapter 2 which relate to the speed of a cyclone, and those from a study of the turning motion of tropical cyclones by Chan et. al. (1980). Results obtained from these data sets generally agree with those predicted from the theoretical analysis.

Chapter 6 presents calculations of the vorticity budget for the data sets studied in Chapter 5. The theoretical results of Chapter 4 appear to agree very well with these calculations.

Both observational (Chapters 5 and 6) and theoretical results (Chapter 4) point to the importance of the vorticity budget in determining tropical cyclone motion. By synthesizing these results, a physical hypothesis of the physical processes responsible for tropical cyclone motion is proposed in Chapter 7. Observational evidence of this hypothesis is found in the turning motion data set used by Chan et al. (1980). Future possible research and potential applications of this

study in operational forecasting of tropical cyclone movement are discussed in Chapter 8.

CHAPTER 2 - RELATIONSHIPS BETWEEN TROPICAL CYCLONE MOVEMENT AND ITS SURROUNDING FLOW(1)

2.1 Introduction

As discussed in section 1.2, the main objective of this part of study is to establish the relationships between the movement of a tropical cyclone and its surrounding synoptic-scale flow. In order to accomplish this, data around a large number of cyclones must be analyzed. However, only a few observations are usually available for each 12 h position of the cyclone. These observations may not be representative of the actual surrounding flow. This is one reason for the diversity of results obtained by different researchers as to the location (relative to the cyclone center) at which one should measure the winds or height gradients to get the best description of cyclone movement for all types of cyclones. One way to avoid this is through compositing data around many cyclones with similar characteristics. Two such studies had been carried out in the past.

George and Gray (1976) established statistical relationships between the movement of northwest Pacific tropical cyclones and their surrounding winds averaged between 1-7° latitude(2) radius from the cyclone center. They found that over this broad radial belt, the composite 500 mb winds have the strongest correlation with the direction of cyclone movement while the 700 mb winds best correlate with cyclone

---

(1) Part of this chapter has been accepted for publication (Chan and Gray, 1982b). An extended version of this chapter has also been published as a CSU Atmospheric Science Paper (Chan and Gray, 1982a).

(2) Hereafter, a unit of distance will usually be referred to in degrees latitude (1° latitude = 111.1 km).

speed. Gray (1977) presented a similar composite analysis of the winds at 1-7° radius around west Atlantic tropical cyclones. The results were in general agreement with those obtained by George and Gray (1976). However, the winds in these studies were averaged over an area in which both the cyclone circulation and part of the environmental flow are present. This radial belt, therefore, will not provide the best description of the relationships between the movement of the cyclone and its environmental winds.

The present study is an extension of these two previous analyses. Composite wind data over an area (5°-7° latitude radius from the cyclone center) outside the strong inner circulation of the cyclone (see, for example, Merrill, 1982) were correlated with cyclone movement in the west Atlantic, northwest Pacific and Australian-south Pacific regions. More stratifications for both west Atlantic and northwest Pacific cyclones have been included to test the validity of the conclusions in the two previous studies. Data at individual levels as well as mean layer averages were studied and compared for data sets with different characteristics.

2.2 Methodology and data stratifications

The methodology used in this study, as discussed in the previous section, is to composite data around tropical cyclones with similar characteristics so that a more even azimuthal coverage of data can be obtained. Although such a procedure undoubtedly smooths out features particular to individual cyclones, those characteristics that are common to all cyclones in the same stratification should be isolated. In addition, noise from the data will be largely eliminated through the process of averaging. A more detailed description of this compositing

philosophy can be found in the papers by Williams and Gray (1973), Frank (1977), Gray (1981) and other Colorado State University tropical cyclone research reports. Corrections for balloon drift and mass-balance were made in the same way as described in these papers and reports.

2.2.1. Stratification of the cyclones

Tropical cyclones with maximum sustained wind speed (V_{max}) $\geq$ 18 m s^{-1} in the northwest Pacific (time period: 1961-1970), west Atlantic (1961-1974), and Australian-south Pacific (1961-1970) oceans were studied. The cyclones were stratified according to their direction and speed of movement, latitude, intensity, intensity change and size. These stratifications are listed in Tables 1, 2 and 3.

2.2.2. Compositing technique

Wind data from rawinsonde stations shown in Figs. 1 (northwest Pacific), 2 (west Atlantic) and 3 (Australian-south Pacific region) were composited around cyclones for the stratifications listed in Tables 1-3 using the circular grid shown in Fig. 4. The center of the grid coincides with the cyclone center. The grid has a radius of 15^{o} latitude with eight radial bands. Each radial band is divided into eight equal segments or octants and numbered from 1 to 8 in a counterclockwise fashion, with Octant 1 always being in front of the cyclone.

The $\pm$ 6h (from current position) best-track positions were used to determine the direction and speed of cyclone movement. Each parameter (in this case the wind components) for all soundings falling within any given grid box for a stratification are then averaged. This average value is assigned to the mid-point of the grid box, giving a total of 64 values of each parameter at each pressure level.

TABLE 1

Description of stratifications of tropical cyclones in the northwest Pacific. All cyclones under study had a maximum sustained wind speed (V_{max}) > 18 m s^{-1}. The number of rawinsonde soundings in each group of stratifications within the 5-7° latitude radial band is ~ 1000.

STRATIFICATION	DESCRIPTION
By Latitude	
North Cyclone	Latitude of cyclone > 20°N
South Cyclone	Latitude of cyclone ≤ 20°N
By Speed	
Slow Cyclone	Cyclone speed (V_c) ≤ 3 m s^{-1}
Moderate Cyclone	4 m s^{-1} ≤ V_c ≤ 7 m s^{-1}
Fast Cyclone	V_c > 7 m s^{-1}
By Direction	
Westward Cyclone	250° < Cyclone Direction (CD) ≤ 310°
Northward Cyclone	310° < CD ≤ 350°
Eastward Cyclone	350° < CD ≤ 60°
By Intensity	
Weak Cyclone	980 mb < Central Pressure (CP) ≤ 1000 mb
Intense Cyclone	950 mb ≤ CP ≤ 980 mb
Very Intense Cyclone	CP < 950 mb
By Intensity Change	
Deepening North Cyclone	CP was decreasing at the time of observation; latitude of cyclone > 20°N
Deepening South Cyclone	CP was decreasing at the time of observation; latitude of cyclone ≤ 20°N
Filling North Cyclone	CP was increasing at the time of observation; latitude of cyclone > 20°N
Filling South Cyclone	CP was increasing at the time of observation; latitude of cyclone ≤ 20°N
By Size and Intensity	
Small Tropical Storm	980 < CP ≤ 1000 mb; 1° ≤ ROCI[3] ≤ 3°
Medium Tropical Storm	980 mb < CP ≤ 1000 mb; 4° ≤ ROCI ≤ 5°
Large Tropical Storm	980 mb < CP ≤ 1000 mb; ROCI ≥ 6°
Small Typhoon	CP ≤ 980 mb; 1° ≤ ROCI ≤ 3°
Medium Typhoon	CP ≤ 980 mb; 4° ≤ ROCI ≤ 5°
Large Typhoon	CP ≤ 980 mb; ROCI ≥ 6°

(3) ROCI - radius of outermost closed surface isobar averaged around the cyclone to the nearest whole degree latitude.

TABLE 2

Same as Table 1 except for tropical cyclones in the west Atlantic. The number of rawinsonde soundings in each group of stratifications within the 5-7° latitude radial band is ~ 900.

STRATIFICATION	DESCRIPTION
By Latitude	
Region I Cyclone[4]	Cyclone location: lat. $\leq 18^{\circ}$N, long. $> 45^{\circ}$W or lat. $< 22^{\circ}$N, 75°W $\leq$ long. $\leq 87^{\circ}$W.
Region II Cyclone[4]	Cyclone location: 18°N $<$ lat. $\leq 35^{\circ}$N long. $\geq 45^{\circ}$W except those already included in Region I.
By Speed	
Slow Cyclone	Cyclone speed < 4 m s^{-1}
Fast Cyclone	Cyclone speed ≥ 4 m s^{-1}
By Direction	
Northward Cyclone	Direction of movement: 316°–45°
Westward Cyclone	Direction of movement: 225°–315°
By Intensity	
Hurricane	Maximum sustained wind (V_{max}) ≥ 33 m s^{-1}
Tropical Storm	18 m s^{-1} $\leq V_{max} < 33$ m s^{-1}
By Size and Intensity	
Small Tropical Storm	18 m s^{-1} $\leq V_{max} < 33$ m s^{-1}; $1^{\circ} \leq$ ROCI $\leq 3^{\circ}$
Large Tropical Storm	18 m s^{-1} $\leq V_{max} < 33$ m s^{-1}; ROCI $\geq 4^{\circ}$
Small Hurricane	$V_{max} \geq 33$ m s^{-1}; $1^{\circ} \leq$ ROCI $\leq 3^{\circ}$
Large Hurricane North	Latitude of cyclones $> 25^{\circ}$N $V_{max} \geq 33$ m s^{-1}; ROCI $\geq 4^{\circ}$
Large Hurricane South	Latitude of cyclones $\leq 25^{\circ}$N $V_{max} \geq 33$ m s^{-1}; ROCI $\geq 4^{\circ}$

[4] See Fig. 2 for a more detailed description of the regions.

TABLE 3

Same as Table 1 except for tropical cyclones in the Australian-south Pacific region. The number of rawinsonde soundings in each group of stratifications within the 5-7° latitude radial band is ~ 500.

STRATIFICATION	DESCRIPTION
By Direction	
Eastward Cyclone	CP $\leq$ 990 mb $40^{\circ} \leq$ CD $\leq 150^{\circ}$
Westward Cyclone	CP $\leq$ 990 mb $210^{\circ} \leq$ CD $\leq 320^{\circ}$
By Intensity and Region	
All Hurricanes	CP $\leq$ 990 mb
Coral Sea Hurricanes	Longitude east of 136°E CP $\leq$ 980 mb
Coral Sea Tropical Storm	Longitude east of 136°E 980 mb < CP < 995 mb
West Australian Hurricane	Longitude west of 136°E CP $\leq$ 980 mb

The wind vectors were resolved in two coordinate systems. The first system involves resolving each wind observation into a parallel component (V_P) along the direction of cyclone movement and a component normal (V_N) to this direction, as shown in Fig. 5. This will be referred to as the ROTated (ROT) system. In order to study the environmental flow relative to the cyclone, a second coordinate system is used in which the speed of the cyclone V_c was subtracted from the parallel wind component (V_P) for each sounding. The composite method was then applied to the difference $V_P - V_c$ which is labeled as V_{PM} (see

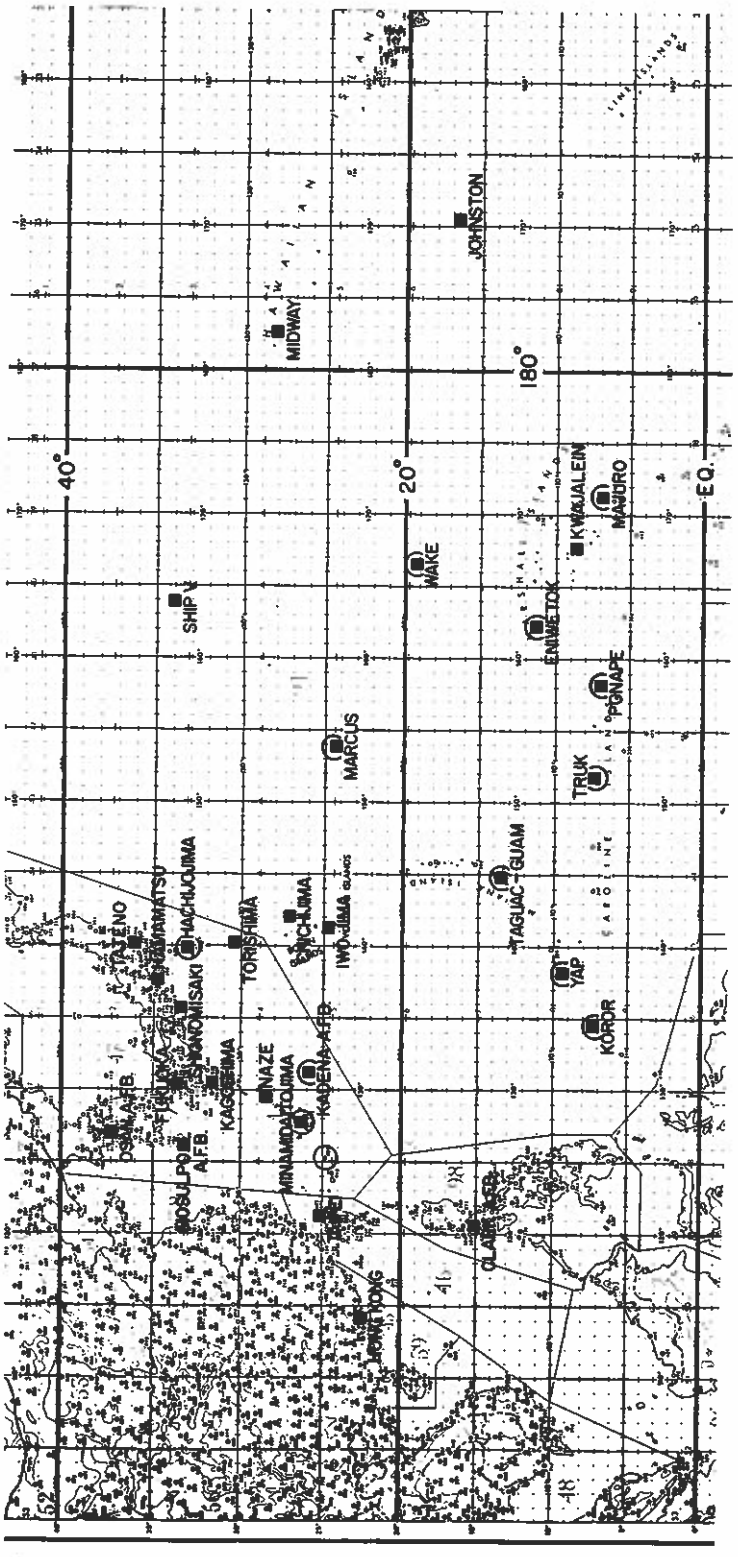

Fig. 1. Northwest Pacific rawinsonde stations.

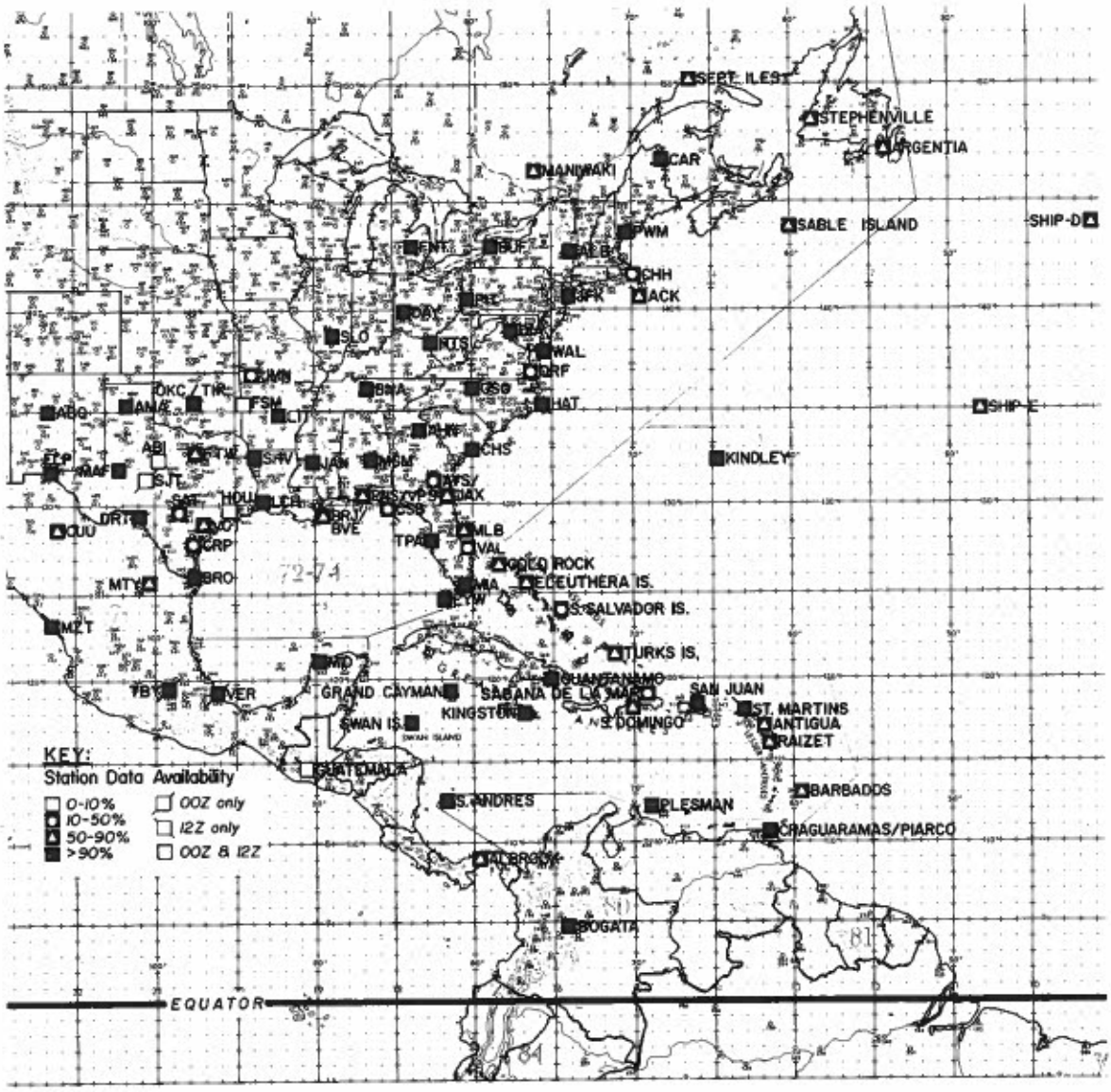

Fig. 2. West Atlantic rawinsonde stations.

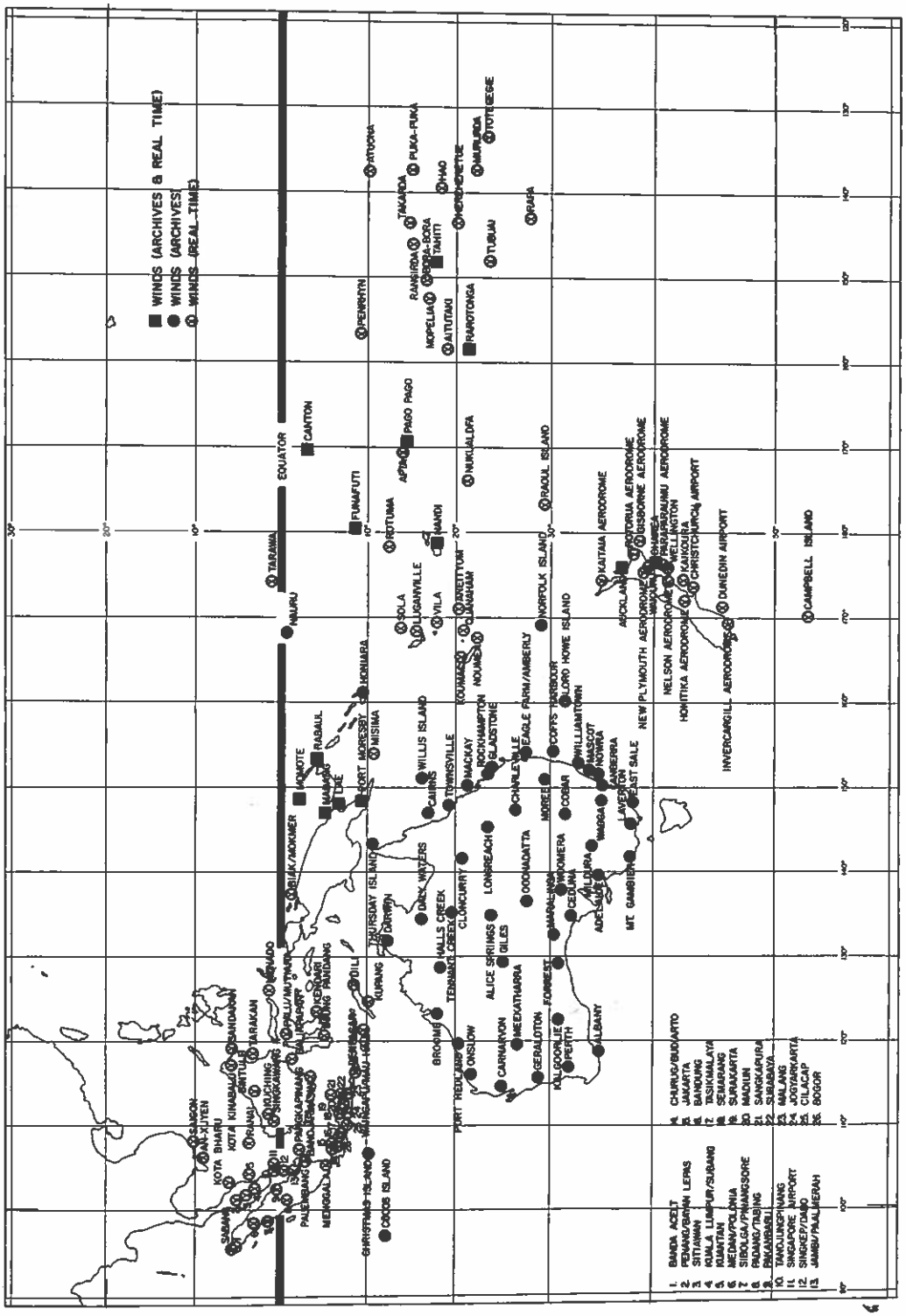

Fig. 3. Australian–south Pacific region rawinsonde stations.

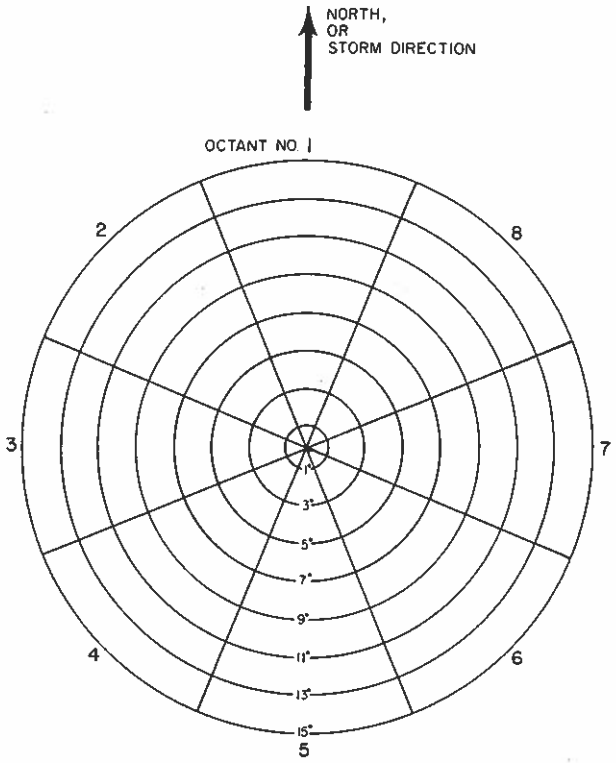

Fig. 4. Grid used for compositing rawinsonde data. The arrow points in the direction of storm motion. Outer numbers denote octants. Numbers inside grid indicate distances from the center in degrees latitude.

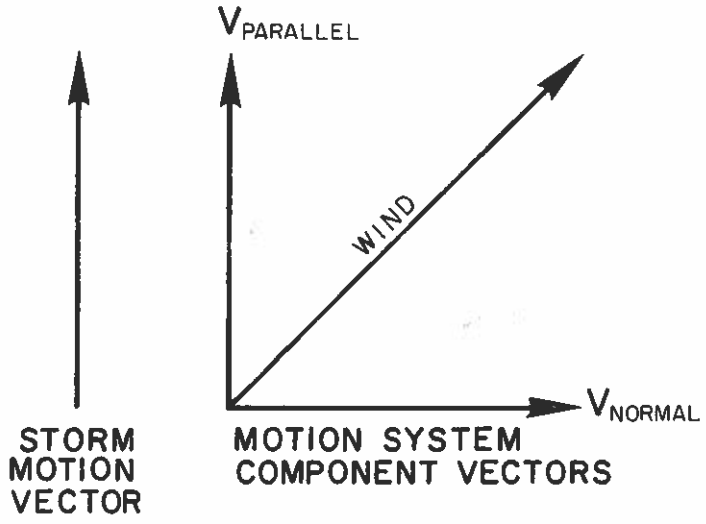

Fig. 5. Parallel (V_P) and perpendicular (V_N) component of a wind vector showing their relation to the storm motion vector in the ROT system.

Fig. 6). This will be referred to as the MOTROT (for MOTion-ROTated) system. The normal component V_N is the same as in the ROT system. See George and Gray (1976) or Chan et al. (1980) for a more detailed description of these two coordinate systems.

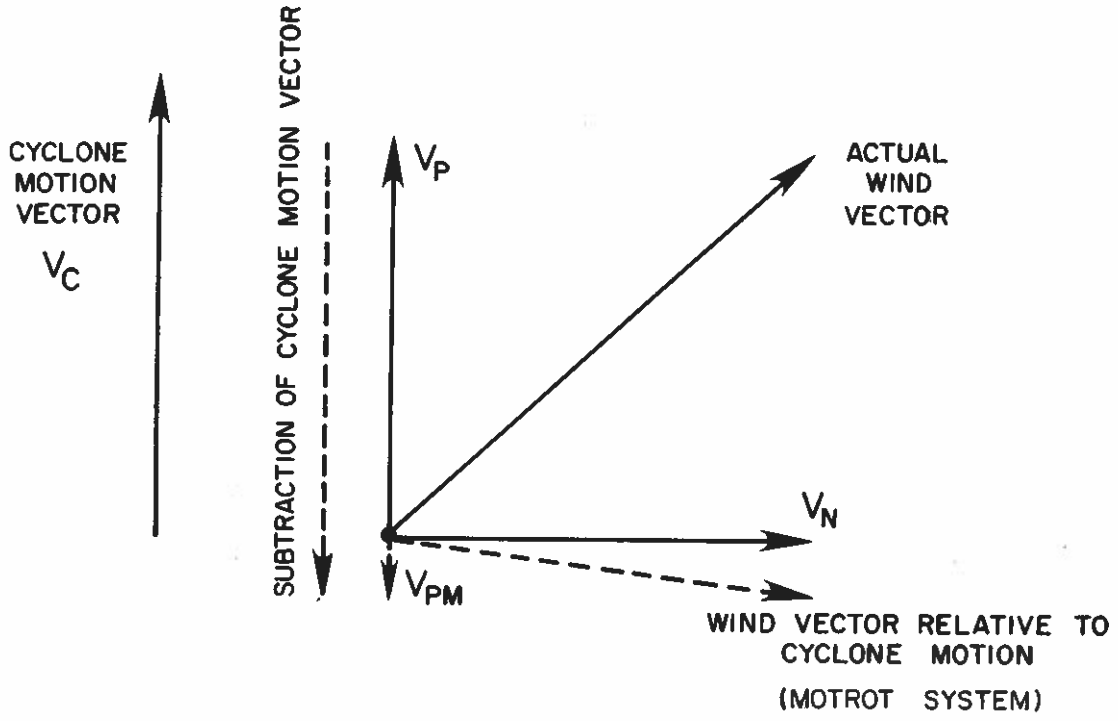

Fig. 6. Illustration of the MOTion-ROTated (MOTROT) coordinate system.

2.3 Relationship between the surrounding flow and the direction of cyclone movement

A convenient parameter to describe the relationship between the surrounding flow and the direction of movement of tropical cyclones is the difference between the direction of the surrounding wind and that of the cyclone motion vector. If the ROT system described in section 2.2.2 is used, this Directional Difference (DD) is given by

$$DD = \begin{cases} \arctan (V_N/V_P) & V_P > 0 \\ \arctan (V_N/V_P) + 180^o & V_N > 0,\ V_P < 0 \\ \arctan (V_N/V_P) - 180^o & V_N < 0,\ V_P < 0 \end{cases} \qquad (1)$$

where V_N and V_P are the components of the composite wind normal and parallel to the direction of cyclone movement. The parameter DD therefore represents the deviation of the composite wind in a particular octant and radial band from the direction of movement of all tropical cyclones in a particular stratification. A positive value of DD means that the cyclone is moving to the left of the composite wind.

The basic hypothesis in the steering-flow concept is that the cyclone can be considered as a point vortex so that its circulation does not interact with that of the environment. That is, the cyclone is simply "advected" along by the environmental flow. If this is the case, the directional difference at the steering level should be about the same for cyclones with different characteristics. Under this assumption, the steering level can be determined by studying the scatter of the values of DD for data sets in the same ocean at each pressure level. The scatter S is defined as

$$S = \sqrt{\frac{1}{N} \sum_{i=1}^{N} (x_i - \bar{x})^2}$$

where N = total number of data sets

x_i = value of parameter x for data set i

$\bar{x}$ = mean value of parameter x for all data sets.

In a sense, the value of S is similar to the standard deviation of

a sample. However, it cannot be interpreted in the same way because the data sets are not all independent and the values of x_i are sample means. Nevertheless, this calculation will provide a measure of the spread of the values of the parameter x among the data sets. The level and radius with the least amount of scatter is then assumed to be the steering level. Mid-tropospheric (700-500 mb) data 5-7° from the cyclone center appear to satisfy this criterion the best. This is not surprising since forecasters have traditionally found these to be the best steering levels.

In some of the track forecast schemes, layer-averaged winds are used to represent the steering current (see, for example, Riehl and Burgner, 1950; E. Jordan, 1952; Miller, 1958; Sanders and Burpee, 1968). To see if this idea would yield better results than 'single-level steering', layer-averaged deviations (pressure weighted) have also been computed.

One problem in determining the 'steering current' is that the environmental flow may not be uniform around the cyclone. Therefore, each part of the cyclone may be subjected to a different current. The best way to avoid this problem is to consider the mean surrounding flow, that is, by relating cyclone movement to the average flow around a radial band. To calculate a radial band average of DD, the values of V_N and V_P in each of the eight octants are averaged to obtain mean V_N (or $\overline{V}_N$) and mean V_P (or $\overline{V}_P$) values. Eq. (1) is then applied using $\overline{V}_N$ and $\overline{V}_P$ to give the radial band average of DD (or $\overline{DD}$). The value $\overline{DD}$ therefore represents the difference between the direction of the mean wind in a particular radial band and that of the cyclone. This was done for all radial bands at each individual pressure level. As

mentioned above, the smallest scatter in the values of $\overline{DD}$ appears 5-7° from the cyclone center. Therefore, only data at this radius will be presented.

2.3.1 Variation with height

Northwest Pacific. Figure 7 shows a plot of the 5-7° belt average winds in the ROT coordinate system (see section 2.2.2) at different levels for all data sets in the northwest Pacific. These winds were plotted using the values of $\overline{V}_N$ and $\overline{V}_P$. The direction of cyclone movement is towards the top of the figure. This figure shows that for all the data sets, the cyclone is moving to the left of the direction of the mean wind at all the cyclonic levels (below 300 mb) except near the boundary layer (below 900 mb). The least variability between data sets appears to be in the mid-troposphere. More variability exists both at the anticyclonic levels (above 300 mb) and in the boundary layer.

The actual variations of the belt average deviation of $(\overline{DD})$ with height for all the data sets in the northwest Pacific are shown in Fig. 8. A positive number means that the cyclone is moving to the left of the mean wind. It can be seen that for most of the data sets, the values of $\overline{DD}$ do not vary much throughout a large portion of the troposphere. This suggests that the average flow around most of these cyclones does not have much directional wind shear in the vertical.

Some variations within each category of cyclones can also be seen in Fig. 8. Cyclones at latitudes north of 20°N seem to move more to the left of the mean wind than those south of 20°N. Similar results have also been obtained by Brand et al. (1981). In the speed category, slow-moving cyclones appear to have a much larger variation of $\overline{DD}$ values in the vertical. Northward-moving cyclones have $\overline{DD}$ values

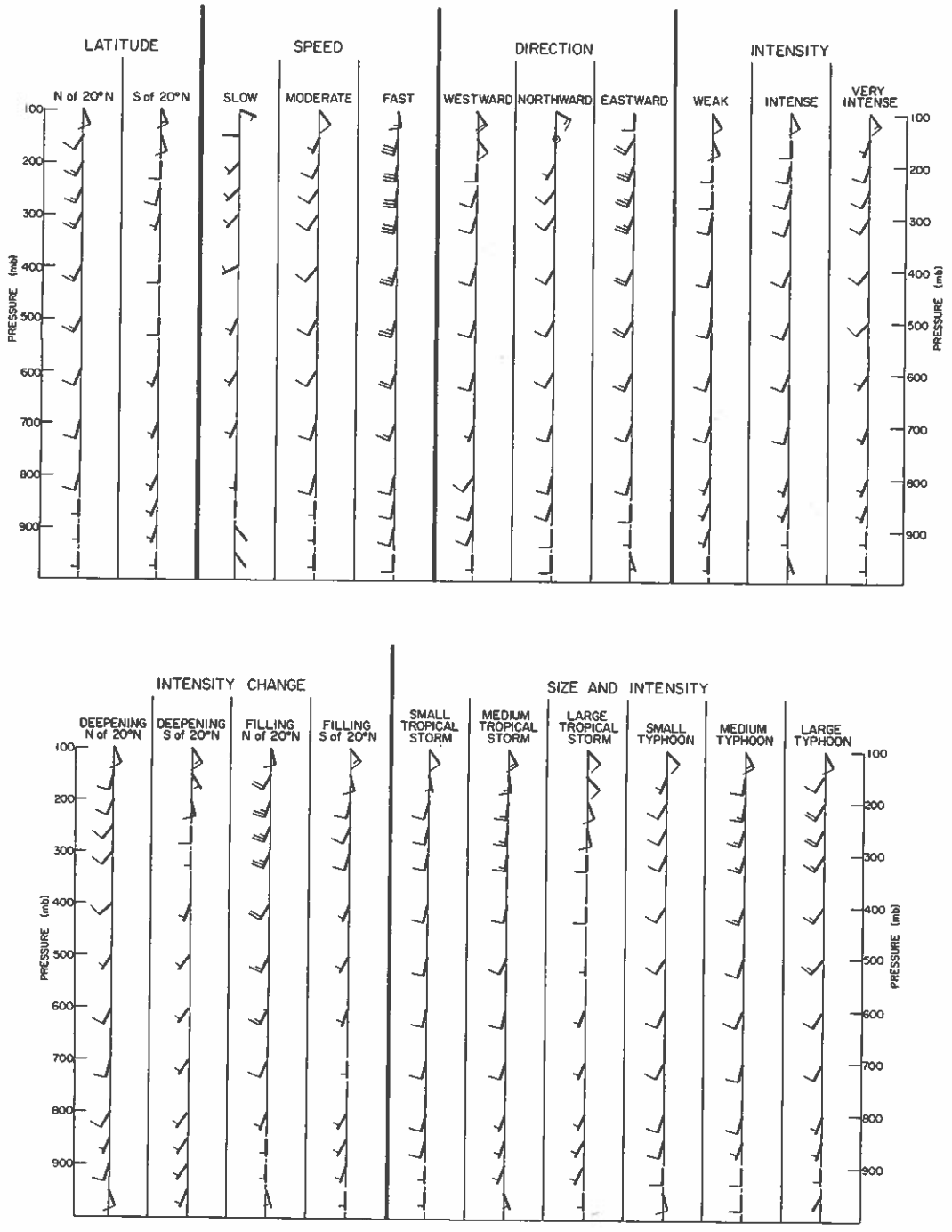

Fig. 7. 5-7° belt average winds in the ROT coordinate system at different pressure levels for all data sets in the northwest Pacific. The direction of cyclone movement is towards the top of the figure. Wind barbs were plotted in the usual meteorological convention, one full barb equivalent to 5 m s^{-1}.

increasing with height while the opposite is true for westward-moving cyclones. As a cyclone increases in intensity it seems to move more to the left of the mean wind. The values of $\overline{DD}$ also appear to increase with the size of the cyclone.

Since little variability in the values of $\overline{DD}$ in the vertical exists, winds at a single level in the mid-troposphere might be used to describe the directional movement of a tropical cyclone equally as well as layer-averaged winds. More discussion of this will follow.

West Atlantic. Figure 9 shows the 5-7° belt average winds in the ROT coordinate system for west Atlantic tropical cyclones. The portion of the atmosphere in which the variability between data sets is small seems to be confined only to the mid-troposphere between 700 mb and 500 mb. For each data set, the variation in the vertical is slightly larger when compared with northwest Pacific tropical cyclones. Most cyclones move either in the same direction or to the right of the mean winds below 800 mb. In the mid- to upper troposphere, however, west Atlantic cyclones move to the left of the mean wind, as in the northwest Pacific. In the mid-troposphere the winds are, in general, weaker than those in the northwest Pacific and the values of $\overline{DD}$ are also smaller.

These observations are more clearly shown in Fig. 10. The values of $\overline{DD}$ appear to increase with height from the surface up to ~ 150 mb for all the data sets with the exception of the westward-moving data set. Westward-moving cyclones tend to move in the same direction or slightly to the right of the mean wind direction. Values of $\overline{DD}$ above 300 mb for this data set were not plotted because the winds are very weak (as shown in Fig. 9) and directional deviations are, therefore, less well defined.

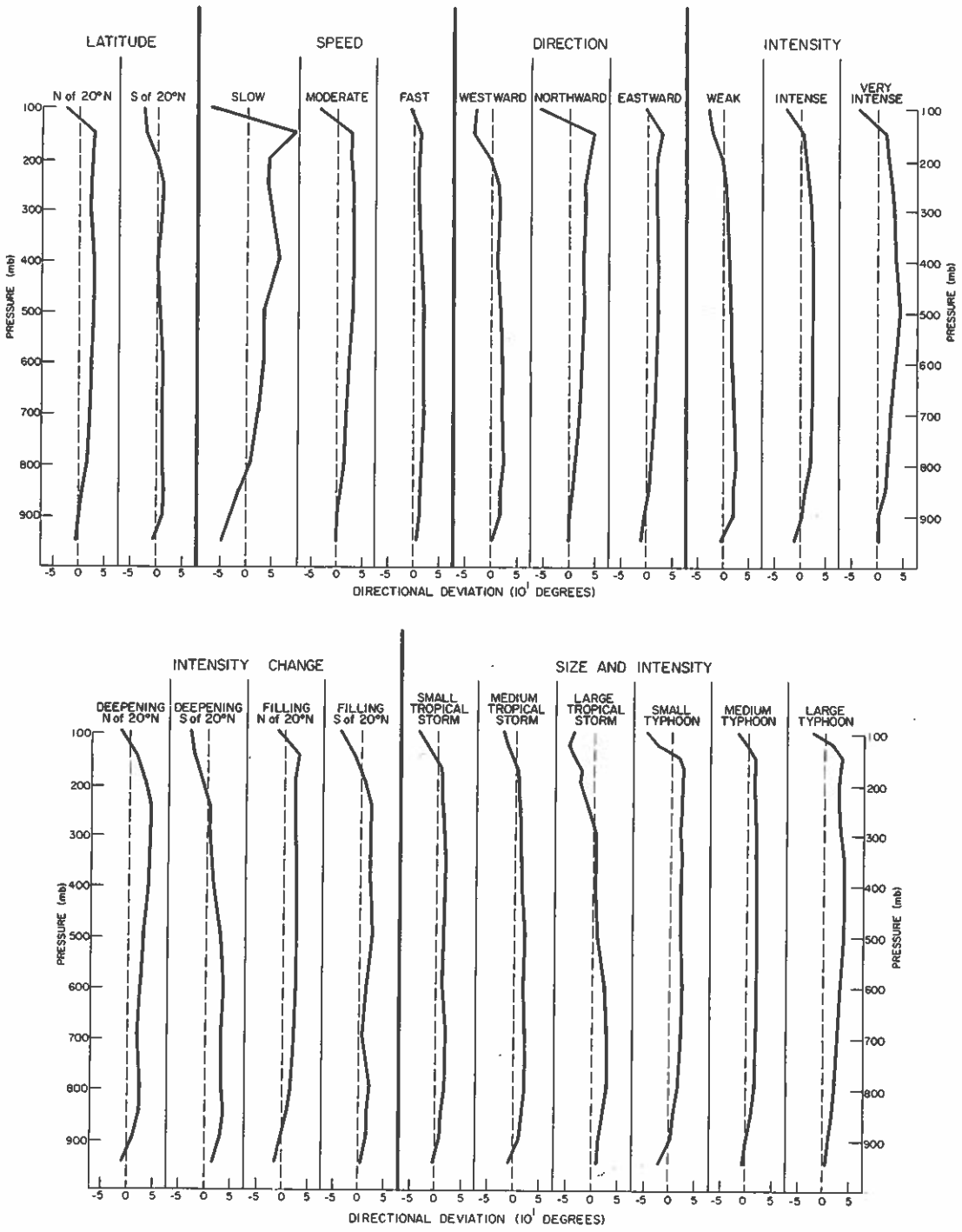

Fig. 8. Variation with height of the 5-7° belt average wind deviation (DD - solid line) for all data sets in the northwest Pacific. The zero (dashed) line represents the direction of cyclone movement. A positive value means that the cyclone is moving to the left of the 5-7° belt average wind direction.

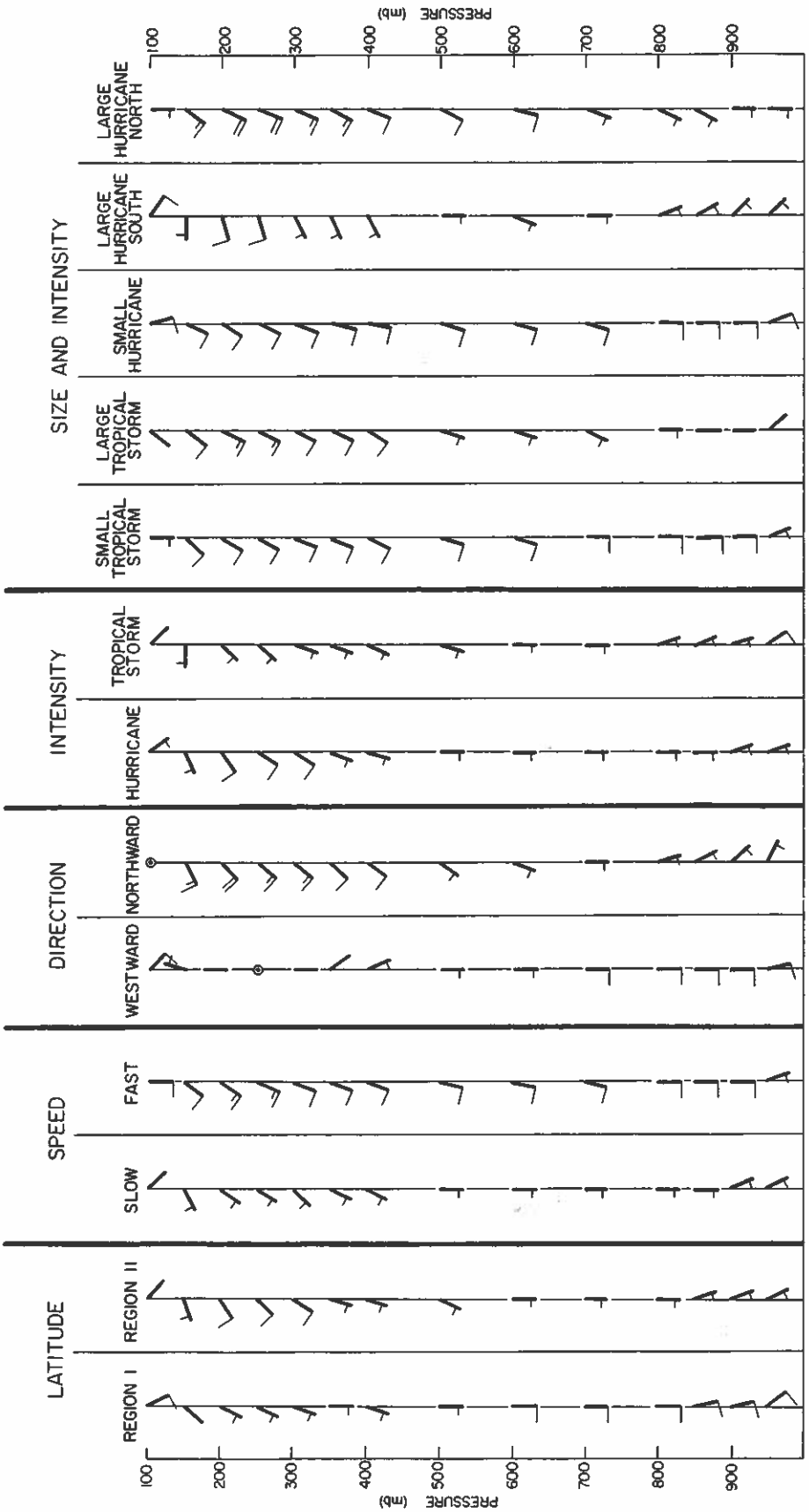

Fig. 9. Same as Fig. 7 except for west Atlantic tropical cyclones.

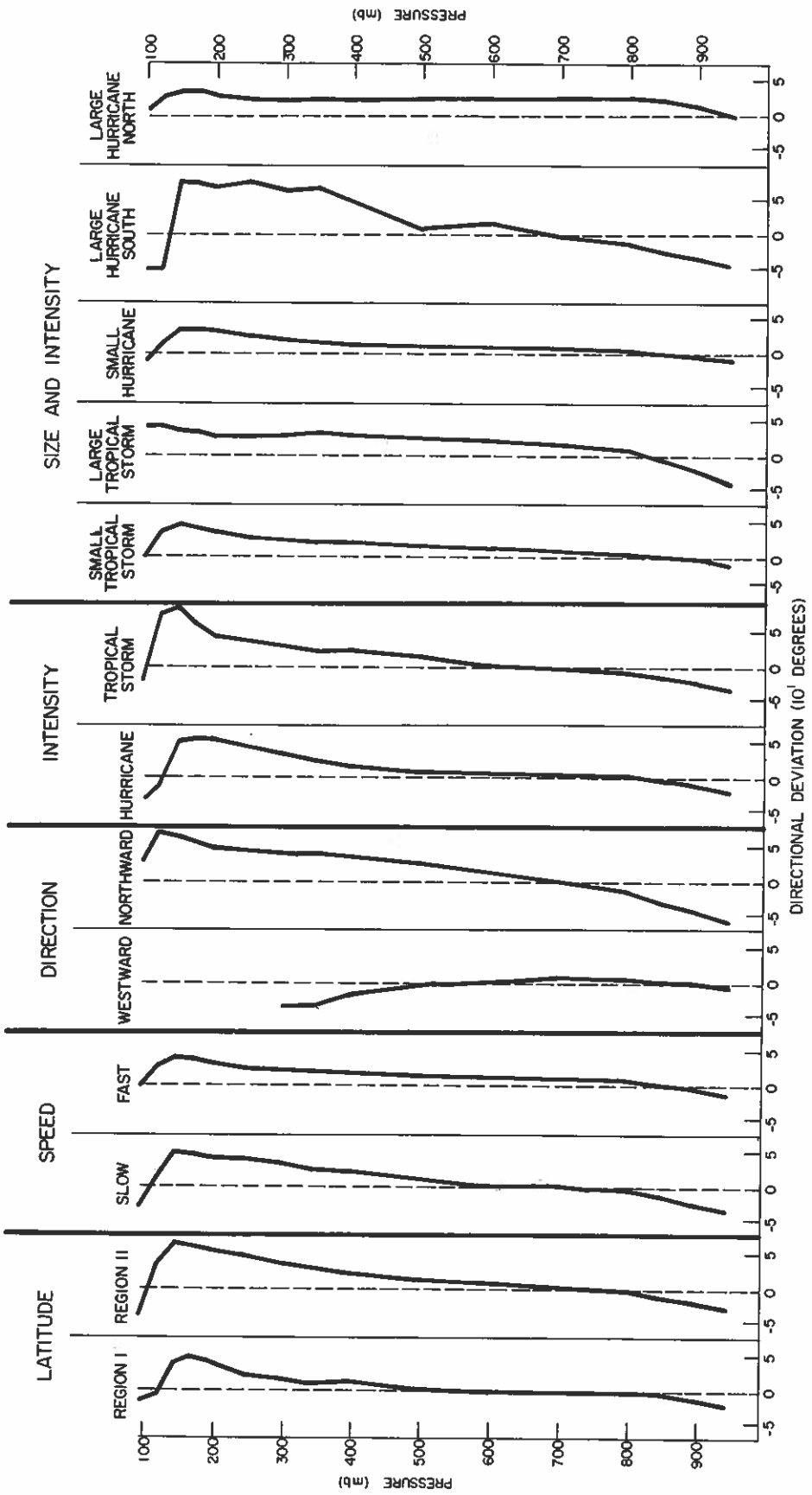

Fig. 10. Same as Fig. 8 except for west Atlantic tropical cyclones.

Variations within each category of cyclones can also be seen in Fig. 10. Region I (~ south of 18°N) cyclones move less to the left of the mean winds than cyclones in Region II (~ north of 18°N). Westward-moving cyclones have quite different values of $\overline{DD}$ than northward-moving cyclones. This is the same as the northwest Pacific except it is more obvious for west Atlantic cyclones. The values of $\overline{DD}$ also appear to increase slightly with the size of the cyclone. However, from a practical point of view, the differences in the values of $\overline{DD}$ between cyclones of different sizes may not be discernable. Therefore, it might be possible to assume that the direction of cyclone movement can be described adequately using the 5-7° mean wind (at least in the mid-troposphere) irrespective of the size of the cyclone. This is true in both the northwest Pacific and west Atlantic.

The general increase in the values of $\overline{DD}$ with height for west Atlantic tropical cyclones suggests that the cyclones are in an environment with a stronger average directional vertical wind shear than northwest Pacific cyclones. This type of shear profile would imply that using layer-averaged steering might be superior to using single-level steering. This will be discussed in greater detail later.

Australian-south Pacific region. Figure 11 gives the 5-7° belt-averaged winds in the ROT coordinate system for tropical cyclones in the Australian-south Pacific region. At first glance, the data appear to be very noisy. However, a closer examination shows that for data sets classified under 'intensity and region', the variability among the data sets in the mid- to upper-troposphere is actually very small, with the cyclone moving to the right of the mean wind direction above 700 mb.

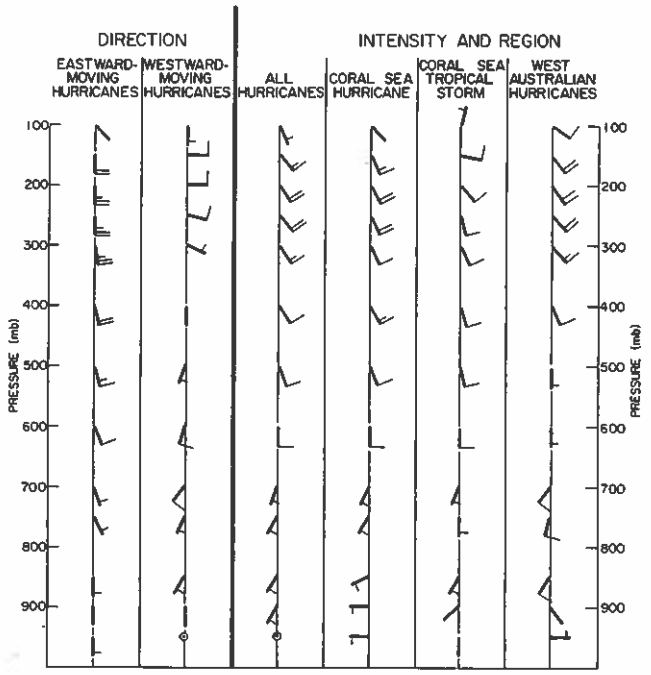

Fig. 11. Same as Fig. 7 except for tropical cyclones in the Australian -south Pacific region.

This is also the case for eastward-moving cyclones. Westward-moving cyclones appear to move to the left of the mean wind at levels up to 400 mb.

These variations are better illustrated in Fig. 12 which gives the 5-7° belt-average deviations ($\overline{DD}$) at different levels. The values of $\overline{DD}$ generally decrease with height, opposite to those of the west Atlantic. These profiles again demonstrate the existence of an average directional wind shear profile in the vertical. This shear appears to be stronger in the lower troposphere (below ~ 600 mb).

Another important feature in Fig. 12 is the difference in the $\overline{DD}$ profiles between westward and eastward-moving cyclones. This same type of difference between cyclones moving in different directions also shows up in the two northern hemisphere ocean basins (see Figs. 8 and 10). It appears that when directional vertical wind shear is present (as in the west Atlantic and Australian-south Pacific regions), this difference in

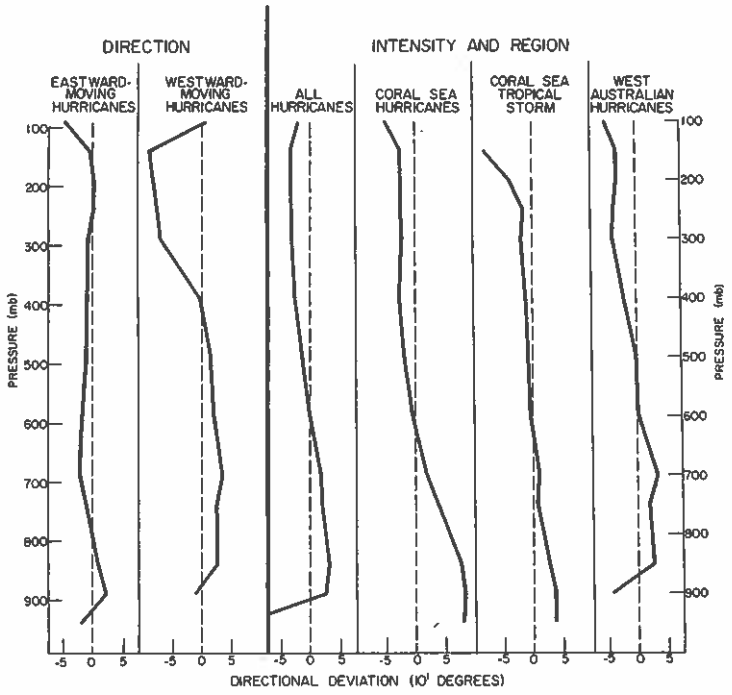

Fig. 12. Same as Fig. 8 except for tropical cyclones in the Australian -south Pacific region.

directional deviations (between cyclones moving in different directions) is more obvious. One must conclude that the deviation of the cyclone direction from that of the mean wind at a given level is related to the zonal and meridional direction of cyclone motion.

Summary. The results in this subsection show that the vertical variation of the deviation of the cyclone direction from the 5-7° belt average wind direction for all three tropical regions depends on the directional vertical wind shear of the environmental winds. The least variability among data sets in a given ocean basin appears to be in the mid-troposphere. Most cyclones in the Northern Hemisphere move to the left of the 5-7° belt average wind (at least in the mid-troposphere) while cyclones in the Southern Hemisphere, in general, move to the right of mid-tropospheric winds at this radius. Such deviations appear to be

slightly modified by latitude, intensity, and size of the cyclone. However, cyclones with different zonal components of motion have large differences in the $\overline{DD}$ values. This, as will be seen in Chapter 4, is very much related to the variation in the Coriolis parameter across a cyclone.

2.3.2 Individual level

Since the mid-tropospheric winds at 5-7° radius give the least amount of difference in the directional deviations between data sets, these levels will now be more closely examined. The actual values of $\overline{DD}$ for all data sets at 700, 600, and 500 mb and the corresponding standard deviations are presented.

Northwest Pacific. Table 4 shows the 5-7° $\overline{DD}$ values for northwest Pacific tropical cyclones at 700, 600, and 500 mb. All cyclones move to the left of the 5-7° mean wind by about the same amount, an indication of the relatively small vertical wind shear in this ocean basin (see also Fig. 8). Since such a consistency exists between data sets with widely different characteristics, one might conclude that the steering flow theory appears quite applicable, particularly in the mid-tropospheric levels. However, if such a theory is correct, one would expect the value of $\overline{DD}$ to be near zero. While this is true in a few stratifications, a systematic difference of ~ 20° exists between the mean 5-7° wind direction and the direction of cyclone movement. This suggests that the large-scale flow, though the dominant factor, is not totally responsible for the directional movement of the tropical cyclone. Other factors, which will become apparent in later chapters, must be present to provide such a systematic directional deviation.

TABLE 4

Directional Difference ($\overline{DD}$) between the 5^{o}-7^{o} radial band average wind and the direction of cyclone movement for northwest Pacific tropical cyclones. (See text for a description of how the averages and the scatter were calculated.) A positive number indicates the cyclone is moving to the left of the mean wind. Unit: degrees.

STRATIFICATION	700 mb	600 mb	500 mb
By Latitude			
North of 20^{o}N	19	22	26
South of 20^{o}N	9	10	4
By Speed			
Slow (1-3 m s^{-1})	23	32	34
Moderate (4-7 m s^{-1})	16	22	29
Fast (> 7 m s^{-1})	19	17	17
By Direction			
Westward (250^{o}-310^{o})	21	21	17
Northward (310^{o}-350^{o})	18	23	28
Eastward (350^{o}-60^{o})	16	18	22
By Intensity			
Weak (1000-980 mb)	21	16	14
Intense (950-980 mb)	23	25	26
Very Intense (< 950 mb)	24	34	42
By Intensity Change			
Deepening North of 20^{o}N	19	23	29
Deepening South of 20^{o}N	29	33	25
Filling North of 20^{o}N	22	24	24
Filling South of 20^{o}N	3	13	23
By Size and Intensity			
Small Tropical Storm	17	11	13
Medium Tropical Storm	19	15	19
Large Tropical Storm	28	22	8
Small Typhoon	22	24	21
Medium Typhoon	17	18	19
Large Typhoon	24	30	36
Mean	19	22	23
Scatter	5.8	6.8	9.1

West Atlantic. Table 5 gives the values of $\overline{DD}$ for west Atlantic tropical cyclones. Similar results are found. Cyclones generally move to the left of the 5-7° mean wind. A few stratifications, however, show different results, particularly the westward-moving tropical cyclones which move slightly to the right of the 500 mb environmental flow.

Australian-south Pacific region. The 5-7° $\overline{DD}$ values for tropical cyclones in the Australian-south Pacific region are shown in Table 6. As discussed earlier, because of the large directional shear of the wind in the lower to mid-troposphere, $\overline{DD}$ values are noisier than those in the other two ocean basins. On the average, cyclones in this region move to the left of the 5-7° 700 mb wind and to the right of the 5-7° 600 mb and 500 mb wind. This is not true for cyclones having a large zonal component. Westward-moving cyclones move consistently to the left of the 5-7° mean wind at all three levels while the opposite is true for eastward-moving cyclones.

Apart from the differences that occur between cyclones with east and west directions of movement, these results suggest that, in exact opposite to the Northern Hemisphere, cyclones in the Southern Hemisphere generally move to the right (rather than to the left) of the mid-tropospheric flow. This should be expected if the same physical processes are involved.

Summary. Although some variations exist in the $\overline{DD}$ values between different composite data sets, a general consistency is found. Table 7 summarizes the mean values and the corresponding scatter for each of the three ocean basins. It can be seen that cyclones in the northwest Pacific have the smallest variability, a reflection of the small mean

TABLE 5

Same as Table 4 except for west Atlantic tropical cyclones.

STRATIFICATION	700 mb	600 mb	500 mb
By Latitude			
Region I (South)	-5	-3	1
Region II (North)	3	7	12
By Speed			
Slow (1-3 m s^{-1})	-1	0	11
Fast (> 3 m s^{-1})	9	11	13
By Direction			
Northward (316^{o}-45^{o})	0	12	25
Westward (225^{o}-315^{o})	5	-2	-8
By Intensity			
Hurricane	2	3	5
Tropical Storm	-5	0	12
By Size and Intensity			
Small Tropical Storm	7	10	14
Large Tropical Storm	16	20	23
Small Hurricane	8	8	10
Large Hurricane North	23	22	24
Large Hurricane South	-3	15	7
Mean	5	8	11
Scatter	8.2	8.1	9.3

TABLE 6

Same as Table 4 except for tropical cyclones in the Australian-south Pacific region.

STRATIFICATION	700 mb	600 mb	500 mb
By Direction			
Eastward (40^{o}-150^{o})	-24	-20	-13
Westward (210^{o}-320^{o})	33	19	12
By Intensity and Region			
Hurricane	15	-3	-16
Coral Sea Hurricane	16	-7	-22
Coral Sea Tropical Storm	9	-5	-9
West Australian Hurricane	32	1	-2
Mean	14	-3	-8
Scatter	20.8	12.7	12.0

TABLE 7

Summary of the mean directional differences between cyclone motion and the 5-7° radial band mean wind averaged for all data sets in each ocean basin. The corresponding scatter within each ocean basin is given in parentheses.

Ocean Basin	700 mb	600 mb	500 mb
Northwest Pacific	19 (5.8)	22 (6.8)	23 (9.1)
West Atlantic	5 (8.2)	8 (8.1)	11 (9.3)
Australian-south Pacific Region	14 (20.8)	-3 (12.7)	-8 (12.0)

directional vertical wind shear. The direction of movement of west Atlantic cyclones tends to deviate less to the left of the mid-tropospheric mean wind (~ 10°) than those in the northwest Pacific (~ 20°). On the contrary, but with similar physical agreement, cyclones in the Southern Hemisphere move to the right of the mean winds at 600 and 500 mb. Parts of these results are consistent with those obtained by George and Gray (1976) and Brand et al. (1981) for the northwest Pacific and those of Gray (1977) for the west Atlantic.

It is important to note that the means given in Table 7 are meant to provide an idea of the average deviation of the cyclone direction from the environmental flow direction. The deviation in individual cases will differ from the mean, although in most cases not significantly. The amount of this difference depends on the various characteristics of the cyclone, as discussed above.

2.3.3 Layer-averages

Four averages were calculated: surface to 100 mb, surface to 300 mb, surface to 500 mb and 700 mb to 500 mb. The layer-averaged

component winds are denoted by $\langle \bar{V}_N \rangle$ and $\langle \bar{V}_P \rangle$, where

$$\langle \bar{V}_N \rangle = \frac{\int_{p_1}^{p_2} \bar{V}_N \, dp}{p_2 - p_1} \tag{2a}$$

and

$$\langle \bar{V}_p \rangle = \frac{\int_{p_1}^{p_2} \bar{V}_p \, dp}{p_2 - p_1} , \tag{2b}$$

with p_1 and p_2 being the lower and upper pressure levels of the layer. The layer-averaged directional deviation is then calculated by substituting $\langle \bar{V}_N \rangle$, $\langle \bar{V}_P \rangle$ into Eq. (1).

The reason for choosing the surface to 100 mb layer-average is to test the validity of the suggestion by Sanders and Burpee (1968) and Sanders et al. (1975) that the integrated tropospheric flow is the most applicable 'steering' current. Riehl and Burgner (1950) and E. Jordan (1952) used the surface to 300 mb mean flow as their predictor. The surface to 500 mb mean flow is calculated for comparison with the deeper surface to 300 mb mean flow pattern. The results in the previous subsection indicate the importance of mid-tropospheric flow and hence the 700 mb to 500 mb mean flow was also calculated.

Northwest Pacific. Table 8 shows the layer-averaged values of $\overline{DD}$ for northwest Pacific tropical cyclones. Little variation exists between the different pressure-weighted averages. This small variation is also reflected in the mean for all the data sets. However, within each category, slight differences that are consistent with the discussion in the last two sub-sections exist between data sets.

TABLE 8

Directional deviations between cyclone direction and direction of layer-averaged 5°-7° mean winds for different combination of levels for northwest Pacific tropical cyclones. See text for a description of how these averages were calculated (Eq. 2).

	$\int_{\text{surface}}^{100\text{mb}}$	$\int_{\text{surface}}^{300\text{mb}}$	$\int_{\text{surface}}^{500\text{mb}}$	$\int_{700\text{mb}}^{500\text{mb}}$
By Latitude				
North of 20°N	19	19	15	23
South of 20°N	2	6	8	8
By Speed				
Slow (1-3 m s^{-1})	29	27	10	30
Moderate (4-7 m s^{-1})	20	20	14	23
Fast (> 7 m s^{-1})	12	14	15	18
By Direction				
Westward (250°-310°)	9	17	18	20
Northward (310°-350°)	16	17	13	23
Eastward (350°-60°)	17	16	13	19
By Intensity				
Weak (1000-980 mb)	8	14	16	16
Intense (950-980 mb)	16	20	18	25
Very Intense (< 950 mb)	23	26	22	34
By Intensity Change				
Deepening North of 20°N	23	23	17	23
Deepening South of 20°N	14	24	30	30
Filling North of 20°N	19	20	17	23
Filling South of 20°N	8	13	10	13
By Size and Intensity				
Small Tropical Storm	9	12	11	13
Medium Tropical Storm	9	14	16	18
Large Tropical Storm	1	14	19	19
Small Typhoon	15	16	15	22
Medium Typhoon	12	15	14	18
Large Typhoon	27	29	26	31
Mean	15	18	16	21
Scatter	7.5	5.6	5.2	6.4

Cyclones south of 20°N move less to the left of all the layer-averaged flow than those north of 20°N. Slow-moving cyclones have the largest deviations in the speed category. An increase in the direction deviation is also found to correlate very well with an increase in cyclone intensity. The deviation also increases with cyclone size. The scatter among the data sets is about the same for the different layer-averages. The mean flow corresponding to the layer of cyclonic flow (surface to 300 mb or surface to 500 mb) has slightly smaller $\langle\overline{DD}\rangle$ values than the other levels. These results again demonstrate the absence of appreciable mean directional wind shear in the vertical.

West Atlantic. Table 9 indicates that the directional variability between data sets in the west Atlantic is larger than that in the northwest Pacific. The smallest variation appears to be for the surface to 300 mb average and the 700-500 mb average. These results again point to the existence of directional wind shear in the vertical. When integrated over the lower troposphere (surface to 500 mb), the shear near the boundary layer gives a large variability among data sets. However, when the integration is made up to 300 mb or just in the mid-troposphere (700-500 mb), the effect of the boundary layer is quite small. If the upper tropospheric flow is included (surface to 100 mb), a large variability exists because of the strong shear at the upper levels. Therefore, it appears that in the west Atlantic where directional wind shear is present in the upper and lower troposphere, either the mid-troposphere or a deep layer corresponding to the cyclonic rotation of the vortex is a better predictor of cyclone direction.

As in the northwest Pacific, small variations between data sets exist within each category. North cyclones move more to the left of the

TABLE 9

Same as Table 8 except for west Atlantic tropical cyclones.

	$\int_{\text{surface}}^{100\text{ mb}}$	$\int_{\text{surface}}^{300\text{mb}}$	$\int_{\text{surface}}^{500\text{mb}}$	$\int_{700\text{mb}}^{500\text{mb}}$
<u>By Latitude</u>				
Region I (South)	-1	-3	-7	-3
Region II (North)	16	5	-4	7
<u>By Speed</u>				
Slow (1-3 m s^{-1})	11	3	-7	4
Fast (> 3 m s^{-1})	14	10	7	11
<u>By Direction</u>				
Northward (316°-45°)	27	13	-5	13
Westward (225°-315°)	-9	-5	-2	-1
<u>By Intensity</u>				
Hurricane	10	3	-3	3
Tropical Storm	6	-1	-8	2
<u>By Size and Intensity</u>				
Small Tropical Storm	14	9	5	10
Large Tropical Storm	22	18	11	20
Small Hurricane	12	8	5	9
Large Hurricane North	22	21	21	23
Large Hurricane South	18	4	-12	6
Mean	13	7	0	8
Scatter	9.7	7.7	9.2	7.6

layer-averaged winds than south cyclones. In fact, south cyclones move slightly to the right of the mean flow. This is also the case for westward moving cyclones. These two data sets (south and westward-moving) probably include almost the same cyclones since cyclones south of 20°N usually move westnorthwestward. Northward-moving cyclones, on the other hand, are usually at higher latitudes. Therefore, consistent with north cyclones, they move more to the left of the mean wind. These results suggest the importance of the latitude (which relates to the Coriolis parameter) in cyclone motion. This question has been addressed in some theoretical studies (for example, Holland, 1982). See also a more complete discussion of this in Chapters 3 and 4. Anthes (1982) also presented a review of this topic. In the intensity category, hurricanes generally move more to the left of the layer-averaged flow than tropical storms. The deviation also appears to increase with cyclone size. The small (or even negative) deviation for the large hurricane south data set is probably a result of the latitude of the cyclones.

Australian-South Pacific region. Table 10 gives the layer-averaged $\overline{DD}$ values for tropical cyclones in the Australian-south Pacific region. The striking result is the consistency among data sets for the surface to 100 mb layer-average. It shows that Australian cyclones move to the right of the 5-7° mean tropospheric wind. Because of the large directional vertical wind shear, a relatively large variability exists among the different layer-averages for a given data set, with the exception of eastward-moving hurricanes (see Fig. 12).

Summary. The mean $\overline{DD}$ values for all data sets for each level- or layer-average for the three ocean basins are shown in Table 11. It

TABLE 10

Same as Table 8 except for tropical cyclones in the Australian-south Pacific region.

	$\int_{\text{surface}}^{100\text{mb}}$	$\int_{\text{surface}}^{300\text{mb}}$	$\int_{\text{surface}}^{500\text{mb}}$	$\int_{700\text{mb}}^{500\text{mb}}$
By Direction				
Eastward (40°-150°)	-10	-13	-14	-17
Westward (210°-320°)	-9	14	22	22
By Intensity and Region				
Hurricane	-20	-12	3	-5
Coral Sea Hurricane	-15	-7	12	-12
Coral Sea Tropical Storm	-13	-2	5	-4
West Australian Hurricane	-22	-8	10	14
Mean	-15	-5	6	0
Scatter	5.3	10.0	12.0	15.2

TABLE 11

Same as Table 7 except for level- or layer-averaged winds.

Ocean Basin	$\int_{\text{surface}}^{100\text{mb}}$	$\int_{\text{surface}}^{300\text{mb}}$	$\int_{\text{surface}}^{500\text{mb}}$	$\int_{700\text{mb}}^{500\text{mb}}$
Northwest Pacific	15 (7.5)	18 (5.6)	16 (5.2)	21 (6.4)
West Atlantic	13 (9.7)	7 (7.7)	0 (9.2)	8 (7.6)
Australian-south Pacific Region	-15 (5.3)	-5 (10.0)	6 (12.0)	0 (15.2)

shows that the mean tropospheric flow (surface to 100 mb) gives almost the same results for all the three ocean basins. It seems that the mean tropospheric flow, on the average, would be the best descriptor or predictor for direction of cyclone movement, with cyclones in the Northern Hemisphere moving to the left of this flow by ~ 15^{o} and those in the Southern Hemisphere moving to the right by about the same amount. However, it appears that, for individual ocean basins, the best layer depends on the directional vertical shear of the environmental wind in that region. In general, the more directional shear there is with height the deeper the steering layer. When little directional shear is present, mid-tropospheric and deep layer steering are comparable.

2.4. Relationship between the surrounding flow and the speed of tropical cyclones

In both coordinate systems described in section 2.2.2, the winds are resolved into two components, one normal (V_N) and one parallel (V_P) to the direction of cyclone movement. The normal component V_N obviously does not contribute to the scalar speed of the cyclone. The study of the relation between the surrounding flow and the speed V_c of a cyclone therefore reduces to relating the parallel component of the wind V_P to V_c. If the large-scale surrounding flow is the determining factor in cyclone speed, as is the case with cyclone direction, then values of V_P relative to cyclone movement should be about the same for different data sets. The MOTROT coordinate system described in section 2.2.2 is used for this purpose. That is, for every wind observation, the value of V_P relative to the cyclone (V_{PM}) is calculated from

$$V_{PM} = V_P - V_c.$$

See Fig. 6 for an illustration of how this is done. A composite was

then made using the individual values of $V_P - V_c$. The parameter V_{PM} therefore represents the composite relative (to the cyclone) wind component parallel to the cyclone direction. A negative value of V_{PM} means that the cyclone is moving faster than the composite wind.

Again, as in the last section, the surrounding flow averaged around a radial band is studied. That is, at each pressure level and each radius, the average of the V_{PM} for all eight octants in that radial band, denoted by $\bar{V}_{PM}$, is computed. To find the 'best' steering level and radius for cyclone speed, the standard deviations of $\bar{V}_{PM}$ for data sets at various levels and radii were calculated. Again, the 5-7° radial band at the three mid-tropospheric levels (700, 600 and 500 mb) have the smallest scatter among data sets for all three ocean basins. Following the procedure used in section 2.3, the variation of 5-7° $\bar{V}_{PM}$ with height will be presented, followed by individual level and then layer-averaged winds.

2.4.1 Variation with height

Northwest Pacific. Figure 13 shows the vertical profile of $\bar{V}_{PM}$ at 5-7° for northwest Pacific tropical cyclones. Little variation in the vertical exists for most data sets except for the data set north of 20°N, the fast-moving, eastward-moving, filling north of 20°N and large typhoon data sets. This means that with the exception of these five stratifications, the other cyclones are generally embedded in an environment with relatively small vertical speed shear. The variation among different data sets, if those five stratifications are excluded, is very small. For all data sets, the values of $\bar{V}_{PM}$ are negative, at least below ~ 600 mb. This means that tropical cyclones in the

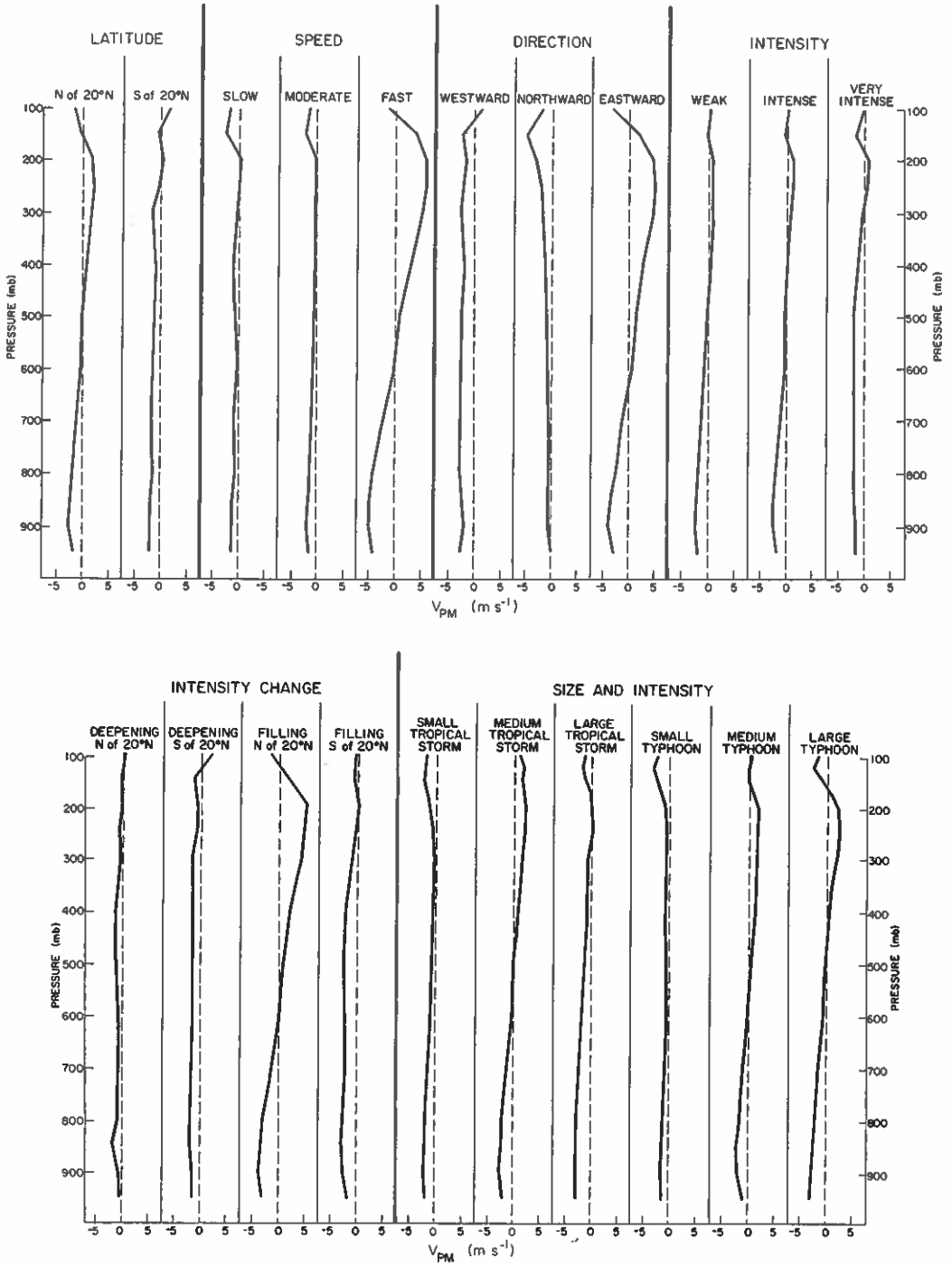

Fig. 13. Variation with height of the 5-7° belt average relative component of the wind parallel to cyclone direction $\overline{V}_{PM}$ for northwest Pacific tropical cyclones (solid line). The zero (dashed) line represents the cyclone speed. A negative value of V_{PM} means that the cyclone is moving faster than the 5-7° surrounding wind.

northwest Pacific generally move faster than their surrounding mean 5-7° winds in the lower to mid-troposphere.

West Atlantic. The vertical profiles of 5-7° $\bar{V}_{PM}$ values for west Atlantic tropical cyclones are shown in Fig. 14. The variation with height for most data sets is not very large. Noticeable exceptions are westward- and northward-moving cyclones, large tropical storms and large hurricanes north of 25°N. Again, all cyclones move faster than the lower and mid-tropospheric winds ($\bar{V}_{PM} < 0$). Between data sets, very little difference between the values of $\bar{V}_{PM}$ can be noticed, especially in the mid-troposphere. It is also of interest to note that the same relationship between the 5-7° wind speed and the cyclone speed holds for cyclones of different sizes in both the northwest Pacific and the west Atlantic. It therefore appears that despite the difference in the sizes of cyclones, the 5-7° surrounding flow can be used to describe cyclone movement.

Australian-south Pacific region. Figure 15 shows the vertical profiles of 5-7° $\bar{V}_{PM}$ values for tropical cyclones in this region. Considerable variation of $\bar{V}_{PM}$ with height exists for most data sets, indicating a large speed shear in the vertical. Similar to those in the Northern Hemisphere, all cyclones move faster than the mean wind in the lower troposphere (below ~ 600 mb). Although strong shear is present, the values of $\bar{V}_{PM}$ in the mid-troposphere are about the same among different data sets.

Summary. The vertical profiles of $\bar{V}_{PM}$ at 5-7° do not show much variation among cyclones in the three ocean basins, when compared to the vertical profiles of directional deviations. Exceptions arise when the cyclone is in an environment with strong vertical speed shear. However,

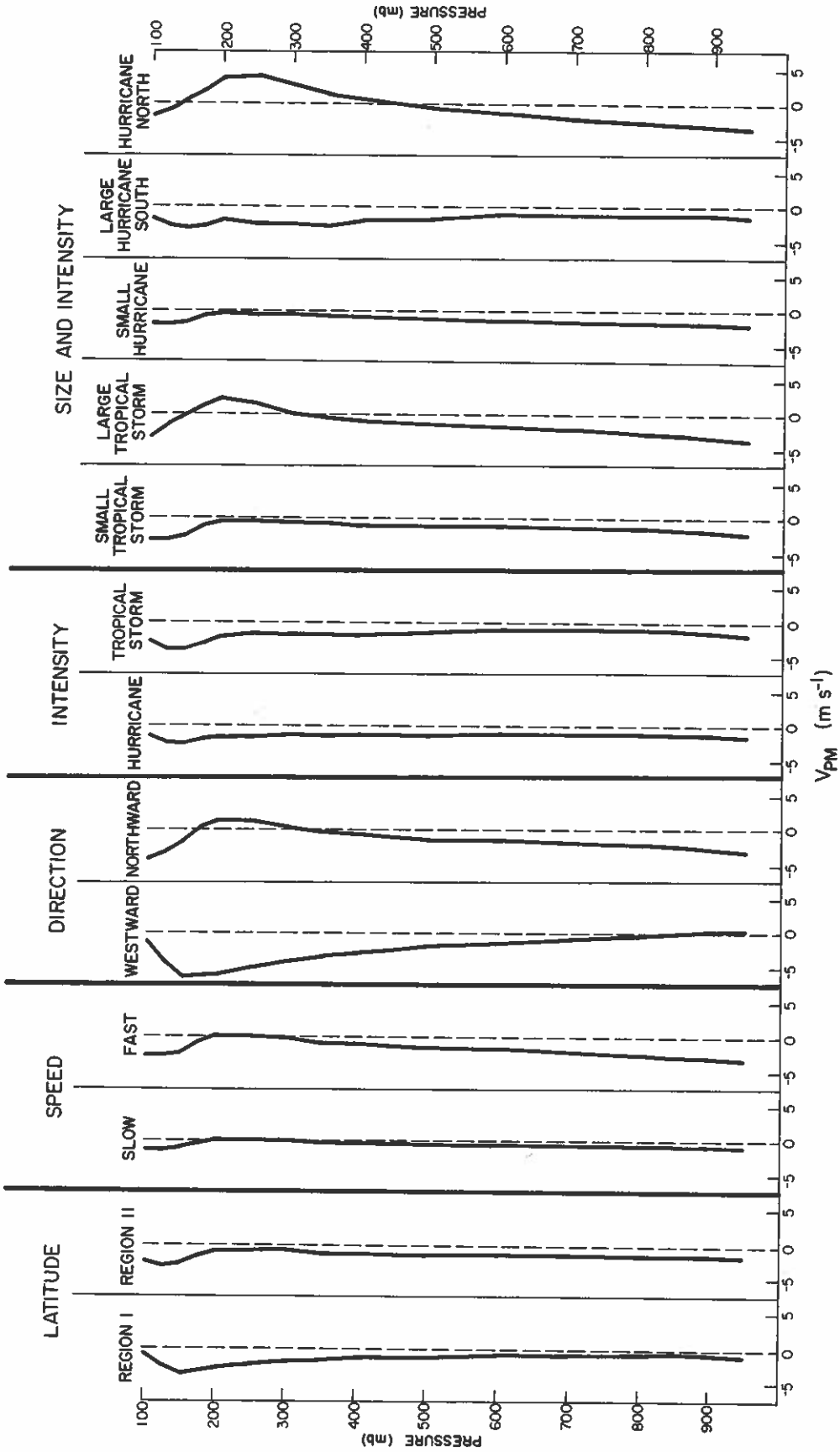

Fig. 14. Same as Fig. 13 except for west Atlantic tropical cyclones.

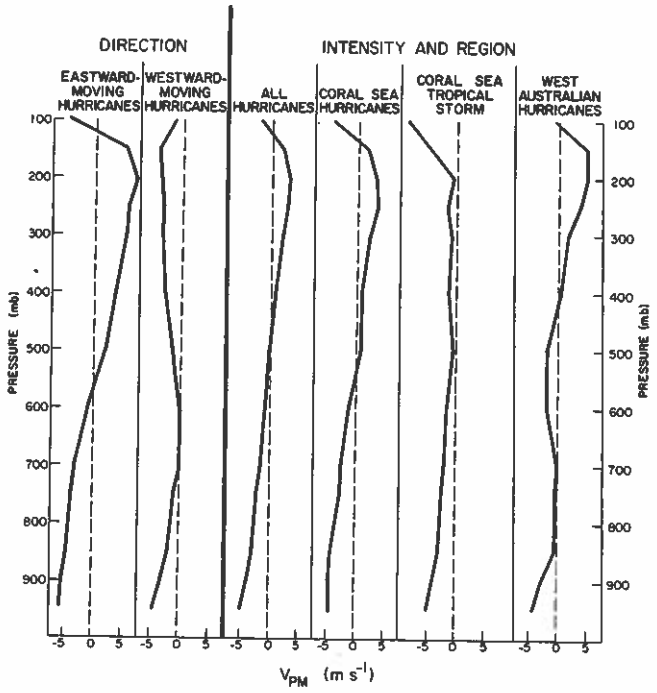

Fig. 15. Same as Fig. 13 except for Australian-south Pacific region tropical cyclones.

all the data sets indicate that cyclones tend to move <u>faster</u> than the 5-7° mean wind at the mid-troposphere. This is consistent with the results obtained by George and Gray (1976) and Gray (1977). If the assumption in the steering flow concept is correct, one would expect $\bar{V}_{PM}$ to be near zero. The fact that $\bar{V}_{PM}$ is always negative, at least in the mid-troposphere, suggests that the cyclone is not simply being "advected" along by the steering flow. This will be discussed further in later chapters.

2.4.2 Individual levels

The results in the last subsection suggest that mid-tropospheric data correlate best with cyclone speed. To quantify these results, the values of $\bar{V}_{PM}$ at 700, 600 and 500 mb and the corresponding standard deviations between data sets are specifically portrayed.

Northwest Pacific. Table 12 gives the values of $\bar{V}_{PM}$ at 5-7° for three mid-tropospheric levels for northwest Pacific tropical cyclones. It can be seen that the $\bar{V}_{PM}$ values at 700 mb have the least spread among data sets. Notice that all data sets show a negative $\bar{V}_{PM}$, meaning that a tropical cyclone travels faster than its 6° mean 700 mb wind. Similar observations can be made about the 600 and 500 mb data. This was also reported by George and Gray (1976).

Note, however, that fast-moving and eastward-moving cyclones and those filling at latitudes north of 20°N all move slower than the 500 mb wind. These cyclones have a strong northward and/or eastward component of motion. Therefore, it seems that the zonal and meridional components of cyclone motion have some effect on the speed of the cyclone relative to its environmental wind. This will be explored more in Chapter 4.

West Atlantic. The values of 5-7° $\bar{V}_{PM}$ at 700, 600 and 500 mb for west Atlantic tropical cyclones are shown in Table 13. Very little scatter exists in the data sets for all three mid-tropospheric levels, as evidenced by the standard deviations. The results also show that a cyclone travels faster than its surrounding 6° mid-tropospheric winds.

Australian-south Pacific region. Table 14 presents the mid-tropospheric 5-7° values of $\bar{V}_{PM}$ for tropical cyclones in the Australian-south Pacific region. As mentioned in the last sub-section, although large vertical speed shear exists in this region, the values of $\bar{V}_{PM}$ do not differ very much between data sets. Again, cyclones travel ~ 1 m s^{-1} faster than their surrounding mid-tropospheric winds.

Summary. To compare results obtained from the different ocean basins, the mean values of $\bar{V}_{PM}$ for all data sets in a given ocean basin and the corresponding scatter are presented in Table 15. One

TABLE 12

Radial band average of the relative (to the cyclone) component of the wind parallel to the direction of cyclone movement ($\bar{V}_{PM}$) at 5°–7° radius for northwest Pacific tropical cyclones. A negative value of $\bar{V}_{PM}$ means the cyclone moves faster than the mean wind. Units: m s^{-1}.

STRATIFICATION	700 mb	600 mb	500 mb
By Latitude			
North of 20°N	-1.4	-0.5	-0.2
South of 20°N	-1.7	-1.5	-1.3
By Speed			
Slow (1-3 m s^{-1})	-0.9	-0.3	-0.9
Moderate (4-7 m s^{-1})	-1.2	-0.8	-0.8
Fast (> 7 m s^{-1})	-2.4	-0.4	0.7
By Direction			
Westward (250°-310°)	-2.6	-2.3	-2.3
Northward (310°-350°)	-0.6	-0.9	-1.3
Eastward (350°-60°)	-1.3	0.5	1.2
By Intensity			
Weak (1000-980 mb)	-1.4	-1.0	-0.3
Intense (950-980 mb)	-1.4	-0.4	-0.3
Very Intense (< 950 mb)	-1.8	-2.0	-2.1
By Intensity Change			
Deepening North of 20°N	-0.9	-1.0	-1.5
Deepening South of 20°N	-1.7	-1.5	-1.5
Filling North of 20°N	-1.2	0.0	0.8
Filling South of 20°N	-2.2	-2.4	-2.6
By Size and Intensity			
Small Tropical Storm	-1.5	-1.0	-0.8
Medium Tropical Storm	-1.2	-0.5	-0.1
Large Tropical Storm	-2.4	-1.9	-1.4
Small Typhoon	-1.0	-0.6	-0.8
Medium Typhoon	-1.1	-0.2	0.4
Large Typhoon	-1.6	-0.7	-0.5
Mean	-1.5	-0.9	-0.5
Scatter	0.5	0.8	1.2

TABLE 13

Same as Table 15 except for west Atlantic tropical cyclones.

STRATIFICATION	700 mb	600 mb	500 mb
By Latitude			
Region I (South)	-0.6	-0.6	-1.0
Region II (North)	-1.2	-1.2	-1.4
By Speed			
Slow (1-3 m s^{-1})	-0.6	-0.6	-0.5
Fast (> 3 m s^{-1})	-2.0	-1.6	-1.5
By Direction			
Northward (316^{o}-45^{o})	-1.7	-1.5	-1.4
Westward (225^{o}-315^{o})	-0.8	-1.4	-1.9
By Intensity			
Hurricane	-1.0	-1.0	-1.3
Tropical Storm	-1.0	-1.0	-1.4
By Size and Intensity			
Small Tropical Storm	-1.3	-1.2	-1.2
Large Tropical Storm	-2.1	-1.7	-1.4
Small Hurricane	-1.5	-1.3	-1.2
Large Hurricane North	-2.1	-1.5	-0.8
Large Hurricane South	-1.0	-1.1	-1.7
Mean	-1.3	-1.2	-1.3
Scatter	0.5	0.4	0.4

TABLE 14

Same as Table 15 except for tropical cyclones in the Australian-south Pacific region.

STRATIFICATION	700 mb	600 mb	500 mb
By Direction			
Eastward (40^{o}–150^{o})	-3.1	-0.9	2.0
Westward (210^{o}–320^{o})	-0.1	-0.2	-1.5
By Intensity and Region			
Hurricane	-1.6	-0.9	-0.2
Coral Sea Hurricane	-2.6	-1.3	0.8
Coral Sea Tropical Storm	-2.1	-1.6	-0.6
West Australian Hurricane	-0.2	-2.0	-2.1
Mean	-1.6	-1.2	-0.3
Scatter	1.2	0.6	1.5

TABLE 15

Average 5^{o}–7^{o} $\bar{V}_{PM}$ for all data sets in each ocean basin and the corresponding scatter at 700, 600 and 500 mb (in parentheses). Unit: m s^{-1}.

Ocean Basin	700 mb	600 mb	500 mb
Northwest Pacific	-1.5 (0.5)	-0.9 (0.8)	-0.5 (1.2)
West Atlantic	-1.3 (0.5)	-1.2 (0.4)	-1.3 (0.4)
Australian–south Pacific Region	-1.6 (1.2)	-1.2 (0.6)	-0.3 (1.5)

might conclude from this table that cyclones in both hemispheres generally move faster than the mid-tropospheric winds at 5-7° by an average of ~ 1 m s^{-1}. Both 700 and 600 mb appear to be better levels than 500 mb.

2.4.3 Layer-averages

To calculate the pressure-weighted averages of $\overline{V}_{PM}$, Eq. (2b) was used with $\overline{V}_{PM}$ in the integrand of the numerator instead of $\overline{V}_{P}$. Similar pressure-weighted averages were calculated: surface to 100 mb, surface to 300 mb, surface to 500 mb and 700 to 500 mb.

Northwest Pacific. Table 16 shows the pressure-weighted layer averages of $\overline{V}_{PM}$ for all northwest Pacific cyclones. As with the layer-averaged directional deviations, not much variation exists among the different averages. This is also evident from the mean for all the data sets. Slight variations within each category are also apparent. Cyclones south of 20°N move faster than the layer-averaged flow by a larger amount than those north of 20°N. The values of the integrated $\overline{V}_{PM}$ for eastward-moving cyclones are usually the least negative among the direction data sets. Very intense cyclones tend to move faster than the mean wind by the largest amount within the intensity category. For the same intensity change, north cyclones have $\overline{V}_{PM}$ values less than those of south cyclones. This is consistent with the results for cyclones in the latitude category.

The results in Table 16 seem to suggest that a relatively shallow layer would be nearly as representative of cyclone speed as a deep layer average. This is of course a reflection of the relatively small speed shear of the environmental wind.

TABLE 16

Layer-averaged 5°-7° $\bar{V}_{PM}$ for different combination of levels for northwest Pacific tropical cyclones. See text for a description of how the averages were calculated. Unit: m s^{-1}.

Stratification	$\int_{\text{surface}}^{100\text{mb}}$	$\int_{\text{surface}}^{300\text{mb}}$	$\int_{\text{surface}}^{500\text{mb}}$	$\int_{700\text{mb}}^{500\text{mb}}$
By Latitude				
North of 20°N	-0.6	-1.0	-1.7	-0.6
South of 20°N	-1.3	-1.6	-1.7	-1.5
By Speed				
Slow (1-3 m s^{-1})	-0.9	-0.9	-0.9	-0.6
Moderate (4-7 m s^{-1})	-1.1	-1.1	-1.3	-0.9
Fast (> 7 m s^{-1})	-0.1	-1.3	-3.0	-0.6
By Direction				
Westward (250°-310°)	-2.2	-2.3	-2.4	-2.4
Northward (310°-350°)	-1.5	-1.0	-0.8	-0.9
Eastward (350°-60°)	0.2	-0.5	-1.8	0.2
By Intensity				
Weak (1000-980 mb)	-0.8	-1.1	-1.6	-0.9
Intense (950-980 mb)	-0.7	-1.1	-1.6	-0.6
Very Intense (< 950 mb)	-1.4	-1.7	-1.9	-2.0
By Intensity Change				
Deepening North of 20°N	-1.0	-1.1	-1.1	-1.1
Deepening South of 20°N	-1.5	-1.7	-1.7	-1.5
Filling North of 20°N	0.2	-0.7	-1.9	-0.1
Filling South of 20°N	-1.9	-2.3	-2.5	-2.4
By Size and Intensity				
Small Tropical Storm	-1.3	-1.2	-1.5	-1.1
Medium Tropical Storm	-0.2	-0.7	-1.4	-0.6
Large Tropical Storm	-1.7	-1.9	-2.3	-1.9
Small Typhoon	-1.2	-1.0	-1.0	-0.8
Medium Typhoon	-0.1	-0.4	-1.0	-0.3
Large Typhoon	-0.7	-1.0	-1.7	-1.0
Mean	-0.9	-1.2	-1.7	-1.0
Scatter	0.7	0.5	0.6	0.7

West Atlantic. The layer-averaged 5-7° $\bar{V}_{PM}$ values for west Atlantic tropical cyclones are shown in Table 17. The variation among different averages is also small for most data sets. The scatter among data sets is about the same for all four layer-averages.

Australian-south Pacific region. Table 18 shows the level- and layer-averaged $\bar{V}_{PM}$ 5-7° for tropical cyclones in this region. As mentioned before, the vertical speed shear in this region is relatively large (see Fig. 15). Therefore, a large variation among different layer-averages exists for a given data set, as seen in Table 18. Both the surface to 500 mb and the 700 mb to 500 mb layer-averages are extremely consistent. The deep layer averages have a larger spread. This is different than the layer-average directional deviations discussed in section 2.3.3 in which the mean tropospheric flow best describes the directional movement of a cyclone in this region. It appears from Fig. 15 that the speed shear is too variable among data sets to give a consistent $\bar{V}_{PM}$ when integrated over a deep layer. However, if the integration is through a shallower layer, the effect of the shear would be less.

Summary. Layer-averaged $\bar{V}_{PM}$ for all data sets in each of the three ocean basins is shown in Table 19. It can be seen that in the three ocean basins, cyclones, on the average, move faster than the mean 5-7° level- or layer-averaged winds. The most consistent layer-average appears to be the surface to 300 mb average. The mid-tropospheric average is also about the same between the three oceans. Therefore, it seems that the best layer-average depends very much on the vertical wind shear profile in the environment.

TABLE 17

Same as Table 16 except for west Atlantic tropical cyclones.

Stratification	$\int_{\text{surface}}^{100\text{ mb}}$	$\int_{\text{surface}}^{300\text{mb}}$	$\int_{\text{surface}}^{500\text{mb}}$	$\int_{700\text{mb}}^{500\text{mb}}$
By Latitude				
Region I (South)	-1.3	-0.9	-0.7	-0.7
Region II (North)	-1.4	-1.3	-1.3	-1.3
By Speed				
Slow (1-3 m s^{-1})	-0.5	-0.5	-0.6	-0.6
Fast (> 3 m s^{-1})	-1.7	-1.8	-2.2	-1.7
By Direction				
Northward (316^{o}-45^{o})	-1.4	-1.6	-2.0	-1.5
Westward (225^{o}-315^{o})	-2.2	-1.4	-0.7	-1.3
By Intensity				
Hurricane	1.3	-1.2	-1.1	-1.1
Tropical Storm	-1.6	-1.3	-1.1	-1.1
By Size and Intensity				
Small Tropical Storm	-1.4	-1.3	-1.4	-1.2
Large Tropical Storm	-1.4	-1.8	-2.3	-1.7
Small Hurricane	-1.3	-1.3	-1.5	-1.4
Large Hurricane North	-0.6	-1.3	-2.2	-1.5
Large Hurricane South	-1.7	-1.5	-1.2	-1.3
Mean	-1.4	-1.3	-1.4	-1.3
Scatter	0.4	0.4	0.6	0.3

TABLE 18

Same as Table 16 except for tropical cyclones in the Australian-south Pacific region.

Stratification	$\int_{\text{surface}}^{100\text{mb}}$	$\int_{\text{surface}}^{300\text{mb}}$	$\int_{\text{surface}}^{500\text{mb}}$	$\int_{700\text{mb}}^{500\text{mb}}$
By Direction				
Eastward (40°-150°)	0.2	-0.8	-2.5	-0.5
Westward (210°-320°)	-2.2	-1.9	-1.5	-0.6
By Intensity and Region				
Hurricane	-0.7	-1.3	-2.1	-0.8
Coral Sea Hurricane	-0.8	-1.5	-2.4	-0.9
Coral Sea Tropical Storm	-2.4	-2.1	-2.4	-1.4
West Australian Hurricane	-0.1	-1.0	-1.7	-1.5
Mean	-1.0	-1.4	-2.1	-1.0
Scatter	1.1	0.5	0.4	0.4

TABLE 19

Same as Table 15 except for layer-averaged $\overline{V}_{PM}$.

Ocean Basin	$\int_{\text{surface}}^{100\text{mb}}$	$\int_{\text{surface}}^{300\text{mb}}$	$\int_{\text{surface}}^{500\text{mb}}$	$\int_{700\text{mb}}^{500\text{mb}}$
Northwest Pacific	-0.9 (0.7)	-1.2 (0.5)	-1.7 (0.6)	-1.0 (0.7)
West Atlantic	-1.4 (0.4)	-1.3 (0.4)	-1.4 (0.6)	-1.3 (0.3)
Australian- south Pacific Region	-1.0 (1.1)	-1.4 (0.5)	-2.1 (0.4)	-1.0 (0.4)

2.5. Summary

The main findings of this study are:

a) the large-scale circulation is very well related to the movement of tropical cyclones;

b) wind data at the mid-troposphere (700, 600 and 500 mb) correlates best with both the direction and speed of cyclone movement;

c) on the average, tropical cyclones in the Northern Hemisphere moves ~ 10^{o}–20^{o} to the left of the surrounding mid-tropospheric winds at ~ 6^{o} latitude radius from the cyclone center; an approximate opposite directional deviation occurs for cyclones in the Southern Hemisphere;

d) on the average, tropical cyclones move faster by ~ 1 m s^{-1} than the surrounding mid-tropospheric winds at ~ 6^{o} radius from the cyclone center;

e) cyclones having different zonal components of motion have different relationships with their 5–7^{o} surrounding flow; and

f) deep tropospheric flow appears to be a good descriptor of cyclone movement; for cyclones in a relatively weak shear environment a shallow layer-average flow is equally suitable.

Some of these same conclusions were also made by George and Gray (1976), Gray (1977) and Brand et al. (1981). Bell and Lam (1980) found that northwest Pacific tropical cyclones move, on the average, 0.9 m s^{-1} more northward and 3.4 m s^{-1} more westward compared to the geostrophic steering flow. This means that cyclones having a westward component of motion, which is normally the case, move faster than and to the left of the geostrophic flow, in qualitative agreement with the present study.

From a forecasting point of view, these results imply that if one makes a forecast from a scheme based on steering flow, he would tend to predict the cyclone to move to the right of the actual track and slower than observed. This in fact was found to be the case by Kasahara (1957) using a barotropic non-divergent model. Since then, other numerical forecasts of tropical cyclone movement based primarily on steering flow also produced a systematic rightward deflection of the predicted trajectory relative to the actual path and a predicted speed slower than the observed speed. See for example, Kasahara (1959, 1960), Birchfield (1960), Jones (1961, 1977a, 1977b), Sanders and Burpee (1968), Sanders et al. (1975), Anthes and Hoke (1975), Harrison (1981), etc. Such systematic direction and speed biases have also been discussed by Neumann and Pelissier (1981) in the analyses of operational track forecast errors. These apparent discrepancies between theory and observation will be discussed further in later chapters.

This chapter has only dealt with the relationship between the belt-averaged flow and cyclone movement. For a discussion of how tropical cyclone motion is related to winds at individual octants around the cyclone, the reader is referred to the report by Chan and Gray (1982a).

CHAPTER 3 - REVIEW OF PREVIOUS THEORETICAL AND NUMERICAL STUDIES OF TROPICAL CYCLONE MOVEMENT

3.1 Introduction

This chapter reviews previous theoretical and numerical studies of tropical cyclone movement. This should provide the reader with an idea of what has so far been accomplished in terms of the understanding of the basic physical processes of tropical cyclone motion. Since most of these studies are highly mathematical, only the final results will be presented. Discussions will center on how realistic and significant these past studies have been.

3.2. The Beta Effect

One of the earliest theoretical studies on the movement of atmospheric vortices was made by Rossby (1948). He tried to relate vortex motion with the latitudinal variation of the Coriolis parameter across the cyclone. According to Rossby, the Coriolis force acting on an air parcel on the poleward side of a vortex is greater than that acting on a corresponding parcel on the equatorward side of the vortex. The difference between these two forces depends on the variation of the Coriolis parameter with latitude across the cyclone. Integrating this difference for all parcels in the vortex, the net result would be a force acting on the vortex in the north-south direction. Assuming a symmetric vortex, Rossby calculated this force F (per unit height) to be given by:

$$F = \frac{\rho\pi}{4} \beta \bar{\omega} R^4 , \qquad (3)$$

where ρ = density of air

$\bar{\omega}$ = mean angular velocity within the vortex

R = radial outer boundary of the vortex, beyond which the air does not participate in the vortex motion and

β = the variation of Coriolis parameter f with latitude, given by

$$f = f_o + \beta y ,$$

where f_o = value of f at the latitude of the vortex center and y the meridional distance from the center of the vortex. If no extra pressure gradient is present in the environment to balance this force F, then for $\bar{\omega} > 0$ (cyclonic vortex), a poleward acceleration should result. Equation 3 also suggests that such an acceleration should be greater for larger (with the size defined by R) and/or stronger (related to $\bar{\omega}$) vortices. This poleward acceleration has been known as the Rossby effect.

Kasahara (1957) studied the interaction between a vortex and its surrounding flow within the framework of a non-divergent barotroic model. He found that for a uniform flow, the analytic solution shows a <u>westward</u> drift due to the variation of the Coriolis parameter. His model will be discussed in greater detail in section 3.4.1. Adem and Lezama (1960) solved the non-divergent barotropic vorticity equation for an axisymmetric vortex and found that the variation of the Coriolis parameter results in a northwestward movement of the vortex. By changing the differential friction superimposed on a vortex, Rao (1970) was able to change the magnitude of this northwestward motion. Mathur (1974), Anthes and Hoke (1975), Madala and Piacsck (1975), Jones

(1977a), Kitade (1980) and Nitta (1980) studied asymmetric vortices on a β-plane and obtained a northward drift. They all attributed this to the Rossby effect.

The question is: why do some models produce only a northward movement while others give a northwestward motion? It seems obvious that the northward drift, which is present in all models, can be easily explained by the Rossby effect. However, one very important consideration was not made in Rossby's study. This is the pressure-gradient force. If the vortex is in a balanced state, then on the poleward side, the pressure-gradient force will be stronger than that on the equatorward side, thus balancing the 'excess' force that Rossby hypothesized. If this is the case, then this northward acceleration should not be present. However, some of the numerical models use as the initial condition a balanced vortex (for example, Kitade, 1981) and still obtain a poleward acceleration. Therefore, some other explanation must be given to this modeling result.

This apparent discrepancy can be explained using the concept of conservation of absolute vorticity. Consider a cyclone in the Northern Hemisphere. On the west side of the cyclone, air is moving southward, thus reducing its earth vorticity. To conserve absolute vorticity, it must increase its relative vorticity, resulting in the development of a cyclonic flow west of the cyclone center. Similarly, on the east side of the cyclone, air would have to reduce its relative vorticity by setting up an anticyclone. This is similar to the Rossby Wave effect (Rossby, 1939). The cyclonic (anticyclonic) flow to the west (east) of the cyclone therefore sets up a net southerly flow which then advects the vortex vorticity northward. This would then cause the cyclone to

move northward. Anthes and Hoke (1975) were the first to propose such an explanation. Holland (1982) also explained the northward drift with similar arguments. The increase in relative vorticity to the west side of the cyclone would also produce a westward movement of the cyclone. The net result is therefore a northwestward motion. Thus, the northward drift of a cyclone produced in numerical models is not a result of the effect proposed by Rossby (1948) but rather the response of the model atmosphere to the westward (eastward) increase (decrease) of relative vorticity.

Bell (1980) found from an observational study of more than 2000 tropical cyclones in the northwest Pacific that cyclone size (although not defined in the paper) and poleward acceleration are significantly correlated in the sense indicated by the Rossby effect. Poleward displacement is also found to correlate with cyclone intensity. Bell pointed out that although the statistical significance of these correlations is very high, the correlation coefficients are small. This is possible due to the large sample size. From these results, Bell concluded that this is probably a secondary effect.

3.3 Trochoidal Motion

The positions of tropical cyclones are often found to oscillate about a mean path. A good example was hurricane Carla in 1961 (see, for example, Fig. 9-1 in WMO, 1979). This type of oscillation often takes the form of a trochoid with a period of ~ 6h. The present paper, however, concerns mainly with tropical cyclone motion of a longer time scale (~ 12-24h). Therefore, only a brief review of some of the theoretical results will be presented here. For more detailed

descriptions of these studies, the reader is referred to the original papers.

Yeh (1950) was the first one to analyze such a problem. He studied a Rankine vortex embedded in a homogeneous, incompressible basic current of uniform speed on a f-plane. Under these conditions, he found that the centroid of the vortex moves in a trochoidal path with a period that depends on the intensity and size of the vortex. Kuo (1969) performed a theoretical study on vortex movement in which frictional drag and a shearing current were included. He also found an oscillatory motion of the vortex about its mean path. Recent numerical experiments, for example, Jones (1977b), Kitade (1980, 1981) and Nitta (1980), on either a f-plane or a β-plane, also obtained a trochoidal motion of the model vortex.

Earlier models (Yeh, 1950; Kuo, 1969) assumed the vortex to be a solid rotating cylinder. The oscillatory motion obtained was thus attributed to the Magnus effect. However, more recent models did not have such an assumption. It would seem that such oscillations may not be due to the Magnus effect. In fact, Kitade (1981) showed that his model results do not agree with those predicted by Yeh's theory. Kitade (1981) used a simple divergent barotropic model to solve numerically for the movement of the vortex on a beta-plane. The only physics in this model is the adjustment between the wind and pressure fields as governed by the momentum equations. A possible explanation of the oscillatory motion in this model is that because of the changes in vorticity created by both advection and stretching processes, the vortex is constantly distorted. The pressure field therefore has to adjust to these changes and a non-linear process sets in. A similar argument has also been

advanced by Holland (1982). Whether this is the actual physical mechanism that causes the oscillatory motion still needs to be further documented with both theory and observations. A study of this type of short-term motion is beyond the scope of this paper which is to consider cyclone motion on a longer time scale.

3.4 Interaction Between a Cyclone and its Surrounding Flow

3.4.1 Barotropic Model

Kuo (1950) studied the motion of atmospheric vortices in a non-divergent, barotropic model with pure horizontal motion. He found the presence of a force which drives cyclonic vortices towards regions with higher absolute vorticity. This may be explained in terms of the process of geostrophic adjustment. Because of the non-uniform distribution of absolute vorticity, the kinetic energy associated with the flow is also not uniform. The flow therefore readjusts by converting part of the "excess" kinetic energy to potential energy. The final result is the formation of a cyclonic vortex which "traps" the potential energy.

If divergence is included, an extra force exists that tends to drive westward-moving cyclones towards the south and eastward-moving cyclones towards the north. Kuo found, however, that this force is about one order of magnitude smaller than that caused by the gradient of vorticity.

Kasahara (1957) studied the interaction between a cyclone and its surrounding flow in a different way. A barotropic and non-divergent model was used. The total streamfunction was separated into two parts, that of the vortex and that of the environment (which is equal to the total streamfunction minus the vortex streamfunction). Under these

conditions, the instantaneous velocity C of the center of a symmetric vortex is found to be

$$\mathbb{C} = \tilde{\mathbb{V}}_o + K(\mathbb{k} \times \nabla \tilde{\eta}_o) , \qquad (4)$$

where

$\tilde{\mathbb{V}}_o$ = velocity of the steering (environmental) current at the center

K = characteristic constant prescribed by the pattern of the streamfunction of the vortex (usually > 0)

$\mathbb{k}$ = unit vector in the vertical

$\tilde{\eta}_o$ = absolute vorticity of the steering current at the center center of a cyclone.

The second term in Eq. 4 arises from the interaction between the vortex field and the steering current. If the steering current is uniform or of constant meridional shear, then $| \nabla \tilde{\eta}_o | = \beta$, where β = variation of the Coriolis parameter with latitude. In this case, the interaction term will produce a westward movement. This is the Rossby wave type effect discussed in section 3.2. If one traces back to the development of Eq. 4, one finds that this term can be interpreted as the advection of earth's vorticity by the vortex flow.

Because of this westward movement, a vortex under the influence of a uniform easterly (westerly) flow will move faster (slower) than the flow. In addition, since the vector $\mathbb{k} \times \nabla \tilde{\eta}_o$ always points towards the west, the velocity vector $\mathbb{C}$ in Eq. 4 will not necessarily be parallel to the steering flow vector $\tilde{\mathbb{V}}_o$. For a flow with a southerly (northerly) component, the vector $\mathbb{C}$ should be to the left (right) of the vector $\tilde{\mathbb{V}}_o$. This interpretation qualitatively agrees with the observational

results of Chapter 2. A more thorough discussion will be given in Chapter 4.

Kasahara applied this model in the prediction of the movement of two hurricanes using the rawinsonde data (at 500 mb) around them. The vortex streamfunction was defined as the azimuthal average of the total streamfunction. The environmental streamfunction is then the difference between the total streamfunction and the vortex streamfunction. The forecast tracks obtained in this way were always to the right of the observed track. Kasahara did not explore further the reason for such a discrepancy. However, he did point to the sensitivity of the track to the constant K in Eq. 4.

Hubert (1959) performed a number of 500 mb barotropic predictions with a steering flow model under operational conditions. He found the same rightward bias and interpreted this as a tendency for hurricanes to move to the left of the geostrophic wind at that level. This interpretation qualitatively agrees with the observational results in Chapter 2. The causes for such an apparent leftward deflection will be discussed later.

3.4.2 Two-level Baroclinic Model

In order to simulate the three-dimensional nature of actual cyclone motion, Kasahara (1960) extended the barotropic model described above to a two-level baroclinic model. The basic methodology was still the same: at each level, separate the vortex and the 'steering flow' streamfunctions and predict their individual evolution with time. The coupling between the two levels is through the thermodynamic equation with no diabatic heating and constant static stability.

The instantaneous velocity C_i at level i (i=1,2) for a symmetric vortex is then given by

$$C_i = \tilde{V}_{oi} + K_i (k \times \nabla \tilde{\eta}_{oi}) - \frac{Q}{\nabla^2 \psi_i} , \qquad (5)$$

where Q = coupling term between the two levels which is a function of the static stability, the wind shear between the two levels and the relative vorticity of the steering flow at both levels,

ψ_i = streamfunction of the vortex at level i,

and $\tilde{V}_{oi}$, K_i, $\tilde{\eta}_{oi}$ have the same meaning as before. Compared with Eq. 4, it can be seen that the first two terms on the RHS are the same in both cases. However, an additional term exists in Eq. 5 which represents the coupling between the vortex and the steering current at both levels. Kasahara found that for a vortex of the size of a tropical cyclone, this effect acts upon the movement of the upper and lower vortices in such a way as to let the common axis of their horizontal circulations remain vertical during the movement, in agreement with common observations. He also claimed that the effects of this and the vorticity gradient ($k \times \nabla \tilde{\eta}_{oi}$) terms are insignificant for time scales of less than 1 day. From the information given by Kasahara, it is not possible to see if such claims are justified, at least for the coupling term. However, it appears that from what was discussed in the last sub-section, the vorticity gradient term should be important in determining cyclone direction and speed. Nevertheless, Kasahara made all his forecasts by assuming that the instantaneous velocity of a tropical cyclone is the vector mean of the steering velocities at the two levels evaluated at the center of the cyclone.

The predicted movements of the hurricanes from Kasahara's two-level model again displayed a tendency to deflect to the right of the actual paths. After examining the observed tracks in relation to the steering flow, Kasahara came to the same conclusion as Hubert (1959) that "it is more appropriate to say that the actual path deflected leftward relative to the mean steering flow". This is exactly what was discussed earlier. Had Kasahara included the vorticity-gradient term, he might have had better results.

3.4.3 Using the Concept of Potential Vorticity

3.4.3.1 Frictionless Flow

To investigate the interaction between the vortex and the environment further, Kasahara and Platzman (1963) analyzed the potential-vorticity equation in a homogeneous and incompressible atmosphere with the following assumptions:

a) quasi-hydrostatic (vertical acceleration neglected),

b) quasi-horizontal (horizontal velocity components independent of z, vertical velocity component a linear function of z where z is the vertical coordinate),

c) quasi-geostrophic (Rossby number $R_o \ll 1$),

d) Froude number $\sim R_o$ (Froude number $=U/(gH)^{1/2}$, where U is the velocity scale and H the mean depth of the fluid) and

e) $L/R_E \sim R_o$ (where R_E = radius of earth and L the length scale).

The most severe problem here is the assumption of quasi-geostrophy. The authors did not address the issue in depth but claimed that this could be resolved partly by the use of the gradient (instead of geostrophic) wind and partly by breaking up the flow into that of the vortex and of the steering flow.

With these assumptions and partitioning the potential vorticity into those of the vortex and the environment, the authors solved a simplified form of the potential vorticity equation and obtained the instantaneous velocity $\mathbb{C}$ of an axisymmetric vortex as:

$$\mathbb{C} = \tilde{\mathbb{V}}_o + \sigma[\mathbb{k}x(\nabla\zeta)_o] + \tau\{\mathbb{k}x[\nabla(\Gamma + f)]_o\} + 0(b^{-4}) , \quad (6)$$

where $\tilde{\mathbb{V}}_o$, ζ and Γ are the velocity, relative vorticity and relative potential vorticity of the steering flow respectively, f the Coriolis parameter, σ and τ are parameters that depend on the potential vorticity of the vortex, and $b = L_s/L_v$, with L_s, L_v being the characteristic length scales of the steering flow and the vortex respectively. The subscript o indicates evaluation at the center of the vortex. The last term on the RHS means that it is of the order of b^{-4}.

The third term on the RHS in Eq. 6 is analogous to the second term on the RHS in Eq. 4 because for a non-divergent atmosphere, $\Gamma = \zeta$ so that $\Gamma + f = \zeta + f = \eta$. The second term on the RHS of Eq. 6 does not appear in Eq. 4. Tracing back to the development of Eq. 6, it was found that this term represents the advection of the vortex vorticity by the steering flow while the term $\tau\{\mathbb{k}x[\nabla(\Gamma + f)]_o\}$ came from the advection of absolute potential vorticity of the steering flow by the vortex.

To understand the difference between this model and the one with zero divergence, consider again the case of a uniform flow. Then, $(\nabla\zeta)_o$ is zero and the only interaction term is $\tau\{\mathbb{k}x[\nabla(\Gamma+f)]_o\}$. In a non-divergent atmosphere, $\nabla\Gamma = 0$ and the term $\mathbb{k}x(\nabla f)_o$ will produce a westward movement as discussed in section 3.4.1. For a divergent model, $\nabla\Gamma$ (negative of the gradient of the steering flow potential vorticity)

is a non-zero vector that points to the right of the flow direction (facing downstream). Therefore, $\mathbf{k} \times \nabla \Gamma$ will be in the direction of the steering flow. This contributes to an increase of the cyclone speed $|\mathbf{C}|$. This means that a cyclone embedded in an easterly flow will move even faster than the flow compared with the non-divergent case. For a cyclone in a westerly current, the term $\nabla \Gamma$ may overcompensate the westward drift produced by the β-effect so that the cyclone would still move faster than the flow. In the non-divergent model, this cannot happen since $\nabla \Gamma = 0$.

Kasahara and Platzman did not consider this aspect of their model. Instead, they analyzed the acceleration of the vortex for the case of a uniform flow. This is given by

$$\frac{d\mathbf{C}}{dt} = G \nabla (\Gamma + f) \qquad (7)$$

where G is a function of σ, τ and $\lambda (= f_o/(gH)^{1/2})$. The sign of G is negative for cyclonic vortices. Therefore, the acceleration is proportional to the gradient of the absolute potential vorticity of the steering flow. This is similar to the results obtained by Kuo (1950). Since G is negative and $\nabla \Gamma$ points to the right of the flow, the term $G \nabla \Gamma$ gives a leftward acceleration of the vortex. The part ∇f gives the β-effect deflection discussed in section 3.4.1. Such a result should cause the cyclone to move more to the left of its steering current and should therefore produce forecast tracks that are closer to the observed ones. Indeed, the authors demonstrated that in the case of Hurricane Betsy, the rightward bias obtained in a non-divergent model was almost completely eliminated.

Therefore, it appears that the assumption of non-divergence might not be appropriate in the prediction of cyclone tracks. However, how the divergence contributes physically to cyclone motion is still unclear at this point. More discussion of the possible physical processes involved will be given in the next chapter.

3.4.3.2 Effect of Friction

To investigate the effect of land on the movement of a cyclone, Rao (1969) solved a simplified potential-vorticity model by imposing a stronger frictional drag on the left hand side of the cyclone than the right hand side, thus creating an asymmetry in the wind field. The result is a leftward deflection of the vortex relative to the frictionless case. The differential friction alone should cause more frictional convergence on the left hand side than the right hand side and thus more ascending motion. However, the numerical integration (for a hypothetical vortex) shows that ascending motion is stronger on the right hand side.

Rao suggested that the reason for the stronger ascending motion on the right hand side is a result of a stronger wind on this side, despite a weaker frictional stress. He therefore concluded that the differential frictional drag across the cyclone is of secondary importance. The leftward deflection is primarily a result of the asymmetry in the wind field. Indeed, he obtained a leftward deflection in a real situation where asymmetry was present, with the total wind stronger on the right hand side. His explanation for this deflection was that "the stronger ascending motion to the right causes a faster reduction of vorticity (above the boundary layer) that eventually

results in a leftward deflection". The contribution of asymmetric wind fields to vortex motion will be discussed more thoroughly in Chapter 5.

3.5 Discussion

The theoretical studies discussed in this chapter point to two very important factors that influence the movement of a tropical cyclone. These are (1) the variation of the Coriolis parameter with latitude across the cyclone and (2) the interaction between the cyclone and environmental circulations. Table 20 gives a summary of the major findings from these theoretical and numerical studies of tropical cyclone movement.

The effect of the variation of Coriolis parameter across a cyclone appears to cause the cyclone to drift in a northwestward (in the Northern Hemisphere) direction. This is primarily a result of the advection of the earth's vorticity by the vortex tangential wind. Such an advection increases the relative vorticity to the west of the cyclone. An induced circulation is then set up which tends to advect the vortex vorticity poleward. As a result, the vortex will tend to move both poleward and westward. This β-effect is always present. A more detailed analysis of the importance of this effect and the coupling between the earth's vorticity and the divergence of the vortex and/or environmental flows will be presented in the next chapter.

The mechanism by which the environmental flow affects cyclone motion is apparently through the advection of vortex vorticity. How this interaction occurs is still not clear at this point.

Most motion studies to date have concentrated on very simple flow fields. What if the surrounding flow is not uniform or changes with

TABLE 20

Summary of the major findings of previous theoretical and numerical studies of tropical cyclone movement.

Author(s)	Model	Major Finding(s)
Rossby (1948)	Axisymmetric vortex	Poleward acceleration of vortex due to variation of Coriolis parameter across cyclone
Kuo (1950)	Barotropic	Presence of a force that drives cyclonic vortices towards regions with higher absolute vorticity
Yeh (1950)	Rankine vortex	Trochoidal motion of vortex
Kasahara (1957)	Non-divergent barotropic	(1) Westward movement of vortex under a uniform flow (2) Forecast tracks to the right of observed tracks
Hubert (1959)	Non-divergent barotropic	Vortex moves to the left of geostrophic wind
Adem and Lezama (1960)	Non-divergent barotropic	Northwestward movement of vortex due to variation of Coriolis parameter across the vortex
Kasahara (1960)	Two-level baroclinic	Forecast track to the right of observed tracks
Kasahara and Platzman (1963)	Divergent barotropic	Presence of force which drives the vortex in the direction of increasing absolute potential vorticity. This direction is to the left of the steering flow if the flow is uniform
Rao (1969)	Barotropic with frictional drag	Leftward deflection of vortex from environmental flow.
Kuo (1969)	Barotropic with frictional drag	Trochoidal motion of vortex
Rao (1970)	Barotropic with frictional drag	Change in magnitude of northwestward motion of vortex due to variation of Coriolis parameter across the vortex and frictional effects

TABLE 20 (cont'd)

Author(s)	Model	Major Finding(s)
Mathur (1974), Anthes and Hoke (1975), Madala and Piacsck (1975), Jones (1977a), and Kitade (1980)	Primitive equation 3-dimensional	Northward drift of cyclone
Kitade (1981)	Barotropic	Northward drift of cyclone
Holland (1982)	Divergent barotropic	(1)Northwestward movement of vortex due to variation of the Coriolis parameter across the vortex (2) Difference between vortex speed and environmental flow speed due to variation of the Coriolis parameter across the vortex

time? What is physically happening under these circumstances? To answer these questions, one can study the behavior of vortices under different environmental conditions using a theoretical or numerical model. Or, one can analyze observations around tropical cyclones which underwent different behavioral changes. Both these approaches are employed in this paper. In the next chapter, a simple theoretical study of cyclone motion will be presented.

CHAPTER 4 - ANALYTICAL STUDY OF TROPICAL CYCLONE MOTION USING THE VORTICITY EQUATION

4.1 Introduction

The results in Chapter 2 demonstrate the significance of the environmental flow in describing tropical cyclone motion. Previous theoretical and numerical studies described in Chapter 3 also point to the importance of this flow in determining the direction and speed of a cyclone. Moreover, models which permit interactions between the environmental flow and that of the vortex appear to predict cyclone tracks with higher accuracy (for example, Kasahara and Platzman, 1963). Models developed on a β-plane also suggest the relevance of the earth's rotation in cyclone motion. The basic question, however, still remains: what are the physical processes that are actually occurring during the movement of a cyclone?

This chapter will attempt to answer part of this question. A simplified form of the vorticity equation is solved analytically for different types of environmental flow. The contribution of each term in the vorticity equation to the local change in relative vorticity is identified. The results imply certain physical mechanisms responsible for cyclone motion. The rationale behind this is that a local change in relative vorticity will cause the cyclone to adjust its mass field and 'propagate' towards the area of maximum increase in relative vorticity. This rationale will be justified in Chapter 7 with observations. Although some of the assumptions may not be strictly valid, these

results do provide some physical explanations of the observed relationships (presented in Chapter 2) between the motion of tropical cyclones and its surrounding flow.

4.2 The Model

The vorticity equation in cylindrical, isobaric coordinates can be written as

$$\frac{\partial \zeta}{\partial t} = - \mathbb{V} \cdot \nabla(\zeta+f) - (\zeta+f) \nabla \cdot \mathbb{V} - \omega \frac{\partial \zeta}{\partial p} + \left(\frac{\partial u}{\partial p} \frac{\partial \omega}{r \partial \theta} - \frac{\partial v}{\partial p} \frac{\partial \omega}{\partial r} \right) + Z \quad (8)$$

where

ζ = relative vorticity

f = Coriolis parameter

$\mathbb{V}$ = horizontal wind vector

u = radial wind

v = tangential wind

ω = vertical p-velocity and

Z = frictional effects.

Outside about 100-200 km from the center of a cyclone, the vertical p-velocity is relatively small and the third and fourth terms on the right hand side of Eq. 8 can usually be neglected. Such an assumption may be justified by performing a simple scale analysis of the first four terms on the right hand side of Eq. 8. Using the composite data from Frank (1977) for typhoons, the magnitude of these terms in the mid-troposphere at ~ 2-4^{o} latitude radius from the cyclone are:

$$\mathbf{V}\cdot\nabla(\zeta+f) \sim 10 m s^{-1} \cdot \frac{10^{-5} s^{-1}}{2 \times 10^{5} m} \sim 5 \times 10^{-10} s^{-2}$$

$$(\zeta+f)\nabla\cdot\mathbf{V} \sim 5 \times 10^{-5} s^{-1} \cdot 10^{-5} s^{-1} \sim 5 \times 10^{-10} s^{-2}$$

$$\omega \frac{\partial \zeta}{\partial p} \sim 200 \times 10^{-5} mb\ s^{-1} \cdot \frac{5 \times 10^{-6} s^{-1}}{200\ mb} \sim 5 \times 10^{-11} s^{-2}$$

$$\frac{\partial v}{\partial p}\frac{\partial \omega}{\partial r} \sim \frac{2 m s^{-1}}{200\ mb} \cdot \frac{100 \times 10^{-5} mb\ s^{-1}}{2 \times 10^{5} m} \sim 5 \times 10^{-11} s^{-2} .$$

It can be seen clearly that the vertical advection term is negligible compared with the advection and stretching terms. The other component of the tilting term cannot be evaluated from Frank's (1977) data because the azimuthal variation of the vertical motion field was not presented. However, the term $(\partial v/\partial p)(\partial \omega/\partial r)$ is of secondary importance compared with the horizontal terms. In fact, as will be seen in Chapter 6, the tilting term has only a magnitude comparable to the vertical advection term. The data presented in Chapter 6 will also justify the assumption of neglecting the vertical advection and tilting terms.

Lee (1982) showed that frictionless effects in the mid-troposphere due to convection are relatively small compared with those in the lower and upper troposphere. Therefore, to a first approximation, the frictional effects Z in Eq. 8 can be neglected. This approximation will become more evident in Chapter 6 where comparisons are made between $\partial \zeta/\partial t$ and the sum of the first four terms on the right hand side of Eq. 8. With these two assumptions, Eq. 8 can then be written as

$$\frac{\partial \zeta}{\partial t} = \underbrace{-u\frac{\partial \zeta}{\partial r}}_{A} \underbrace{-v\frac{\partial \zeta}{r\partial \theta}}_{B} \underbrace{-\zeta \nabla\cdot\mathbf{V}}_{C} \underbrace{-u\frac{\partial f}{\partial r}}_{D} \underbrace{-v\frac{\partial f}{r\partial \theta}}_{E} \underbrace{-f \nabla\cdot\mathbf{V}}_{F} . \qquad (9)$$

This will be the basic equation used in the present study. Terms A and B represent the horizontal advection of relative vorticity by the radial and tangential wind respectively. Term C is the coupling between divergence and relative vorticity. Terms D and E represent the horizontal advection of the earth's vorticity by the radial and tangential wind respectively. Term F is the coupling between divergence and the earth's vorticity.

In order to solve the equation analytically, the u and v fields cannot be too complicated. Therefore, following Holland (1982), a Rankine-combined vortex with a radial wind having the same radial dependence as the tangential wind is assumed, that is,

$$\bar{u} = a v_o r^{-x} \qquad (10a)$$

and

$$\bar{v} = v_o r^{-x} , \qquad (10b)$$

where a and v_o are constants, r the distance from the center of the cyclone and x determines the structure of the vortex, such that

$$0 < x \leq 0.8.$$

The quantity a is actually the tangent of the inflow angle (ϕ), that is,

$$\tan\phi = \frac{\bar{u}}{\bar{v}} = a.$$

Note that Eq. 10a and 10b apply only outside the radius of maximum wind,

which is indirectly implied in the present case when the terms involving ω are dropped. Equations 10a and 10b also imply that the vortex is symmetric. This is approximately valid in the mid-troposphere within ~ 400 km from the cyclone center (see, for example, the data in Shea and Gray (1973) and Frank (1977)).

In order to study the movement of the vortex relative to the environmental flow, the coordinate system used is such that the Y-axis is along the direction of the basic environmental flow V. A cross flow U can be superimposed on the basic flow in a direction (X) perpendicular to the Y-direction. This X-Y coordinate system is shown in Fig. 16. In the present study, only in one case is U non-zero (section 4.6). Resolving the U and V flows at any point A into radial (u') and tangential (v') components,

$$u' = V\cos\theta - U\sin\theta \qquad (11a)$$

and

$$v' = -V\sin\theta - U\cos\theta \ . \qquad (11b)$$

Combining Eq. 10a and Eq. 11a, and Eq. 10b and Eq. 11b give the total wind components

$$u = av_o r^{-x} + V\cos\theta - U\sin\theta \qquad (12a)$$

and

$$v = v_o r^{-x} - V\sin\theta - U\cos\theta \ . \qquad (12b)$$

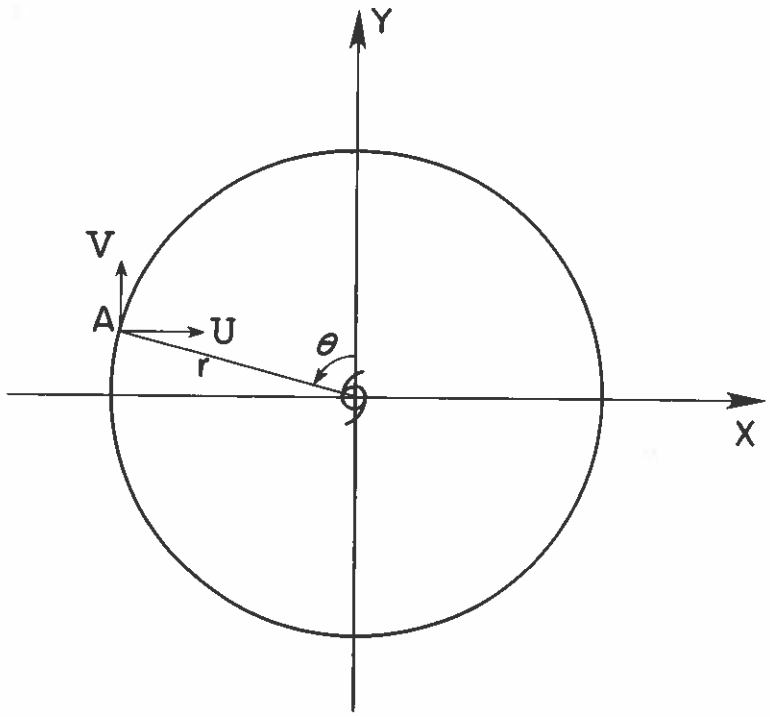

Fig. 16. Schematic diagram showing the superposition of a basic environmental flow V in the Y-direction. A cross flow U can be superimposed along the X-direction.

These will be the wind components used in this study. Note that both U and V can be functions of r and θ.

As mentioned in Chapter 3, the effect of the earth's rotation is very important in tropical cyclone motion. Therefore, a β-effect is included in the model by writing

$$f = f_o + \beta \delta$$

where f_o = Coriolis parameter at the latitude of the cyclone center and δ = meridional distance from the cyclone center. From Fig. 17,

$$\delta = r \cos (\alpha + \theta) .$$

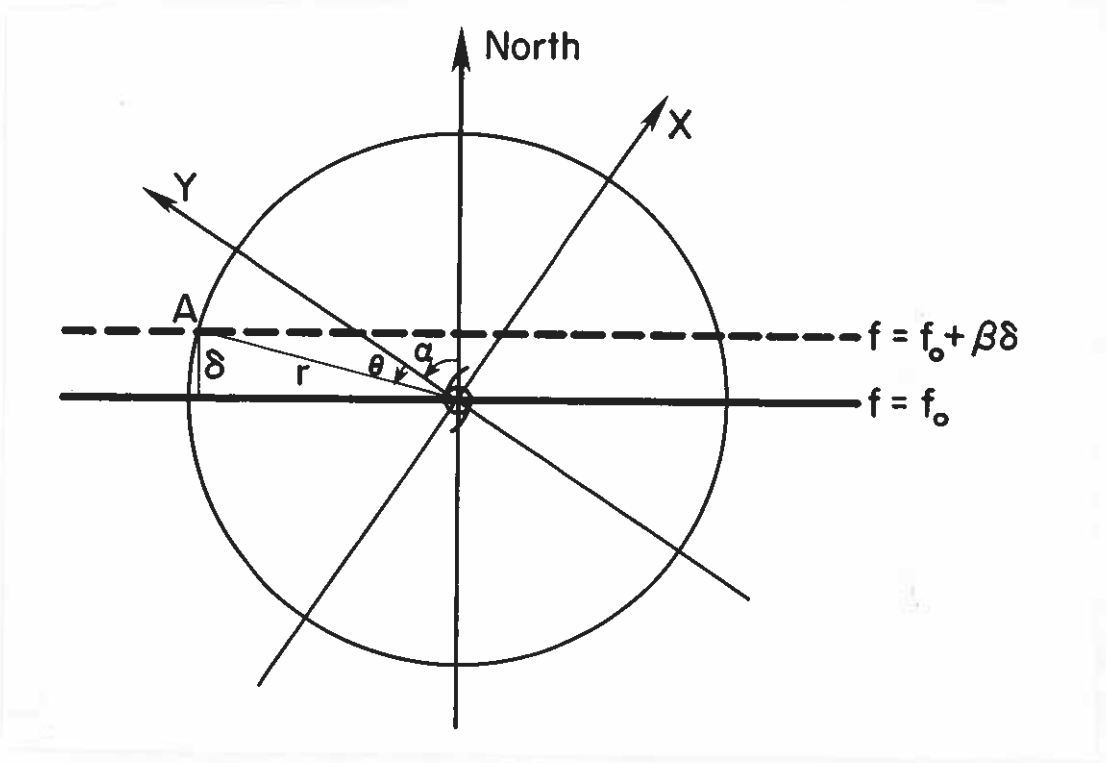

Fig. 17. Schematic showing how the β-effect is included in the model. The X-Y coordinate system is depicted in Fig. 16.

Therefore,

$$f = f_o + \beta\, r \cos(\alpha + \theta) \qquad (13)$$

where α = angle between the Y-axis in Fig. 17 and north, positive if the Y-axis is counterclockwise from north.

In order to solve for $\partial\zeta/\partial t$ in Eq. 9, the relative vorticity and divergence have to be calculated. Now,

$$\zeta = \frac{\partial rv}{r\partial r} - \frac{\partial u}{r\partial\theta} .$$

Substituting from Eq. 12, after some algebraic manipulations,

$$\zeta = (1-x)v_o r^{-(x+1)} - \frac{\partial V}{\partial r}\sin\theta - \frac{\partial U}{\partial r}\cos\theta - \frac{1}{r}\left[\frac{\partial V}{\partial\theta}\cos\theta - \frac{\partial U}{\partial\theta}\sin\theta\right]. \qquad (14)$$

Note that if U = V = constant, as would be the case when a uniform

environmental flow is superimposed onto the vortex, then

$$\zeta = (1-x)\, v_o r^{-(x+1)},$$

which is equal to the relative vorticity of the vortex itself.

The horizontal divergence, $\nabla\cdot\mathbb{V}$, in cylindrical coordinates is given by

$$\nabla\cdot\mathbb{V} = \frac{\partial ru}{r\partial r} + \frac{\partial v}{r\partial\theta}$$

Again, substituting from Eq. 12,

$$\nabla\cdot\mathbb{V} = (1-x)av_o r^{-(x+1)} + \frac{\partial V}{\partial r}\cos\theta - \frac{\partial U}{\partial r}\sin\theta - \frac{1}{r}\left[\frac{\partial V}{\partial\theta}\sin\theta + \frac{\partial U}{\partial\theta}\cos\theta\right]. \tag{15}$$

If only a uniform flow exists,

$$\nabla\cdot\mathbb{V} = (1-x)av_o r^{-(x+1)}$$

which is the same as that for the vortex itself.

The advection terms A, B and D, E in Eq. 9 can now be calculated. To obtain an analytic solution, it is sufficient to solve for the derivatives of ζ and f without having to multiply u or v to the derivatives algebraically. These derivatives can be solved to give:

Term A:

$$\frac{\partial\zeta}{\partial r} = -(1-x^2)v_o r^{-(x+2)} - \frac{\partial^2 V}{\partial r^2}\sin\theta - \frac{\partial^2 U}{\partial r^2}\cos\theta$$

$$- \frac{1}{r}\left[\frac{\partial^2 V}{\partial r\partial\theta}\cos\theta - \frac{\partial^2 U}{\partial r\partial\theta}\sin\theta\right]$$

$$+ \frac{1}{r^2}\left[\frac{\partial V}{\partial\theta}\cos\theta - \frac{\partial U}{\partial\theta}\sin\theta\right] \tag{16}$$

Term B:

$$\frac{\partial \zeta}{r\partial\theta} = \frac{1}{r}\left[-\frac{\partial^2 V}{\partial r\partial\theta}\sin\theta - \frac{\partial^2 U}{\partial r\partial\theta}\cos\theta - \frac{\partial V}{\partial r}\cos\theta + \frac{\partial U}{\partial r}\sin\theta\right.$$

$$\left. - \frac{1}{r}\left[\frac{\partial^2 V}{\partial\theta^2}\cos\theta - \frac{\partial^2 U}{\partial\theta^2}\sin\theta\right] + \frac{1}{r}\left[\frac{\partial V}{\partial\theta}\sin\theta + \frac{\partial U}{\partial\theta}\cos\theta\right]\right] \qquad (17)$$

Term D:

$$\frac{\partial f}{\partial r} = \frac{\partial}{\partial r}\left[f_o + \beta\, r\cos(\alpha + \theta)\right] = \beta\cos(\alpha + \theta) \qquad (18)$$

Term E:

$$\frac{\partial f}{r\partial\theta} = \frac{1}{r}\frac{\partial}{\partial\theta}\left[f_o + \beta\, r\cos(\alpha + \theta)\right] = -\beta\sin(\alpha + \theta) \qquad (19)$$

If U and V are known functions of r and θ, Eqs. 12a, 12b and 13 through Eq. 19 can be computed. Substituting them into Eq. 9 will give the relative vorticity tendency $\partial\zeta/\partial t$ at any r and θ.

The effect of the environment flow (U,V) on $\partial\zeta/\partial t$ (through modifying the various terms in Eq. 9) can then be studied by using different functional forms of U and V. The direction of cyclone movement θ_m is then determined by differentiating $\partial\zeta/\partial t$ with respect to θ and setting it to zero.

Similar to the formula given by Pettersen (1956) for the speed of movement of pressure centers, the vortex speed V_c can be estimated by assuming that the vortex moves into the area of maximum $\partial\zeta/\partial t$. In this case,

$$\left(\frac{\partial \zeta}{\partial t}\right)_{\theta=\theta_m} = - V_c \left(\frac{\partial \zeta}{\partial r}\right)_{\theta=\theta_m}$$

or

$$V_c = - \frac{(\partial \zeta/\partial t)_{\theta=\theta_m}}{(\partial \zeta/\partial r)_{\theta=\theta_m}} \quad . \tag{20}$$

The negative sign is to compensate for the fact that $\partial\zeta/\partial r$ is negative outside the radius of maximum wind. As will be seen later, the value of θ_m and V_c may be a function of r. Therefore, an additional assumption has to be made before the movement of the cyclone can be completely determined. This will be addressed in the next section. Note also that Eq. 20 also assumes a steady-state vortex.

In the rest of this chapter, five special cases which can provide some physical insights into the problem of cyclone motion will be analyzed. These five cases are listed in Table 21.

TABLE 21

The five special cases analyzed in the analytical study of the vorticity equation.

CASE	EFFECTS(S) TO BE STUDIED
I	Differential in Coriolis parameter across a non-divergent symmetric vortex (β-effect)
II	(Case I) + divergence/convergence of a symmetric vortex
III	(Case II) + uniform environmental flow
IV	(Case III) + horizontally-sheared cross wind
V	(Case II) + divergent environmental flow

4.3 CASE I. – Motion of a Non-divergent Vortex With No Environmental Flow

In this case, $U = V = a = \nabla \cdot \mathbb{V} = 0$. This means that

$$v = v_o r^{-x}$$

and

$$\zeta = (1-x) v_o r^{-(x+1)} .$$

Since no environmental flow exists, the angle α can be set to zero without loss of generality. Then,

$$\frac{\partial \zeta}{\partial t} = v_o r^{-x} \beta \sin\theta \qquad (21)$$

which shows that the change in relative vorticity is entirely a result of the advection of the earth's vorticity by the tangential wind. This vorticity tendency is maximum when $\theta = 90^o$, that is, to the west of the vortex. Therefore, the vortex would tend to move towards the west. This is the Rossby wave effect obtained by Kasahara (1957), Adem and Lezama (1960) and other researchers. See the review given in section 3.4.1.

To estimate the speed of the vortex, the term $\partial\zeta/\partial r$ has to be calculated. This is given by

$$\frac{\partial \zeta}{\partial r} = - (1-x^2) v_o r^{-(x+2)}$$

so that the cyclone speed (from Eq. 20) is

$$V_c = - \frac{\beta v_o r^{-x}}{- (1-x^2) v_o r^{-(x+2)}}$$

or

$$V_c = \frac{r^2\beta}{1-x^2}. \qquad (22)$$

Equation 22 suggests that the cyclone speed depends on r, that is, the vortex will tend to be elongated in the east-west direction. Such a distortion of the vortex was also pointed out by Kasahara (1957). But, as suggested by Holland (1982), when this happens, the tangential wind will advect the 'additional' vorticity around to maintain a quasi-symmetric vortex.

In real situations, the whole vortex is assumed to move with only one speed. It might therefore be appropriate to define a mean radius r_E such that by setting $r = r_E$, the cyclone speed will be that given by the equation for calculating V_c. This radius has been referred to as the 'effective radius' (see, for example, Adem and Lezama, 1960; Holland, 1982). It is usually ~ 300 km. In order to compare the results among different cases, a standard effective radius r_E of 300 km will be used in all future calculations in this paper.

4.4 CASE II - Motion of a Symmetric Divergent Vortex with No Environmental Flow

This is similar to Case I except that $a \neq 0$. Then, $u = a\, v_o r^{-x}$,

$$v = v_o r^{-x}, \quad \zeta = (1-x) v_o r^{-(x+1)}, \quad \nabla \cdot \mathbf{V} = (1-x) a v_o r^{-(x+1)}$$

and (with $\alpha = 0$)

$$\frac{\partial \zeta}{\partial t} = v_o \left[2x(1-x) a v_o r^{-2(x+1)} + r^{-x}\beta \sin\theta - f_o(1-x) a r^{-(x+1)} - a(2-x) r^{-x}\beta\cos\theta\right] . \qquad (23)$$

Since v_o and x are characteristics of the vortex, Eq. 23 shows that the local change in relative vorticity is completely determined by the amount of convergence (as given by the parameter a) and the earth's vorticity.

Differentiating Eq. 23 with respect to θ and setting $\partial(\partial\zeta/\partial t)/\partial\theta = 0$,

$$0 = v_o r^{-x} \beta \left[\cos\theta_m + a(2-x) \sin\theta_m\right]$$

or

$$\theta_m = \tan^{-1}\left[-\frac{1}{a(2-x)}\right] . \qquad (24)$$

If a=0, Eq. 24 reduces the $\theta_m = 90^o$, which is Case I. Therefore, the existence of convergence/divergence in the vortex shifts the location where $\partial\zeta/\partial t$ is a maximum. The amount of such a shift will depend on the sign of a. If $a > 0$ (corresponding to a divergent vortex), $\theta_m > 90^o$ and the location of maximum $\partial\zeta/\partial t$ will be shifted equatorward. Conversely, a convergent vortex ($a < 0$) will shift this location poleward. This can be explained physically by considering Fig. 18 for a convergent vortex in the Northern Hemisphere. At point A, both v and u are advecting the earth's vorticity southward. This means that, compared with Case I, the increase in ζ is larger for $0^o < \theta < 90^o$. Therefore, $\partial\zeta/\partial t$ reaches a maximum at $\theta < 90^o$. Notice also that the stronger the inflow, the farther poleward the maximum $\partial\zeta/\partial t$ will be. An example of this is shown in Fig. 19 for x = 1/2. For an inflow angle of 10^o (corresponding to a = -0.18), $\theta_m = 75^o$. As will be seen later, this effect (of the advection of the earth's vorticity by the vortex flow) is of significant importance in determining whether a cyclone will

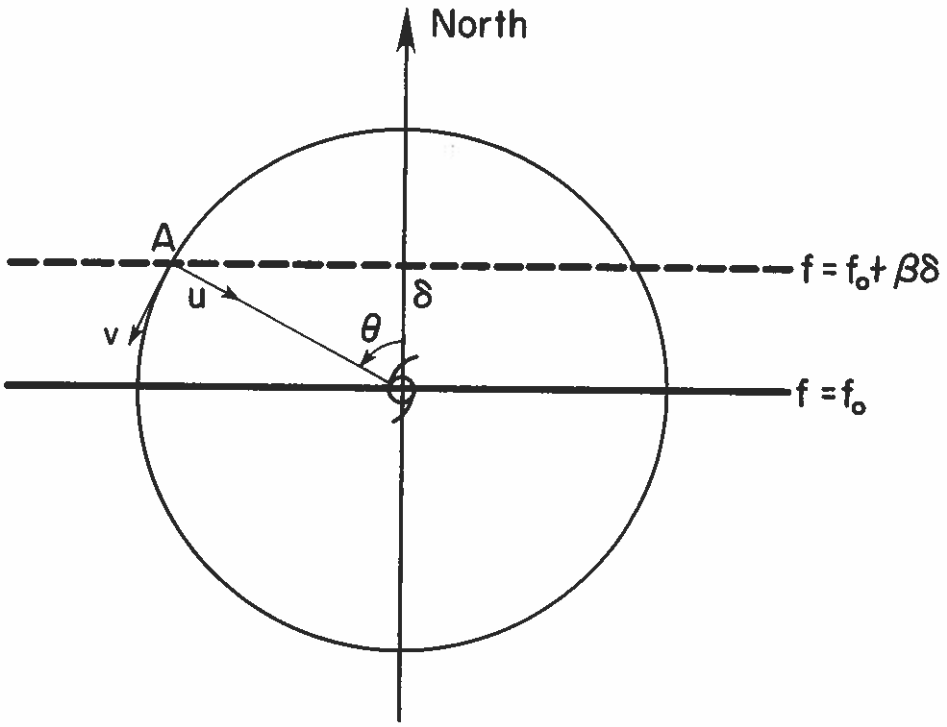

Fig. 18. Schematic of a symmetric vortex with a uniform radial inflow u (<0).

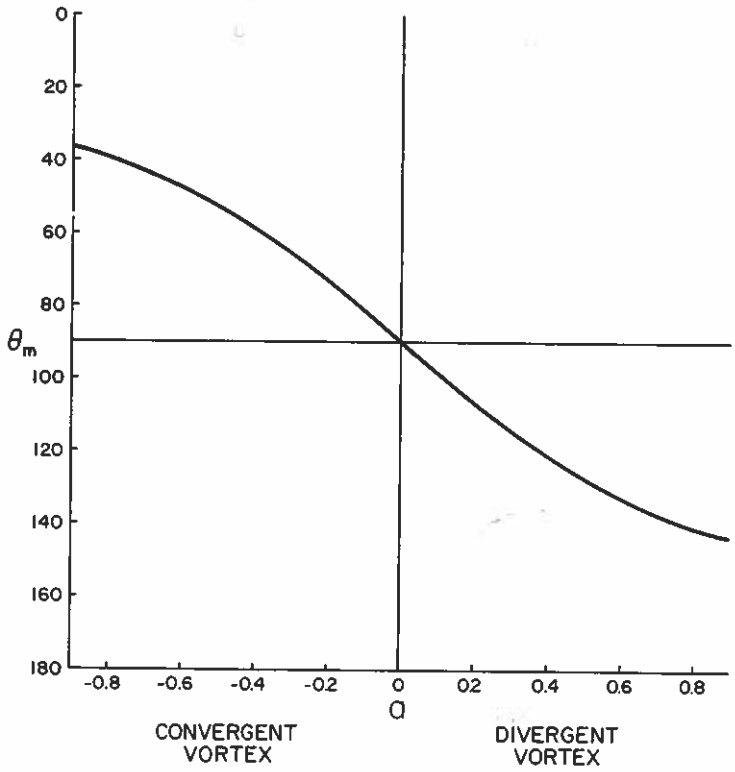

Fig. 19. Variation of θ_m (the azimuthal location of maximum $\partial\zeta/\partial t$) with the tangent of inflow angle a for x = 1/2.

move to the left or right of the environmental flow. Similar ideas have also been discussed by Holland (1982).

The local change in ζ, as given by Eq. 23 has two terms, $2x(1-x)av_o^2 r^{-2(x+1)}$ and $-f_o(1-x)av_o r^{-(x+1)}$, that are due to the convergence/divergence of absolute vorticity caused by the radial wind. Since they are independent of θ, they only spin up/down the vortex but do not contribute to the movement of the vortex. Therefore, to calculate the cyclone speed V_c, it is only necessary to consider the asymmetric terms in Eq. 23. That is,

$$V_c = - \frac{v_o r^{-x} \beta \, [\sin\theta_m - a(2-x)\cos\theta_m]}{- (1-x^2) v_o r^{-(x+2)}}$$

or

$$V_c = \frac{r^2 \beta [\sin\theta_m - a(2-x)\cos\theta_m]}{1-x^2} \qquad (25)$$

Again, if a = 0, Eq. 25 reduces to Eq. 22, that is, Case I. Therefore, the presence of convergence (divergence) increases (decreases) the cyclone speed.

4.5 Case III - Motion of a Symmetric Divergent Vortex Under the Influence of a Uniform Environmental Flow

4.5.1 Theoretical Analysis

In this case, V = constant and U = 0. Then,

$$u = av_o r^{-x} + V\cos\theta$$

$$v = v_o r^{-x} - V\sin\theta$$

$$\zeta = (1-x)\, v_o r^{-(x+1)}$$

and

$$\nabla \cdot \mathbb{V} = (1-x)\, av_o r^{-(x+1)}$$

so that

$$\frac{\partial \zeta}{\partial t} = 2x(1-x)av_o^2 r^{-2(x+1)} - f_o(1-x)av_o r^{-(x+1)} - a(2-x)v_o r^{-x}\beta\cos(\alpha+\theta)$$

$$+ v_o r^{-x}\beta\sin(\alpha+\theta) + (1-x^2)Vv_o r^{-(x+2)}\cos\theta - V\beta\cos\alpha \,. \qquad (26)$$

Compared with Case II (Eq. 23), Eq. 26 shows that the presence of a uniform environmental flow produces two additional terms: (1) the advection of the vortex vorticity by the radial component of the environmental flow $[(1-x^2)Vv_o r^{-(x+2)}\cos\theta]$ and (2) the advection of the earth's vorticity by the meridional component of the flow ($V\beta\cos\alpha$).

4.5.1.1 Direction of Vortex Movement

Of the two additional terms described above, only term (1) (that is, $(1-x^2)\, V\, v_o r^{-(x+2)}\cos\theta$) contributes to the azimuthal location of $\partial\zeta/\partial t$ because the other term, $V\beta\cos\alpha$, is independent of θ. Note also that because α is no longer zero, the other two terms that contribute to θ_m, $-a(2-x)v_o r^{-x}\beta\cos(\alpha+\theta)$ (which is the sum of the advection of earth's vorticity by the vortex radial wind and the coupling of the

divergence of the vortex and the spatially-varying part of earth's vorticity) and $v_o r^{-x}\beta \sin(\alpha + \theta)$ (which is the advection of earth's vorticity by the vortex tangential wind), are now functions of the direction of environmental flow α.

The azimuthal location of maximum $\partial\zeta/\partial t$ (that is, θ_m) can be easily calculated by differentiating Eq. 26 with respect to θ and setting $\partial(\partial\zeta/\partial t)/\partial\theta = 0$. This gives

$$\theta_m = \tan^{-1}\left[\frac{\beta[a(2-x)\sin\alpha + \cos\alpha]}{(1-x^2)Vr^{-2} - \beta[a(2-x)\cos\alpha - \sin\alpha]}\right]. \qquad (27)$$

If $V = 0$ and $\alpha = 0$, Eq. 27 reduces to Eq. 24, that is, Case II. An important point to notice is that if $\beta = 0$, $\theta_m = 0$ for all values of V. That is, the cyclone will move in the direction of the environmental flow. Therefore, <u>the difference between the direction of cyclone motion and that of the environmental flow is entirely a result of the variation in the Coriolis parameter</u>. This result was also obtained by Holland (1982). Equation 27 also shows the dependence of θ_m on the direction of the environmental flow α.

A major difference between this case and the previous two cases is that θ_m depends on r. Such a dependence comes from the advection of the vortex vorticity (which is a function of r) by the radial component of the environmental flow (which is a function of θ). This result therefore points to the importance of the environmental flow in determining cyclone motion.

One finding in observational steering flow studies (for example, George and Gray, 1976; Gray, 1977; Brand <u>et al</u>., 1981 and Chapter 2 of this paper) is that cyclones do not move along the environmental flow

but rather at an angle to it. Equation 27 shows this is the case since θ_m can only be zero if (1) $\beta = 0$ (the case of which has been discussed earlier) or (2)

$$\tan\alpha = -\frac{1}{a(2-x)} \tag{28}$$

which is the same as Case II. For $a = -0.18$ and $x = 0.5$, Eq. 28 gives $\alpha = 75^{\circ}$. Under these conditions, cyclones embedded in an environmental flow with $\alpha < 75^{\circ}$ (that is, with directions $> 285^{\circ}$) will move to the left of the environmental flow. On the other hand, if $\alpha > 75^{\circ}$ a cyclone will move to the right of its environmental flow. A physical explanation of this effect will be given in the next sub-section. Notice that this result is independent of V, r or β. It, however, depends on the shape of the vortex (as determined by the parameter x) and the amount of divergence/convergence (which is related to a).

The variation of θ_m with α can be studied further by keeping V and r constant. An example of this is shown in Fig. 20, with $V = 5$ m s^{-1}, $r = r_E = 300$ km, $a = -0.18$, $x = 0.5$ and $\beta = 2.15 \times 10^{-11} m^{-1} s^{-1}$ (corresponding to latitude 20°N). This figure shows that if the environmental flow has a direction more than 75° west of north or 125° east of north, the cyclone will move to the right of the flow. Otherwise, it will move to the left. A comparison of this result with observations will be made later in this chapter.

The variation of θ_m with the environmental speed V can also be studied by keeping α and r ($=r_E$) constant. Figure 21 shows such a variation for different directions of environmental flow. It appears that in the range $45^{\circ} \leq \alpha \leq 90^{\circ}$, θ_m is fairly constant with V as long as V is greater than or equal to about 5 m s^{-1}. However, when the flow

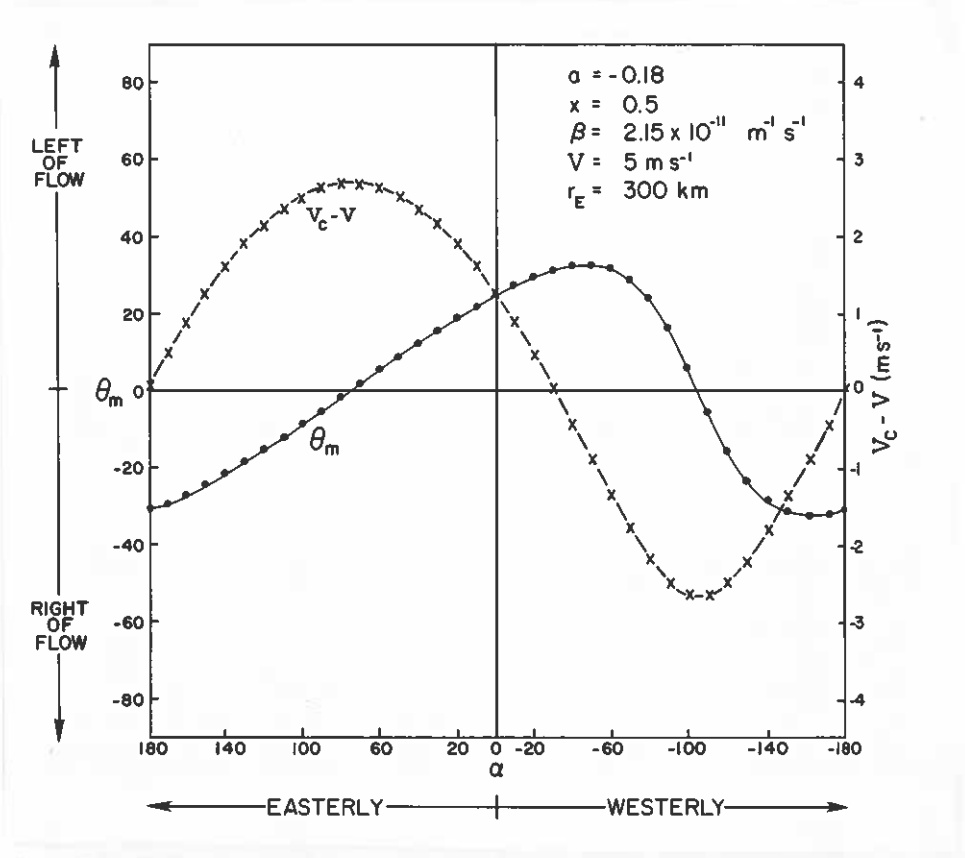

Fig. 20. Variation of θ_m (in degrees) and $V_c - V$ with direction of environmental flow α.

direction is very different from due west, the variation of θ_m with V is significant. This is because $d\theta_m/dV$ depends on both V and α, as can be seen easily from Eq. 27.

4.5.1.2 Speed of Vortex Movement

The speed of movement V_c can be calculated as before, that is,

$$V_c = -\frac{(\partial \zeta/\partial t)_{A,\theta=\theta_m}}{(\partial \zeta/\partial r)_{\theta=\theta_m}}$$

where the subscript A means only the asymmetric terms need to be considered. Then,

$$V_c = V\cos\theta_m + \frac{r^2\beta[\sin(\alpha+\theta_m) - a(2-x)\cos(\alpha+\theta_m)]}{1-x^2}. \qquad (29)$$

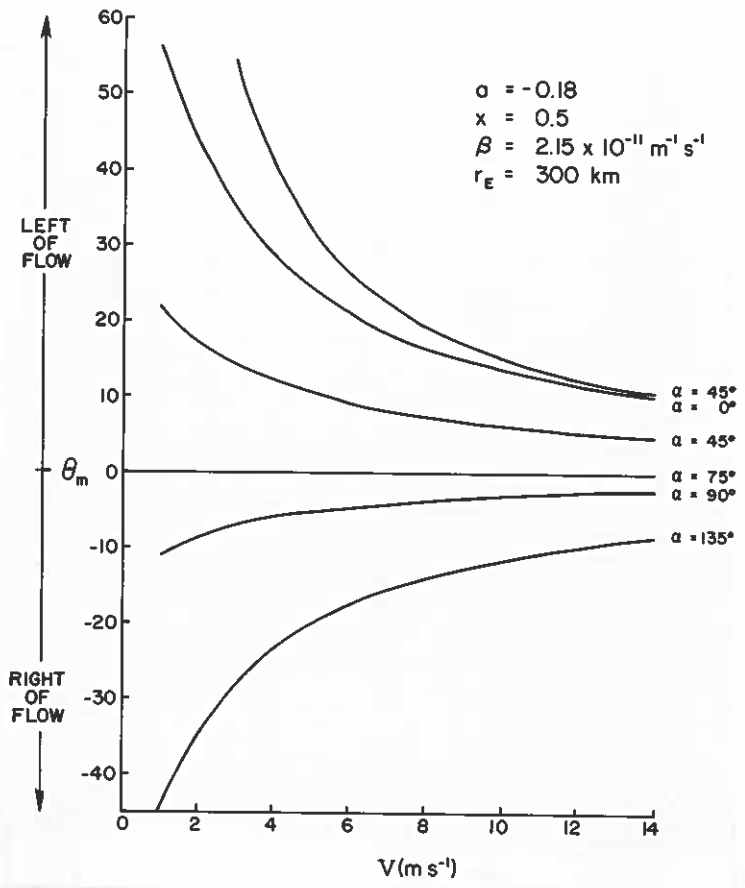

Fig. 21. Variation of θ_m (in degrees) with the speed of the environmental flow V as calculated from Eq. (27).

Compared with Case II, an additional term $V\cos\theta_m$ is present, which is the radial component of V in the direction of cyclone motion.

Another finding in previous steering flow studies and the one described in Chapter 2 is that in most cases, cyclones travel faster than its environmental flow. To investigate this, the quantity $V_c - V$ needs to be calculated. From Eq. 29,

$$V_c - V = V(\cos\theta_m - 1) + \frac{r^2\beta[\sin(\alpha+\theta_m) - a(2-x)\cos(\alpha+\theta_m)]}{1-x^2} . \qquad (30)$$

Keeping V constant, the variation of $V_c - V$ with α can be determined. This is shown in Fig. 20. It can be seen that as long as the

environmental flow is less than ~ 30^{o} east of north ($\alpha = -30^{o}$), the cyclone will move faster than the environmental wind. Otherwise, it will move slower. Since the majority of cyclones move in a direction with $-30^{o} \leq \alpha \leq 90^{o}$, they therefore move faster than their environmental flow. This is entirely a result of the β-effect because from Eq. 30, V_c can only be equal to V if $\beta = 0$ (in which case $\theta_m = 0$, from Eq. 28). Note that the "critical" angle at which a cyclone switches from moving faster to slower than the environmental flow depends on the effective radius r_E and the convergence a. In this case, the critical angle is -30^{o} for r_E = 300 km and a = -0.18.

The maximum value of V_c-V in Fig. 20 (~ 2.5 m s^{-1}) appears to be larger than the observed difference between cyclone and environmental wind speeds (~1-1.5 m s^{-1}). This apparent discrepancy is probably due to the fact that the composite data sets analyzed in Chapter 2 usually include cyclones with a wide range of directions. The difference V_c-V obtained from the composites is therefore a mean value and thus smaller than the predicted difference. Other factors such as different effective radii (r_E), convergence (a) and vortex shape (x) can also cause such a discrepancy. It is also possible that the present analysis does not capture all the physical processes involved.

4.5.1.3 Physical Interpretation

A simple physical picture can now be drawn to explain the motion of vortices under the influence of a uniform environmental flow on a β-plane. Four cases are depicted schematically in Fig. 22. Because of the β-effect and the convergence associated with the vortex, the vortex always has a component towards the west-northwest (at 75^{o} west of north in this case, as indicated in Fig. 22 by the dashed arrow labeled β).

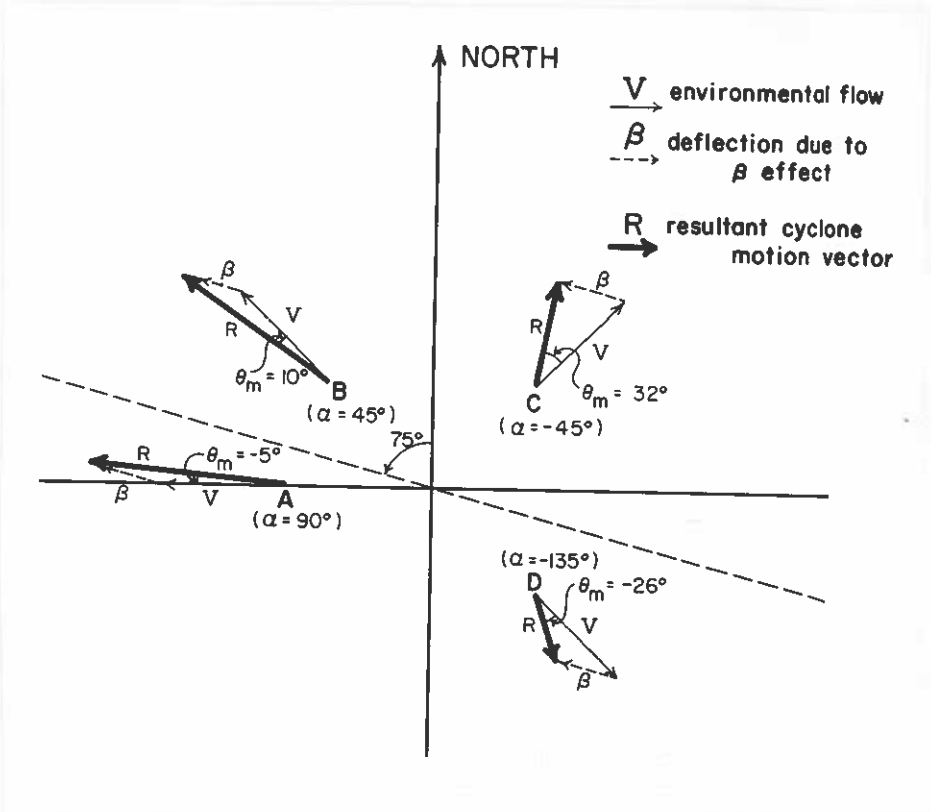

Fig. 22. **Schematic depiction of the resultant motion of a vortex due to a uniform environmental flow and the β-effect with r_E=300 km, a = −0.18, β = 2.15 x 10^{-11} m^{-1} s^{-1}, x = 0.5 and V = 5 m s^{-1}.**

In Case A, the environmental flow V is due west ($\alpha = 90^{o}$). The resultant motion vector R is therefore slightly to the right of V with a magnitude $V_c > V$. In Case B, V is due northwest ($\alpha = 45^{o}$) so that $\theta_m = 10^{o}$ (see Fig. 20) and R is to the left of V with $V_c > V$. In Case C, the flow is from the southwest ($\alpha = -45^{o}$) so that although the resultant motion vector R is still to the left of V, the vortex is moving with a speed $V_c < V$. Lastly, Case D shows that for a northwesterly flow ($\alpha = -135^{o}$), the cyclone travels slower and to the right of the flow. Therefore, the motion of a cyclone must be determined by combining the effects of both the environmental flow and the β-effect which, unfortunately, depends on the convergence/divergence associated with the vortex.

At first glance, Eq. 30 appears to indicate that $V_c - V$ varies linearly with V. But this is not the case because θ_m is also a function of V (see Eq. 28 and Fig. 21). Plots of $V_c - V$ against V for certain values of α are shown in Fig. 23. It appears that the variation of $V_c - V$ with V is not significant especially for large values of V and $\alpha > 0$. Note, however, that although $V_c - V$ decreases with V, V_c actually increases with V. Therefore, combining the results from Fig. 21 and Fig. 23, it can be concluded that increasing the environmental flow reduces the deviation of cyclone direction from the direction of the flow and increases the cyclone speed by an approximately constant magnitude.

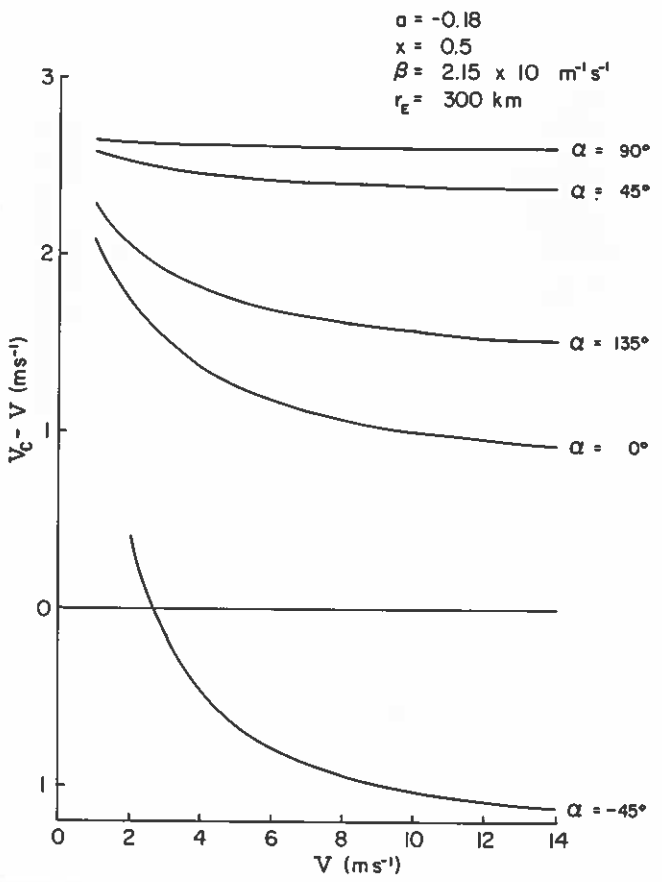

Fig. 23. Variation of $V_c - V$ with V for different directions of environmental flow (α).

4.5.2 Comparison with Observations

Although the environmental flow around the cyclones studied in Chapter 2 may not be uniform, it is useful to compare the results obtained from the present theory with those from observations.

Consider first the directional deviation between the direction of cyclone movement and that of the environmental wind. This was presented in Chapter 2, Tables 4, 5 and 6. From the analysis presented here (Fig. 20), one would expect that westward-moving cyclones have the smallest positive deviation or even a negative deviation while eastward-moving cyclones should have the largest positive deviation. This, however, does not show up in Table 4 (northwest Pacific cyclones). In fact, no systematic pattern is apparent, although all cyclones have a positive deviation. Several factors may contribute to the positive directional deviation of westward-moving cyclones: (1) the surrounding flow might not be uniform, (2) a cross flow might be present (in which cases the present analysis would not apply) and (3) the convergence in each stratification might be different. Again, it is also possible that the present analysis is not adequate.

On the other hand, for west Atlantic cyclones, westward cyclones do move to the right of the surrounding flow while northward cyclones move to the left of the flow, at least at both 600 and 500 mb (see Table 5), as predicted by this analysis. The most significant difference in the angular deviation between cyclones moving in different directions appear in Table 6 which shows these deviations for Australian/south Pacific cyclones. Eastward-moving cyclones move consistently to the right of the surrounding flow while the opposite is true for westward-moving cyclones. This difference is just what the present theory predicts for

the Southern Hemisphere because the combination of the Rossby Wave effect and the convergence associated with the vortex produces a southward deflection (see Case II, Eq. 24).

Another possible comparison between the present theory and the observational results in Chapter 2 is to analyze the variation of the directional deviation with height. Two factors need to be considered. They are the amount of convergence (represented by a) and the vertical wind shear. As shown in Fig. 21, the variation of θ_m with the magnitude of the wind is not very significant except at very low speeds. Therefore, the major consideration in the vertical variation of directional deviation should be the amount of convergence. Figure 24 shows how θ_m varies for different combinations of α and a. For most cyclones, $-45^o \leq \alpha \leq 100^o$. In this range, θ_m increases as the amount of convergence decreases. Now, in tropical cyclones, at about 300 km from the cyclone center, the amount of convergence decreases with height (see, for example, Frank, 1977). Therefore, one would expect the directional deviation to increase with height. Indeed, this is the case for northward and eastward cyclones in the northwest Pacific and northward cyclones in the west Atlantic. The reverse is true for westward cyclones in the south Pacific/Australian region, since they are in the Southern Hemisphere where a is positive for convergent vortices. For westward cyclones in the west Atlantic and, to a lesser extent in the northwest Pacific, θ_m slightly decreases with height. For $\alpha \geq 80^o$, the variation of θ_m with the amount of convergence is very small (see Fig. 24). In this case, other factors (vertical wind shear, change in effective radius, etc.) might become important and give rise to the

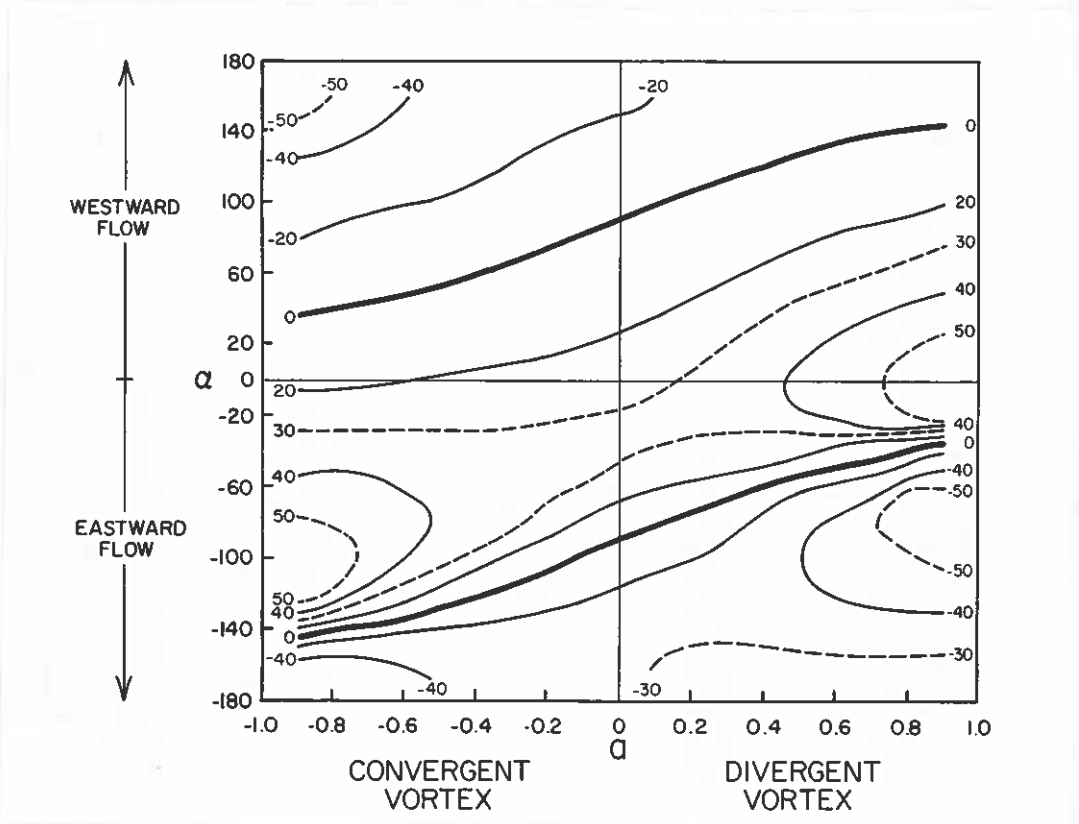

Fig. 24. Values of Θ_m (in degrees) as a function of both the direction of environmental flow α and the tangent of the inflow angle a. The flow is assumed to be uniform at 5 m s^{-1}.

observed results. The slight increase of Θ_m with height for eastward-moving cyclones might be explained in a similar manner.

The difference between cyclone speed and environmental flow speed predicted by the present theory can also be seen in the observations. Figure 20 shows that for $\alpha \geq -30^o$, $V_c > V$. Most of the environmental flows associated with tropical cyclones have directions in this range. Therefore, these cyclones should move faster than their surrounding flow. This is indeed found in Chapter 2 (Figs. 13–15, Tables 12–14). However, when the environmental flow has a strong westerly component, one would expect $V_c < V$. This relationship is observed for eastward-moving cyclones in the northwest Pacific (Fig. 13 and Table 12) for flows at 600 and 500 mb.

Thus, although the cyclones analyzed in Chapter 2 might be embedded in non-uniform environmental flows, the relatively simple theory here is capable of explaining most of the observations.

4.6 Case IV - Motion of a Symmetric Vortex Under the Influence of a Cross-wind

This is to study the situation in which a cyclone moves into a cross-wind. The study by Chan *et al.* (1980) shows that such a cross-wind (especially at 500 mb) correlates very well with a directional change of the cyclone. This analysis may give a better understanding of the possible physical processes involved.

In order to solve the problem analytically but without loss of generality, the cross-wind component will be assumed to vary linearly with Y, that is,

$$U = U_o Y = U_o r \cos\theta \tag{31}$$

where U_o = constant and has a dimension of $[T]^{-1}$. This current will produce a cyclonic (anticyclonic) shear if U_o is negative (positive). The basic environmental flow V along the Y-direction will still be assumed to be uniform, that is, V = constant. Then,

$$\begin{aligned} u &= av_o r^{-x} + V\cos\theta - (U_o r \sin 2\theta)/2 \\ v &= v_o r^{-x} - V\sin\theta - U_o r \cos^2\theta \\ \zeta &= (1-x)\, v_o r^{-(x+1)} - U_o \end{aligned} \tag{32}$$

and

$$\nabla \cdot \mathbb{V} = (1-x)\, av_o r^{-(x+1)}.$$

Notice that this shear flow (Eq. 31) adds its relative vorticity ($-U_o$) onto that of the basic flow. However, since the cross flow is non-divergent, the divergence remains the same as that in Case III. Also, because U_o is constant, $\partial\zeta/\partial r$ and $(\partial\zeta/\partial\theta)/r$ are also the same as those in Case III. Therefore,

$$\frac{\partial\zeta}{\partial t} = \left(\frac{\partial\zeta}{\partial t}\right)_{III} \underbrace{- 1/2\ v_o U_o r^{-(x+1)}(1-x^2)\sin 2\theta}_{(1)} + \underbrace{U_o(1-x)av_o r^{-(x+1)}}_{(2)}$$

$$\underbrace{- U_o r\beta\cos\theta\sin\alpha}_{(3)} \qquad (33)$$

where $(\partial\zeta/\partial t)_{III}$ is the local change of relative vorticity in Case III (Eq. 26).

Equation 33 shows that compared with Case III, the presence of a cross-wind leads to three additional terms in the vorticity equation. These are

1) the advection of the vortex vorticity by the radial component of the cross flow,
2) the coupling of the divergence of the vortex and the vorticity associated with this flow, and
3) the advection of earth's vorticity by the meridional component of this flow.

The effect of these three terms can be seen in the following two examples. In both cases, $0 < \alpha < 90^o$ and the vortex is convergent ($a < 0$).

(a) $U_o > 0$. This implies an anticyclonic shear in the cross-wind, as shown schematically in Fig. 25a. Term (2) is always negative. Term (1) is positive (negative) if the radial component of the cross wind is outward (inward). Term (3) is negative in front of the cyclone and positive behind it. Figure 25a shows that in front of the cyclone, all the terms are negative in region B while region A has a positive contribution from term (1). Therefore, the cyclone would tend to turn to the right of the present track (~ Y-direction). In other words, the right-turning motion of the cyclone is due to the advection of the vortex vorticity by the radial component of the cross-flow.

(b) $U_o < 0$. This means the shear in the cross-wind is cyclonic, as depicted schematically in Fig. 25b. Term (2) in this case is always positive. Term (3) is positive in front of the cyclone and negative behind it. The sign of term (1) is determined in the same way as described previously. In front of the cyclone, region B clearly has the largest increase in ζ and the cyclone would therefore tend to turn to the left of the present track. Again, it is the advection of the vortex vorticity by the radial component of the cross-flow that is responsible for this directional change.

Notice that in both cases, even if the vortex is divergent, the same qualitative conclusion would be drawn since term (2) is independent of θ. These two cases suggest that the environmental flow makes a cyclone change its direction not by 'steering' the cyclone but by creating a maximum increase in the relative vorticity along its future track, primarily through the advection of the vortex vorticity. In Chapter 6, the vorticity budget of cyclones undergoing turning motion is examined. It will be seen that this is indeed the case.

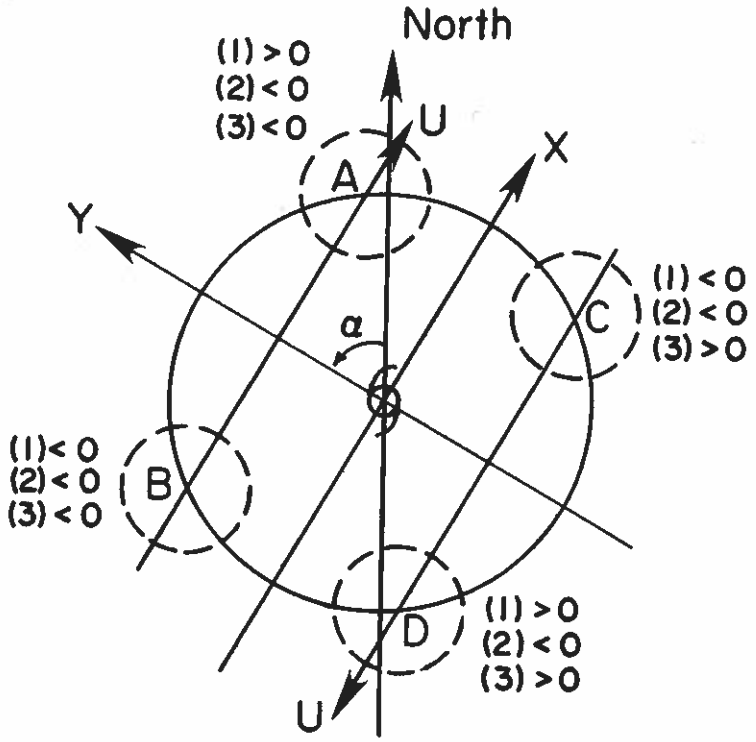

Fig. 25a. Schematic depiction of the U-component of the environmental flow in Case IV with $U_o > 0$ (see Eq. 31) and the sign of the terms in Eq. 33.

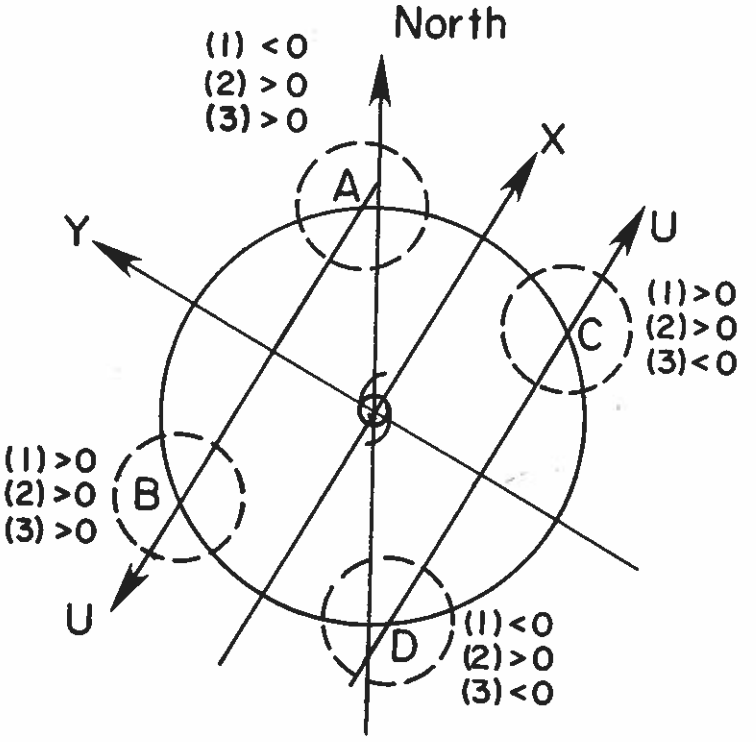

Fig. 25b. Same as Fig. 25a except with $U_o < 0$.

Differentiating Eq. 23 with respect to θ and setting $\partial(\partial\zeta/\partial t)/\partial\theta = 0$ leads to

$$[(1-x^2)Vv_o r^{-(x+2)} - U_o r\beta\sin\alpha]\sin\theta_m$$

$$= [a(2-x)\sin(\alpha+\theta_m) + \cos(\alpha+\theta_m)]\beta v_o r^{-x}$$

$$- U_o v_o r^{-(x+1)} (1-x^2)[\cos^2\theta_m - \sin^2\theta_m] \quad . \tag{34}$$

Instead of solving Eq. 34 (which is a fourth order equation in $\sin\theta_m$) to determine θ_m, a qualitative 'vector analysis' like Fig. 22 will be performed, as depicted in Fig. 26. In this particular case with $\alpha = 45^o$, a cyclone would normally deflect to the left of the flow V, as was shown in Fig. 22. Now, because of the cross-wind component $U(=U_o Y)$, the deflection will change according to the sign of U_o. In case (a), $U_o > 0$ so that the resultant R is to the right of V. In case (b) $U_o < 0$ and R is to the left of V_o, in consistency with Fig. 25. Notice that in case (a), the rightward motion has to overcome the β effect (which tends to deflect the cyclone to the left) while in case (b), the β-effect 'cooperates' with the leftward motion. As a result, the magnitude of θ_m in case (a) is smaller than that in case (b), for the same magnitude of U. Therefore, in order to create a significant rightward motion, a very strong cross-wind will have to be present. This is often the case when a northwestward-moving cyclone encounters a strong baroclinic trough and subsequently turns northward or northeastward.

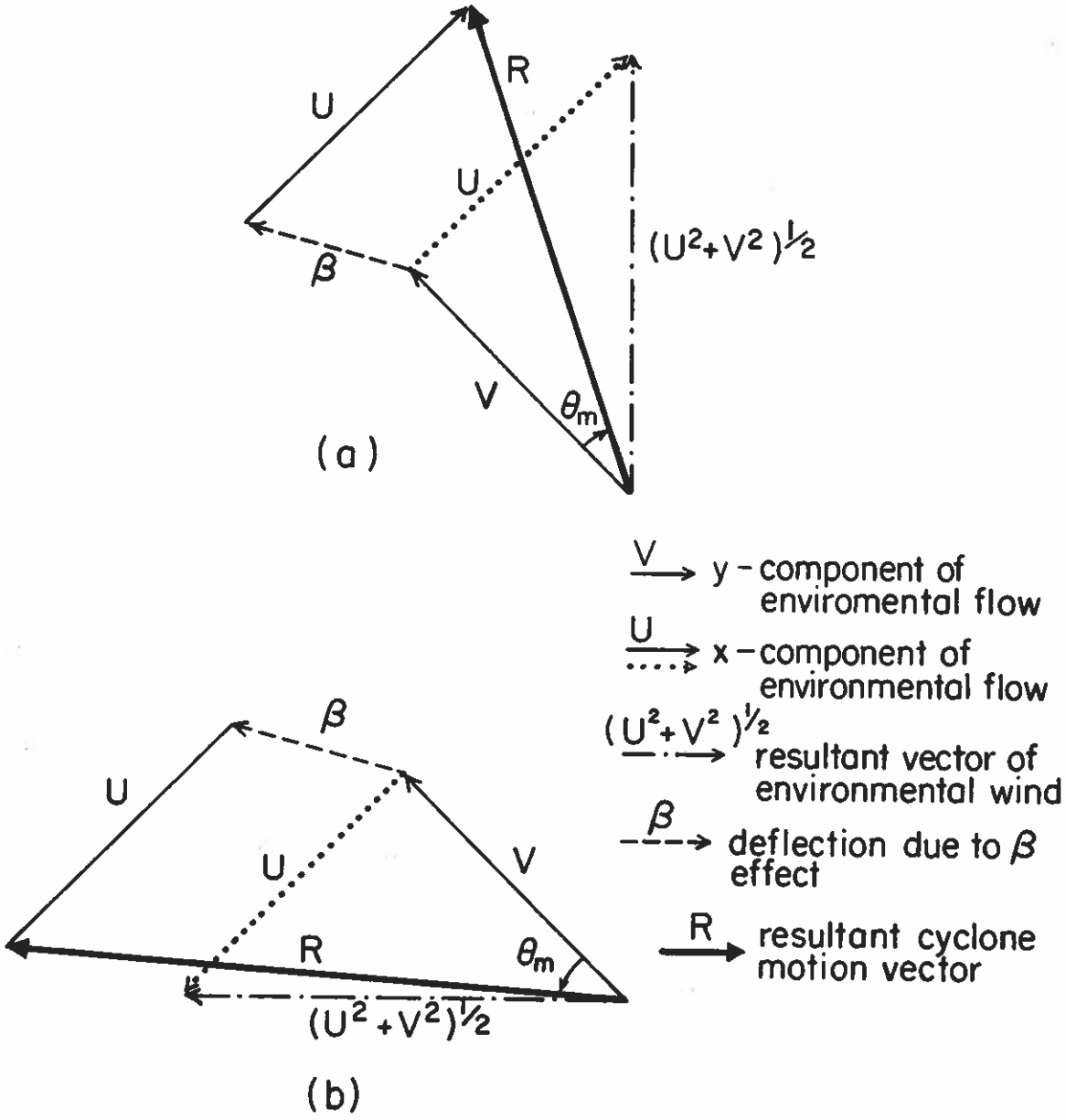

Fig. 26. Schematic depiction of the resultant motion of a vortex due to a uniform environmental flow (V), a cross-wind $U = U_0 Y$ and the β-effect for (a) $U_0 > 0$ and (b) $U_0 < 0$. Other parameters are the same as in Fig. 22.

It also appears from Fig. 26 that the magnitude of the resultant cyclone motion vector R is larger in case (b) than in case (a). This can be seen by calculating V_c from Eq. 33, with $\partial\zeta/\partial r$ being the same as the previous two cases. This is given by

$$V_c = V_{cIII} \underbrace{- (1/2)\, U_o r \sin 2\theta_m}_{(4)} \underbrace{- \frac{U_o r^{(x+3)} \beta \sin\alpha}{(1-x^2)v_o} \cos\theta_m}_{(5)} \qquad (35)$$

where V_{cIII} is the cyclone speed in Case III. For $U_o > 0$, $\theta_m < 0$ so that term (4) is positive and term (5) is negative. For $U_o < 0$, both terms are positive. Therefore, V_c in case (a) ($U_o > 0$) is less than that in case (b) ($U_o < 0$).

4.7 Case V – Motion of a Symmetric Vortex Under the Influence of an Environmental Flow With Speed Shear

This would be the case in which a cyclone moves into a new environment in which the flow has a speed different from that of the present environment. To make the algebra simple, it will be assumed that no cross-wind exists (i.e., U = 0) and V is assumed to vary linearly with Y, that is,

$$V = V_o + V_1 Y = V_o + V_1 r\cos\theta \qquad (36)$$

where V_o and V_1 are constants. An example of this is shown in Fig. 27. Then,

$$\begin{aligned} u &= a v_o r^{-x} + (V_o + V_1 r\cos\theta)\cos\theta \\ v &= v_o r^{-x} - (V_o + V_1 r\cos\theta)\sin\theta \\ \zeta &= (1-x) v_o r^{-(x+1)} \end{aligned} \qquad (37)$$

and $\nabla \cdot \mathbf{V} = (1-x) a v_o r^{-(x+1)} + V_1$.

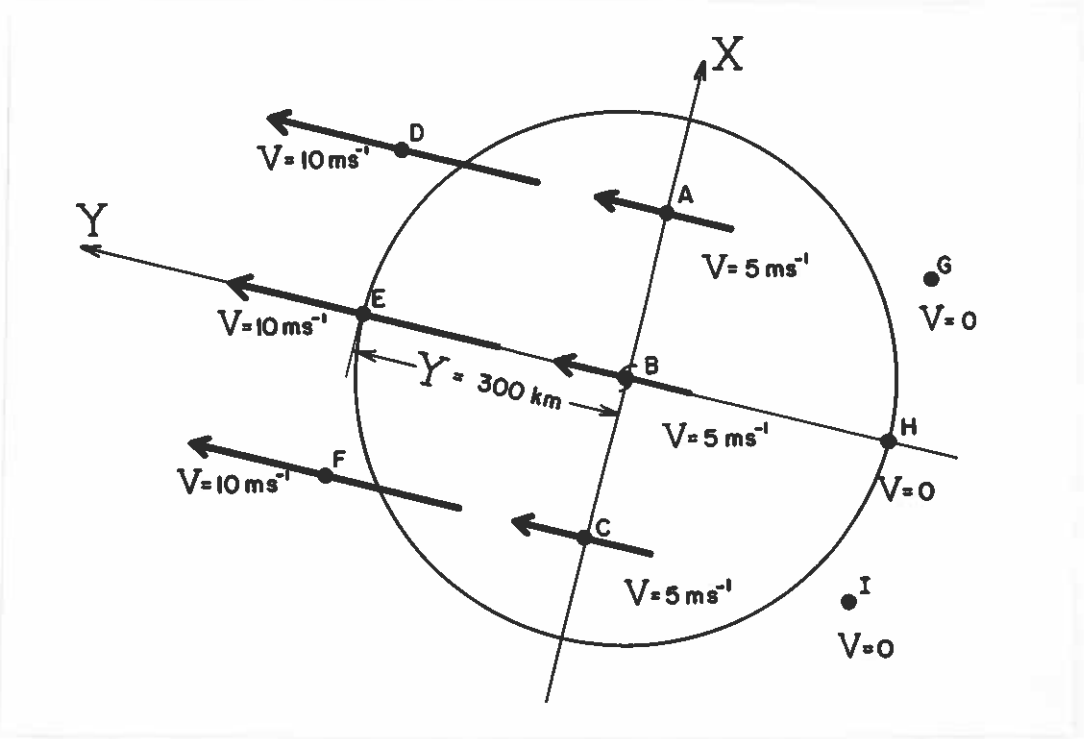

Fig. 27. Schematic depiction of a divergent environmental flow ($V = V_o + V_1 Y$) analyzed in Case V with $V_o = 5$ m s^{-1}, $V_1 = (5/3) \times 10^{-5}$ m^{-1}. This gives a wind of 10 m s^{-1} at Y = + 300 km (points D, E and F), 5 m s^{-1} at Y = 0 (points A, B and C) and 0 m s^{-1} at Y = − 300 km (points G, H and I).

Notice that the flow described by Eq. 36 is a pure divergent flow so that the relative vorticity remains unchanged while an additional so that the relative vorticity remains unchanged while an additional divergence is present, as can be seen in Eq. 37. This also means that $\partial\zeta/\partial r$ and $(\partial\zeta/\partial\theta)/r$ are the same as in Case III. Therefore,

$$\frac{\partial \zeta}{\partial t} = \left(\frac{\partial \zeta}{\partial t}\right)_{III} - (1-x)V_1 v_o r^{-(x+1)} - V_1 f_o + (1-x^2)V_1 v_o r^{-(x+1)}\cos^2\theta$$

(1)

$$- V_1\beta r\cos(\alpha+\theta) - V_1 r\,\beta\cos\alpha\cos\theta, \tag{38}$$

(2) (3)

where $(\partial\zeta/\partial t)_{III}$ is the local change of ζ in Case III with $V=V_o$ (given by Eq. 26). Because of the presence of the speed shear, three additional asymmetric terms appear:

1) the advection of the vortex vorticity by the radial component of V_1,
2) the coupling between the earth's vorticity and the additional divergence, and
3) the advection of earth's vorticity by the meridional component of V_1.

The effects of these terms on the movement of the cyclone will be seen when θ_m and V_c are calculated.

To find θ_m, differentiate the asymmetric part of Eq. 38 with respect to θ and set $\partial(\partial\zeta/\partial t)/\partial\theta = 0$. Then,

$$\tan\theta_m = \frac{\beta[a(2-x)\sin\alpha+\cos\alpha + V_1 v_o^{-1} r^{(x+1)}\sin\alpha]-2(1-x^2)V_1 r^{-1}\sin\theta_m}{(1-x^2)V_o r^{-2}-\beta[a(2-x)\cos\alpha-\sin\alpha+2V_1 v_o^{-1} r^{(x+1)}\cos\alpha]} \tag{39}$$

The most important thing to note in Eq. 39 are the two β-terms, one in the numerator and one in the denominator. Comparing these terms with

those in Case III (Eq. 27), an extra contribution in each term appears. This contribution came from the coupling between the divergence of the environmental flow and the earth's vorticity (term (2) in Eq. 39). It was concluded in section 4.4 (Case II) that a convergence/divergence would change θ_m. Now since extra convergence/divergence associated with the environmental flow is present, this would provide an extra 'forcing' in changing θ_m in a way described in section 4.4. In section 4.5, it was concluded that $\theta_m = 0$ when $\tan \alpha = [a(2-x)]^{-1}$. Now, because of this extra convergence/divergence, θ_m will be zero when

$$\tan \alpha = - \frac{1}{a(2-x) + V_1 v_o^{-1} r(x+1)} \qquad (40)$$

which is different from the case when the environmental flow is non-divergent (Case III, Eq. 27). If $V_1 > 0$ (divergent flow) and $a < 0$, θ_m will be zero when the flow is at an angle west of north ($\alpha > 0$) greater than that for the non-divergent case. Therefore, for the same value of a and x, a divergent environmental flow can cause the cyclone to move to the left of the flow in some cases when the latter would move to the right of the flow had the flow been non-divergent. For a convergent flow, the opposite would occur. Note also that because of this convergence/divergence associated with the environmental flow, θ_m would still be non-zero most of the time even for a non-divergent vortex ($a = 0$).

Equation 39 is a transcendental equation and can only be solved by an iterative process. The results for the case with $V_o = 5$ m s^{-1} and $V_1 = (5/3) \times 10^{-5} m^{-1}$ are shown in Fig. 28. This corresponds to a total

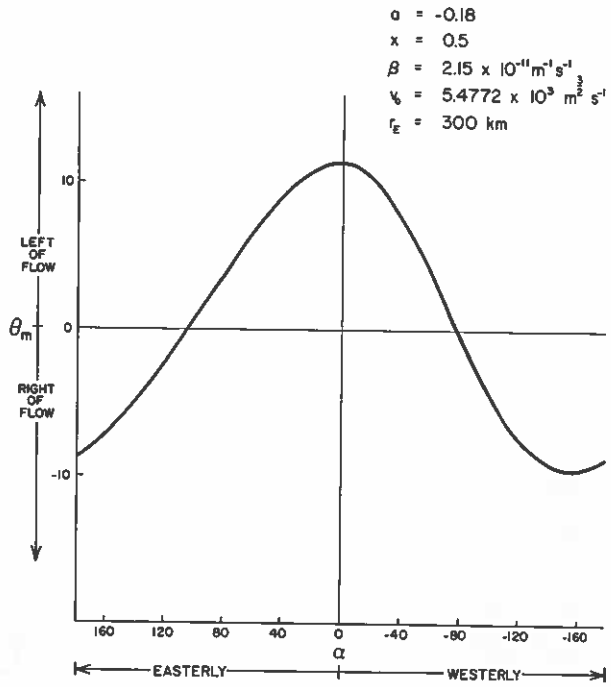

Fig. 28. Variation of θ_m (in degrees) with α for Case V.

wind of 10 m s^{-1} at 300 km in front of the cyclone, as shown schematically in Fig. 28. In Eq. 39, v_o also needs to be defined. Assuming a 10 m s^{-1} tangential wind at 300 km gives a value of v_o = 5.4772 x $10^3 m^{3/2} s^{-1}$. The first thing to note from Fig. 28 is that θ_m has a maximum at α = 0. This is physically reasonable because when α = 0, coupling between the divergence of the environmental wind and β is a maximum. As discussed above, the values of α at which θ_m = 0 will not be the same. This is indeed the case if Fig. 28 is compared with Fig. 22. Such a comparison is possible because in Case III, the values of α at which θ_m = 0 is independent of V.

A conceptual view of the effect of this extra divergence is shown in Fig. 29. Since divergence has the effect of deflecting the cyclone southward (in the Northern Hemisphere), the combined effect of the convergence of the vortex and the divergence in the environmental flow

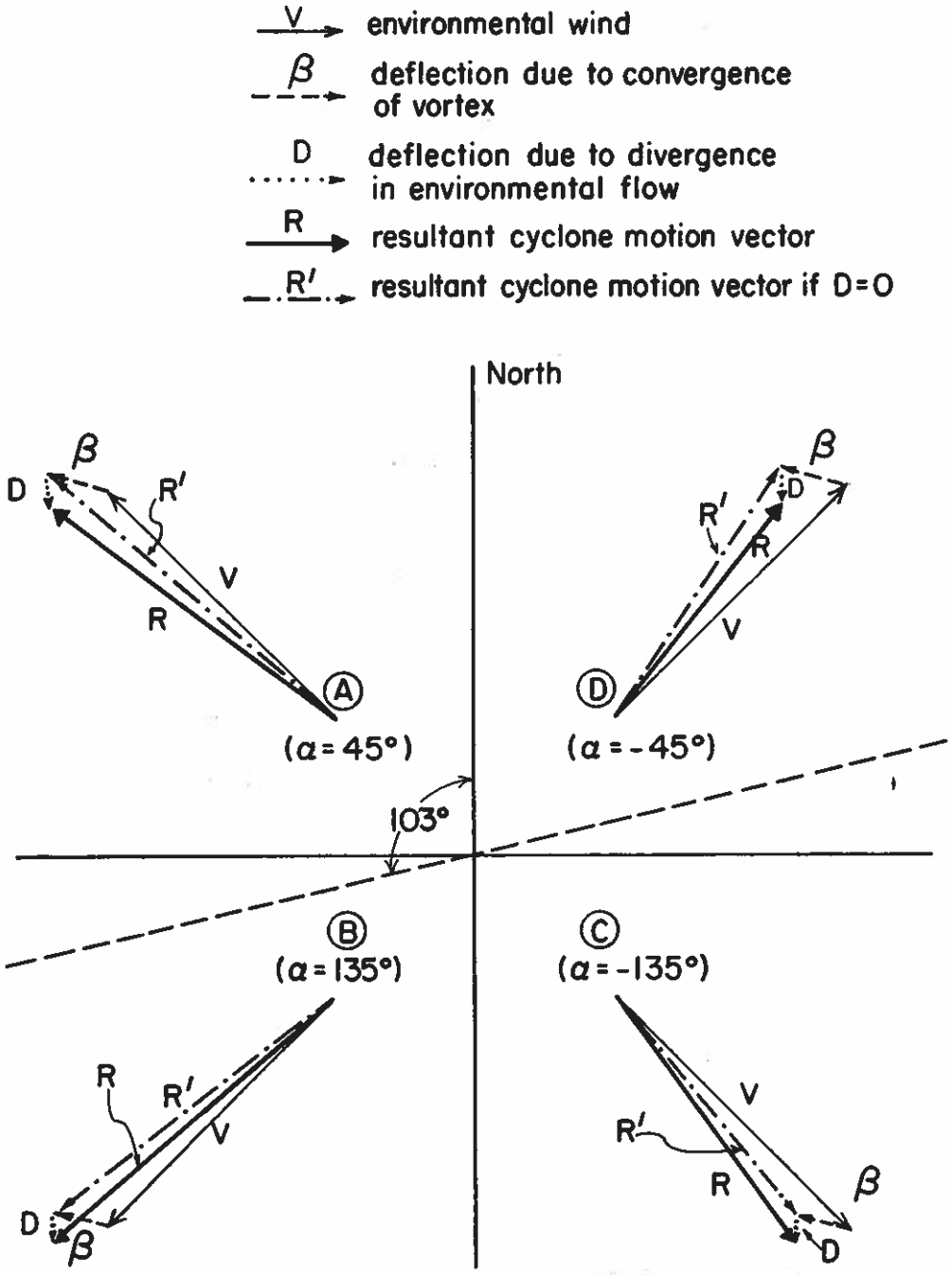

Fig. 29. Schematic depiction of the resultant motion of a convergent vortex with the environmental wind $V = V_0 + V_1 Y$, $V_1 > 0$. Values of the significant parameters are r_E = 300 km, α = -0.18, $\beta = 2.15 \times 10^{-11}$ m^{-1} s^{-1}, $x = 0.5$, $V_0 = 5$ m s^{-1}, $V_1 = 1.667 \times 10^{-5}$ s^{-1}, $v_0 = 5.4772 \times 10^3$ m$^{3/2}$ s^{-1}.

in Case A will cause the cyclone to deflect to the left of V, but by a larger amount than the case of non-divergent flow (as indicated by the arrow R'). In case B, the effect of the divergence is to cause the cyclone to deflect less to the right of the flow than the non-divergent case. Case C shows that under the influence of a divergent northwesterly flow, a cyclone would deflect more to the right of the flow than the case with $V_1 = 0$. Finally, a southwesterly flow (Case D) would cause the cyclone to deflect less to the left of the flow than the non-divergent case. These cases illustrate the importance of a non-uniform environmental flow on the direction of movement of a cyclone.

This importance can be further demonstrated by studying the relationship between θ_m and the divergence/convergence in the environmental flow. This is shown in Fig. 30 for five directions of flow. These curves show that the variation of θ_m with V_1 is much greater for convergent flow ($V_1 < 0$) than for divergent flow ($V_1 > 0$). This is because a convergent flow reinforces the convergence present in the vortex to produce a much stronger β-effect. The cyclone would therefore be deflected more to the left or more to the right depending on what the value of α is. On the other hand, a divergent flow works against the poleward deflection due to the convergence present in the vortex. However, if such a divergence is large enough, it might overcome the latter effect.

To see if a cyclone will speed up (and if so, by how much) under the influence of a divergent flow, the cyclone speed V_c will have to be calculated. Since $\partial\zeta/\partial r$ is the same as Case III, the formula for V_c can easily be derived to give

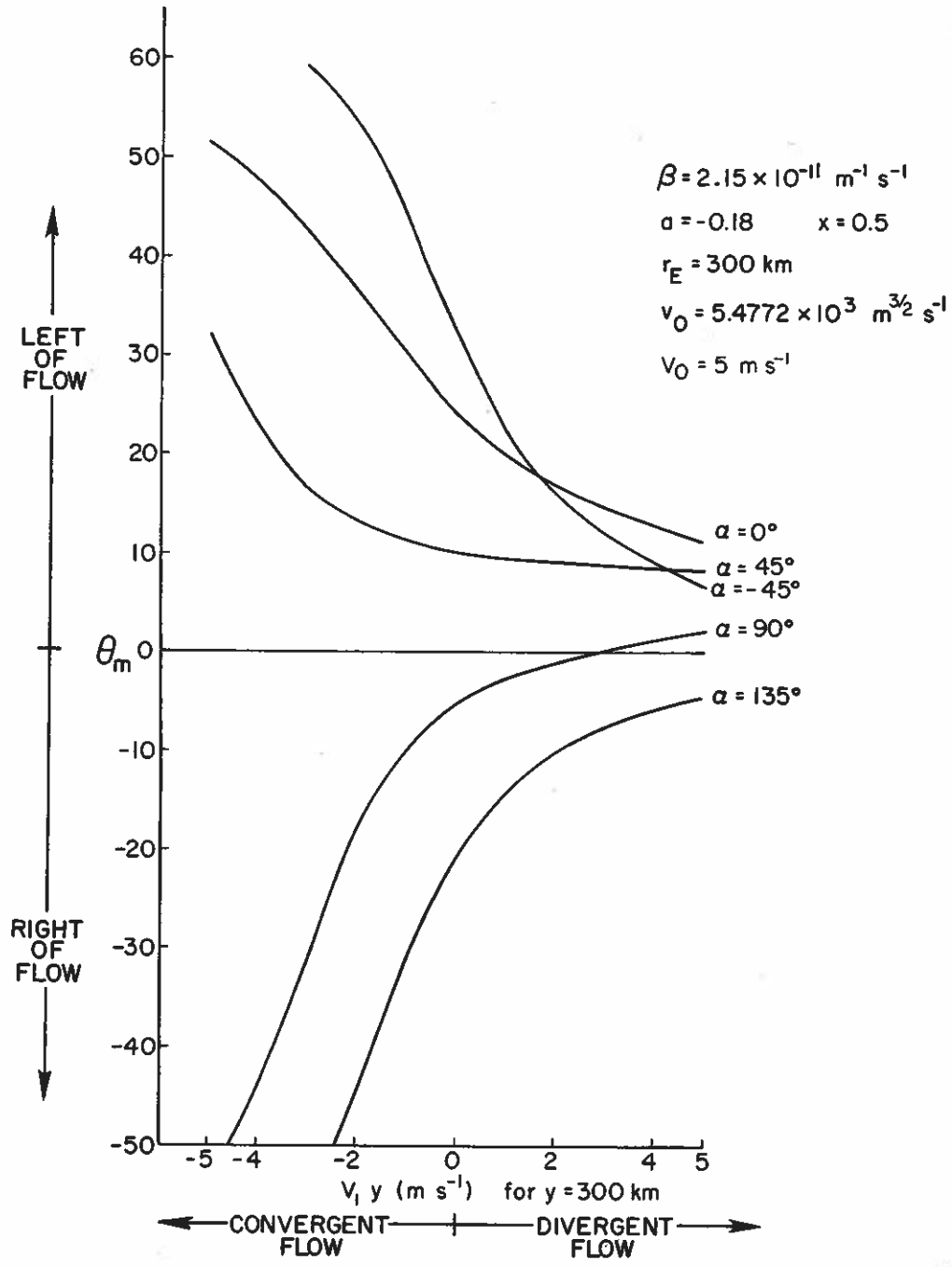

Fig. 30. Variation of θ_m (in degrees) with different values of V_1 for five directions of flow.

$$V_c = (V_o+V_1 r\cos\theta_m)\cos\theta_m + \frac{\beta r^2}{1-x^2}\sin(\alpha+\theta_m) - a(2-x)\cos(\alpha+\theta_m)$$

$$- \frac{V_1 r^{(x+1)}}{v_o}[\cos(\alpha+\theta_m)+\cos\alpha\cos\theta_m] \qquad (41)$$

The first term on the right hand side represents the effect due to the advection of vortex vorticity by the total wind while the second term is the resultant β-effect. It is not obvious from Eq. 41 what the effect of V_1 has on V_c. However, when the actual values of V_c are calculated, a better physical picture emerges. In general, the effect of the term involving V_1 is not as significant as the other terms in Eq. 41. However, it does change the resultant β-effect because θ_m, which appears in all the terms on the right hand side of Eq. 41, is a function of V_1 (see Eq. 39). This is especially true for the β-effect term since θ_m is coupled with α.

Figure 31 shows the variation of cyclone speed V_c with the convergence/divergence associated with the environmental flow for five values of α. A general observation from this figure is that if the flow is slowing down ($V_1 < 0$), V_c is less than V_o. The rate of change of V_c with V_1 varies for different values of α. When the flow is northeasterly ($\alpha = 135^o$), the increase in V_c with V_1 is the largest. This is because at this angle of flow, the cyclone always travels faster than the environmental flow. A divergence in this flow will further enhance the magnitude of V_c (see Case B in Fig. 29). On the other hand, a convergence will actually reduce the increase in V_c caused by the convergence of the vortex. (This can be easily shown using a diagram

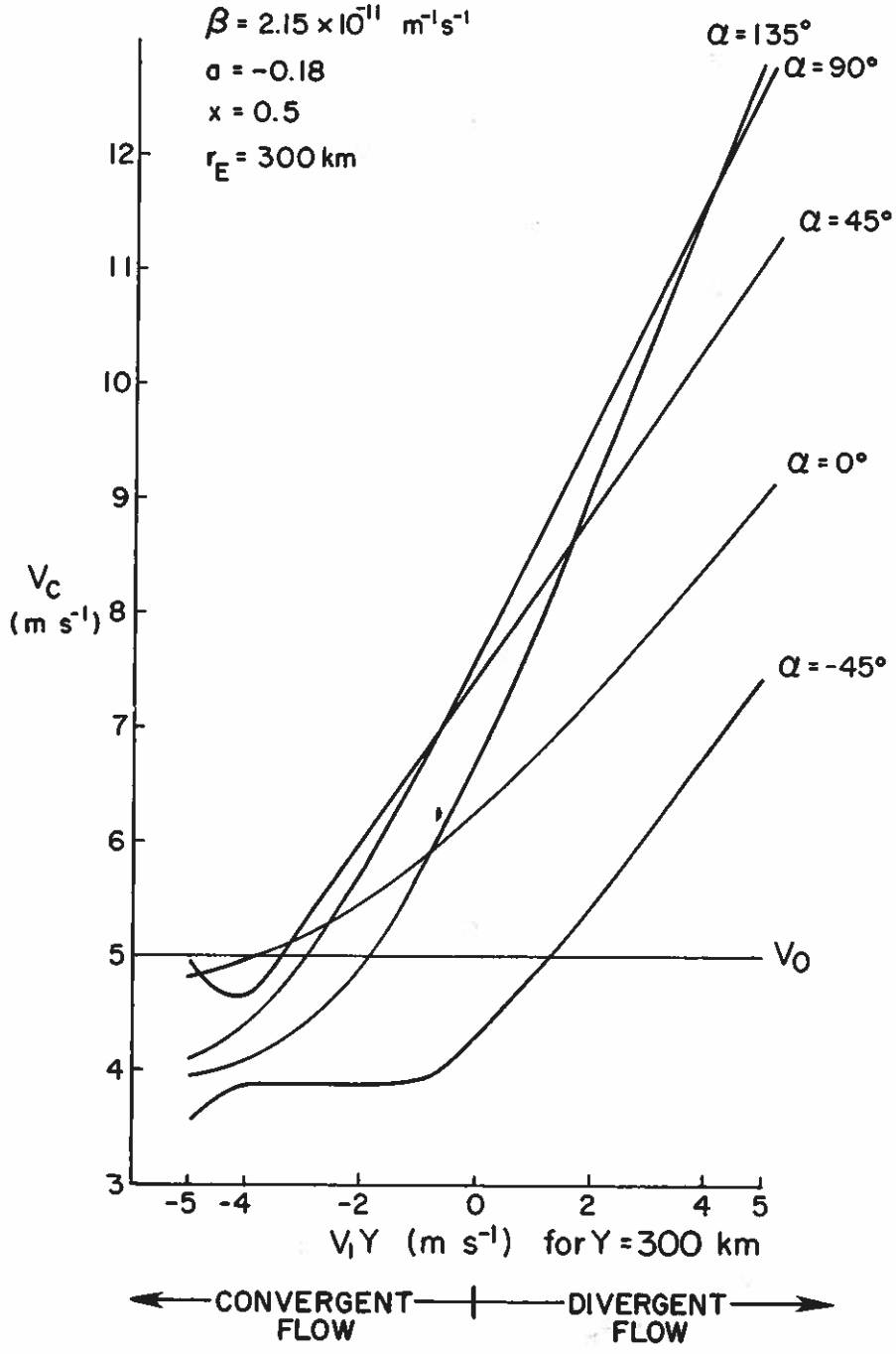

Fig. 31. Variation of cyclone speed V_c with V_1Y for five directions of flow.

similar to Fig. 29.) Therefore, this flow will slow a cyclone down only if the convergence in the flow is strong enough. A divergent northeasterly flow will speed up the cyclone by a great amount.

The curve for a easterly flow ($\alpha = 90^{o}$) is similar. However, for the same V_1, V_c is larger than the case with $\alpha = 135^{o}$. This is because in this case, the flow angle is nearer to that at which $\theta_m = 0$. As indicated in Fig. 20, the difference between V_c and the environmental flow is maximum when $\theta_m = 0$.

For a southeasterly flow ($\alpha = 45^{o}$), a convergence will be "in phase" with that of the vortex to give a greater increase in the magnitude of V_c. Therefore, for the same V_1 (< 0), V_c is larger than the two previous cases. However, a divergence in this flow will work against the convergence of the vortex (as shown by the example in Case A, Fig. 29) and reduce the increase in V_c, and thus the slope of the part of the curve with $V_1 > 0$. Another interesting point is the 'dip' when $V_1 Y = -4$ m s $^{-1}$. This is a result of the fact that the increase in the advection of vortex vorticity by the total flow is not enough to compensate for the decrease in the convergence of the flow when $V_1 Y$ increases from -5 m s^{-1} to -4 m s^{-1}. With the exception of this 'dip' the curve for a southerly flow ($\alpha = 0^{o}$) is similar to that for $\alpha = 45^{o}$ and can be explained with similar physical reasoning. Note also in both cases, the cyclone can only be slowed down if a very strong convergence exists.

In most cases, a cyclone moves slower than its environmental flow if this flow is from the southwest ($\alpha = 45^{o}$). A convergence in this flow will tend to reduce the β-effect due to that of the vortex. A divergence, on the other hand, will 'cooperate' in reducing further the

increase of V_c with increasing environmental wind. These effects are illustrated by the curve in Fig. 30 for $\alpha = -45^{o}$. This curve shows that because of this 'inherent' slow down of the cyclone under such a flow regime it requires a strong divergence in the flow to speed up the cyclone. This is essentially what happens to a real cyclone under the influence of a westerly trough after recurvature. Strong divergence is usually present on the east side of the trough in the mid- to upper troposphre and hence the cyclone will tend to speed up.

Therefore, the problem of predicting a speed change in tropical cyclones is not an easy task. The important parameters are the direction of the flow and the convergence/divergence associated with it.

4.8 Discussion

This chapter presented an analytical study of the motion of a Rankine-combined vortex under the influence of different environmental conditions by solving a simplified, divergent, barotropic vorticity equation. Table 22 summarizes the major findings of the five cases studied. Although these flows were made simple so that the vorticity equation can be solved analytically, examples of them do appear in nature. The results from this study are therefore considered to be generally realistic. They agree reasonably well, at least in a qualitative sense, with many of the observations presented in Chapter 2 (see section 4.5.2). In Chapter 6, more data will be presented to show the importance of the vorticity budget in determining cyclone motion.

The most significant finding from this study is the profound effect of the differential in the Coriolis parameter across the cyclone on both the direction and speed of cyclone movement, especially when it is coupled with a convergence/divergence present in the vortex and/or the

TABLE 22

Summary of the major findings in the five special cases analyzed in the analytical study of the vorticity equation.

Case	Effect to be Studied	Major Findings
I	β-effect	Westward movement of vortex due to advection of earth's vorticity by vortex tangential wind
II	(Case I) + divergence/convergence associated	(1) Effect in Case (I) (2) Poleward (equatorward) deflection of a convergent(divergent) vortex due to (a) advection of earth's vorticity by vortex radial wind, and (b) stretching process
III	(Case II) + uniform environmental flow	(1) Difference between cyclone velocity and environmental flow velocity vectors (that is, both direction and speed) exists as a result of the effects described in Case II (2) This difference depends on the geographical direction of environmental flow as a result of advection of vortex vorticity by radial component of environmental flow
IV	Case III + horizontally-sheared cross wind	(1) Effects in Case III (2)Deflection of vortex due to advection of vortex vorticity by radial component of cross flow
V	Case II + divergent environmental flow	Effects in Case III modified by extra divergence present in environmental flow

environmental flow. The beta-effect obtained by Adem and Lezama (1960), Kasahara (1957) and many other researchers is reproduced in this study. The coupling between the earth's vorticity and the convergence/divergence associated with the vortex has also been studied by Holland (1982) using a slightly different approach. Similar results were obtained. However, the effect of a divergent environmental flow on vortex movement has never been explicitly analyzed before the present study. Likewise, the fact that a 'cross-wind' changes the direction of cyclone movement as a result of changes in the vorticity advection patterns and not by acting as a 'steering flow' has not been discussed in previous studies. The findings in this chapter point to the importance of analyzing the vorticity budget in determining cyclone motion. They also provide insights into the physical processes responsible for cyclone motion. These will provide clues in the interpretation of the results obtained from composite data, as will be seen in Chapter 6.

CHAPTER 5 - WIND-PRESSURE BALANCE IN TROPICAL CYCLONES

5.1 Introduction

In Chapters 3 and 4 the interaction between the circulation of the vortex and that of the environment has been shown to be important in vortex movement. Such an interaction was considered only in terms of the superposition of the two wind fields. Since these two circulations must each be sustained by a pressure gradient, a superposition of the wind fields means that the two pressure fields must also be coupled with each other. It is of interest to investigate whether the winds and pressure gradients are in balance under such circumstances. As will be seen later, this might actually have some potential applications in forecasting a change in direction and/or speed of a cyclone.

To perform such an investigation, a simple theoretical analysis of the problem will first be made. Although the assumptions may limit the applicability of these theoretical results, this analysis could provide a background for interpreting observational results from both aircraft and composite data. The aircraft data consist of those collected by the National Hurricane Research Project during the period 1957-1967 and in 1969. These have been documented by Gray and Shea (1976). Composite data sets stratified according to the speed of the cyclone described in Chapter 2 have also been studied. In addition, calculations have been made on the composite data sets used by Chan *et al*. (1980) in the study of turning motion of tropical cyclones.

5.2 Theoretical Analysis

In order to understand the physics of the problem better, a very simple model will be used. This consists of a cyclonic vortex (not necessarily axi-symmetric) in gradient-wind balance embedded in a geostrophic current. A schematic of such a model is shown in Fig. 32. Note that the term "gradient-wind balance" is used here to mean that

$$\frac{v_R^2}{r} + fv_R - \frac{\partial \Phi_v}{\partial r} = 0 \qquad (42a)$$

and

$$\frac{v_L^2}{r} + fv_L - \frac{\partial \Phi_v}{\partial r} = 0 \ , \qquad (42b)$$

where v_R = tangential wind on the right hand side (RHS) looking in the direction of the cyclone motion

v_L = tangential wind on the left hand side (LHS) looking in the direction of the cyclone motion

f = Coriolis parameter

Φ_v = geopotential of the vortex

and r is the radial distance from the center of the cyclone. If the vortex is not moving, the trajectories and streamlines will coincide and Eqs. 42a and 42b will indeed describe the conditions of gradient-wind balance. However, as soon as the vortex moves, r becomes the instantaneous radius of curvature of the trajectory, which is very difficult to identify. To avoid this problem, the cylindrical coordinate system will be used. In this case, the term 'gradient-wind

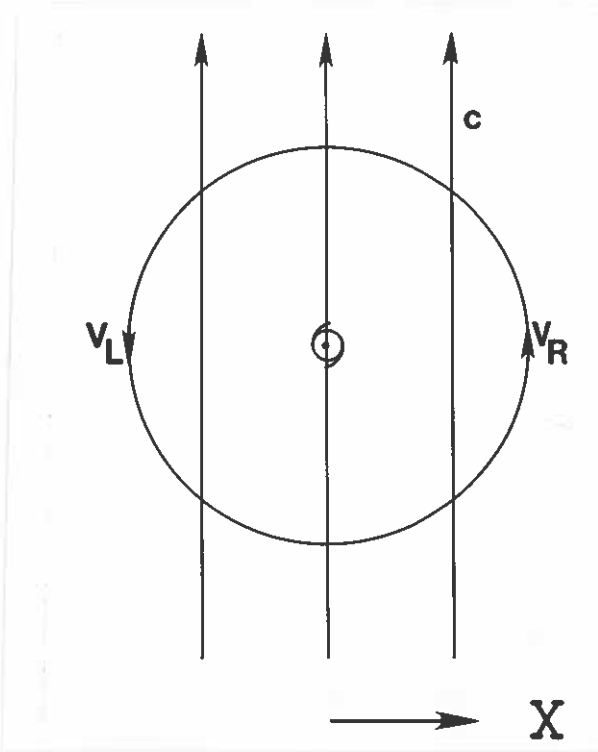

Fig. 32. Schematic diagram showing the superposition of a geostrophic flow (with speed c) onto a vortex with tangential wind V_R on the right-hand-side (RHS) and V_L on the left-hand-side (LHS).

balance' cannot be used. See the definition in the Glossary of Meteorology (Huschke, 1959).

Now, for geostrophic flow,

$$fc = \frac{\partial \bar{\Phi}_c}{\partial X} \tag{43}$$

where

c = speed of environmental flow

and

$\bar{\Phi}_c$ = geopotential of the environmental flow.

On the (RHS) of the cyclone, facing downstream, Eq. 43 becomes

$$fc = \frac{\partial \bar{\Phi}_c}{\partial r} \tag{44a}$$

while on the (LHS) Eq. 43 becomes

$$fc = -\frac{\partial \bar{\Phi}_c}{\partial r} \quad . \tag{44b}$$

Equations 42a,b and 44a,b then describe the wind-pressure balance for the vortex and environmental circulations before any interaction occurs.

To study the interaction of these two fields, consider the radial equation of motion in cylindrical coordinates (assuming frictionless) on the RHS:

$$\frac{du_R}{dt} = \frac{(v_R + c)^2}{r} + f(v_R + c) - \frac{\partial(\bar{\Phi}_v + \bar{\Phi}_c)}{\partial r} \quad , \tag{45a}$$

where d/dt = individual derivative following an air parcel

u_R = radial wind of the vortex on the RHS.

Expanding Eq. 45a,

$$\frac{du_R}{dt} = \underbrace{\left(\frac{v_R^2}{r} + fv_R - \frac{\partial \bar{\Phi}_v}{\partial r}\right)}_{A} + \underbrace{\left(fc - \frac{\partial \bar{\Phi}_c}{\partial r}\right)}_{B} + \frac{2v_R c}{r} + \frac{c^2}{r} \quad . \tag{45b}$$

Equations 42a and 44a show that both terms A and B are zero. Therefore, Eq. 45b becomes

$$\frac{du_R}{dt} = \frac{2v_R c}{r} + \frac{c^2}{r} \quad . \tag{46}$$

Since for a cyclonic vortex, both v_R and r are positive quantities and c is always positive, this analysis shows that a parcel on the RHS of the

cyclone has a positive radial acceleration. Tracing back to the development of Eq. 46, it can easily be seen that the two terms on the RHS of Eq. 46 came from the centrifugal force term in Eq. 45a. Therefore, it is this non-linear term that creates the positive radial acceleration.

On the LHS, the radial equation of motion gives

$$\frac{du_L}{dt} = \frac{(v_L - c)^2}{r} + f(v_L - c) - \frac{\partial(\Phi_v + \Phi_c)}{\partial r} \qquad (47a)$$

where u_L is the radial wind of the vortex on the LHS. Expanding Eq. 47a,

$$\frac{du_L}{dt} = \underbrace{\left(\frac{v_L^2}{r} + fv_L - \frac{\partial \Phi_v}{\partial r}\right)}_{C} - \underbrace{\left(fc + \frac{\partial \Phi_c}{\partial r}\right)}_{D} - \frac{2v_L c}{r} + \frac{c^2}{r} \qquad (47b)$$

Terms C and D are both zero because of Eqns. 42b and 44b. Therefore, Eq. 47b becomes

$$\frac{du_L}{dt} = -\frac{c}{r}(2v_L - c) \; . \qquad (48)$$

Inside a radius of ~ 4^o latitude, $2v_L$ is usually greater than c. Since r is positive for a cyclonic vortex, Eq. 48 shows that a parcel on the LHS of and inside ~4^o of the cyclone would experience a negative radial acceleration. Again, such a negative radial acceleration is a consequence of the extra terms present in the non-linear centrifugal force term in Eq. 47a.

These results suggests that because of the non-linear effects given by the centrifugal force term in the radial equation of motion, the superposition of a geostrophic current and a vortex initially in gradient-wind balance results in parcel accelerations in the radial direction which are positive on the RHS and negative on the LHS. However, these accelerations are only present because the coordinate system used is fixed with respect to the earth. If the same analysis is performed in a coordinate system moving with the environmental speed c, no acceleration is present. This difference my be understood from a kinematic point of view.

Because of the superposition of the environmental flow c onto the vortex, the speed of an air parcel on the RHS of the cyclone would be V_R + c. Similarly, an air parcel on the LHS of the cyclone would have a speed of V_L - c. Therefore, instead of describing a circle, the parcel trajectories will be like the ones portrayed schematicaly in Fig. 33. If the coordinate system is fixed with respect to the earth, the parcel on the RHS will be seen as having an outward radial acceleration and that on the LHS an inward radial acceleration. However, relative to a coordinate system moving with a speed c, these air parcels will be observed to describe circular paths. Thus, the radial accelerations in Eqs. (46) and (48) may be termed "pseudo-accelerations" in the sense that their presence is a result of the coordinate system used. Nevertheless, it is interesting to see whether a computation of these accelerations can provide additional information about cyclone motion.

A net wind-pressure 'imbalance' I can be defined as

$$I = \frac{du_R}{dt} - \frac{du_L}{dt} . \qquad (49)$$

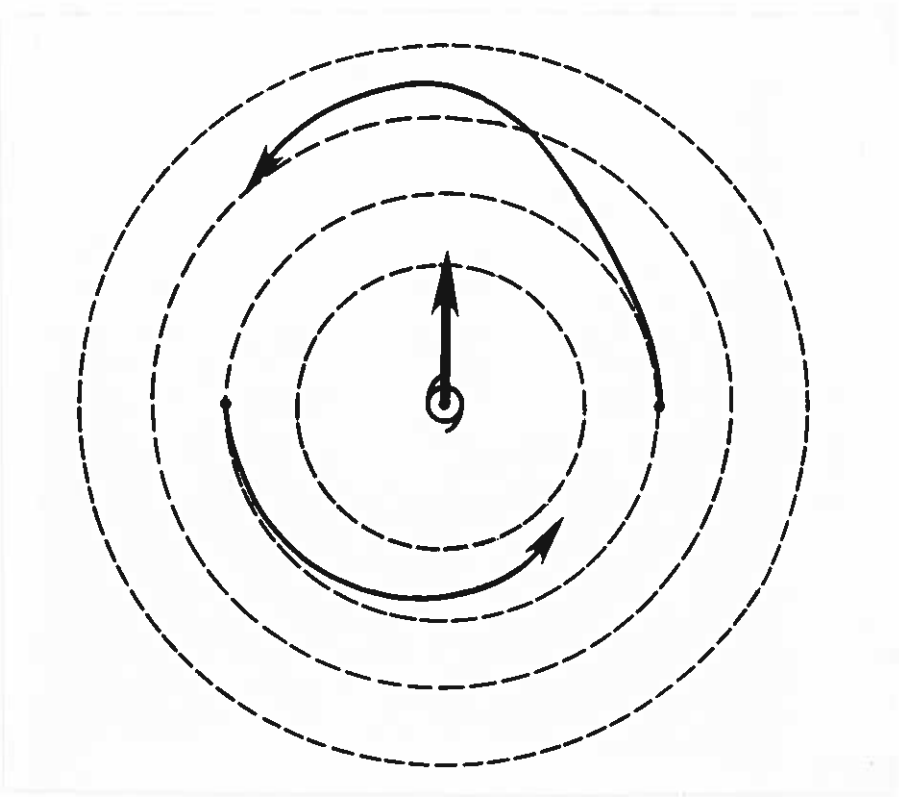

Fig. 33. Schematic diagram showing the trajectories of air parcels (solid lines) on the RHS and LHS of the vortex described in section 5.2. The thick solid arrow indicates the direction of vortex movement.

Substituting in from Eqs. 46 and 48,

$$I = \frac{2c}{r}(v_R + v_L) \quad . \tag{50}$$

Defining the mean tangential wind as

$$\bar{v} = \frac{v_R + v_L}{2} \quad , \tag{51}$$

Equation 50 can be written as

$$I = \frac{4c\bar{v}}{r} \quad . \tag{52}$$

This means that the net imbalance is proportional to the environmental wind speed c, the mean tangential wind $\bar{v}$ and the radius r. Thus, if $\bar{v}$ and r are constant, a calculation of I using Eq. 49 will give an estimate of the environmental wind. Both the observational results in Chapter 2 and the analytical results in Chapter 4 show that the speed of a cyclone exceeds that of the environmental wind by an approximately constant amount of ~ 1 m s^{-1} in most cases. Therefore, the value of I should also be proportional to cyclone speed. A calculation of I might thus provide an estimate of the environmental wind speed.

One basic assumption in this theoretical analysis is that the vortex is initially in a balanced state. In the real atmosphere, cyclones are at best in a quasi-balanced state. Assuming this is true, a cyclone moving into a different environment will be subjected to a condition similar to that portrayed in this analysis. An imbalance will then be created, which will cause a subsequent adjustment of the vortex. Such an imbalance is indeed present in the data sets used by Chan et al. (1980) in their study of the turning motion of cyclones.

In the following sections, calculations of I using different data sets will be presented to demonstrate the existence of such an imbalance.

5.3 NHRP Flight Data

The wind-pressure imbalance suggested in the last section will now be examined using the flight data of the National Hurricane Research Project (NHRP). These data have been fully documented by Shea and Gray (1973) and Gray and Shea (1976). Therefore, only a brief description will be given here.

5.3.1 Brief Description of the Data Set

During the period 1957-1967 and in 1969, the NHRP made about 100 aircraft flights into and out of 22 hurricanes in the Atlantic Ocean on 41 storm days, providing a total of 533 radial legs. Most of the flights were between 900 and 500 mb. Wind, pressure and temperature measurements were made. The accuracy of these measurements has been discussed in the report by Gray and Shea (1976). They provide data at 2.5 n mi intervals between 5 to 50 n mi from the cyclone center. Available parameters include radial and tangential winds, D-values and adjusted temperature. Only the second and the third parameters are needed in this study.

5.3.2 Selection of Cases

In general, a quantitative study of the circulation around an individual cyclone requires an even azimuthal data coverage. Such a requirement is seldom met. For the present purpose, however, only data located to the right and left sides of the cyclone (with respect to cyclone direction) are necessary. Therefore, it should be relatively easy to acquire such data. One restriction, however, is that measurements along the two radial legs cannot be made at two very different times. This is because the time period during which the conditions around the cyclone at close-in distances can remain quasi-constant is relatively short. Therefore, an arbitrary limit of 1 hour was set. That is, only measurements along flight legs that were made less than 1 hour apart were accepted for the present study.

Because of the inherently large cyclone-to-cyclone variability, the best way to 'standardize' the analysis is to compute the imbalance only at the radius of maximum wind (RMW). In deriving Eq. 52, the radius r

is assumed to be the same on both sides. This requires that only those cases in which the radii of maximum wind at both left and right sides are within $\pm$ 2.5 n mi of each other be chosen.

The height gradients $\partial(\bar{\Phi}_v + \bar{\Phi}_c)/\partial r$ were computed using finite differencing with $\Delta r = \pm 5$ n mi. This acts to reduce the noise/fluctuations in the data of scales less than 5 n mi. However, by doing so, a few cases with a radius of maximum wind of $\leq$ 7.5 n mi or $\geq$ 47.5 n mi were eliminated from the sample.

As will be seen later, the wind-pressure imbalance depends on whether the cyclone is changing direction or not. To avoid "contaminating" the data set, only cyclones that moved relatively straight for the 12 hours following the observations were chosen.

With all these restrictions, only 10 cases are available. Although this sample size is very small, the calculated imbalances appear to agree very well with the theoretical results.

5.3.3 Results

Equations 45a and Eq. 47a were used to compute du_R/dt and du_L/dt. The value of I is then calculated using Eq. 49. Since I depends on $\bar{v}$ and r (Eq. 52), and both the maximum wind and the RMW vary from case to case, the value of I has to be 'normalized' in some way so that comparisons between cases can be made. This is accomplished by dividing I (as computed from Eq. 49) by the average maximum wind ($\bar{v}_m$) between the left and right sides and multiplying it by the average radius of maximum wind ($\bar{r}_m$). The normalized value of I will be denoted by I_N. Calculations of I_N are presented in Table 23.

The predominance of the centrifugal force (v^2/r) and the height gradient ($\partial\bar{\Phi}/\partial r$) terms can clearly be seen from Table 23. This is to

TABLE 23

Individual case analysis of the wind-pressure balance in tropical cyclones from NHRP flight data. The symbols are defined as follows: v = tangential wind (m s^{-1}), Φ = geopotential ($m^2 s^2$), u = radial wind (m s^{-1}), I_N = normalized value of I (m s^{-1}). Other symbols are defined in section 5.3. The unit of v^2/r, fv, $\partial\Phi/\partial r$, du/dt and I is m s^{-2} x 10^{-3}. All computations were performed at the RMW.

CYCLONE NAME/DATE	CYCLONE SPEED (m s^{-1})	PRESSURE LEVEL (mb)	POSITION OF RADIAL LEG	v^2/r	fv	$\partial\Phi/\partial r$	du/dt	I	I_N
Carrie 09/15/57	5.66	609	LHS	25.34	2.35	66.24	-38.55	42.05	47.49
			RHS	40.85	3.03	40.39	3.50		
Donna 09/09/60	5.14	811	LHS	105.56	3.06	96.94	11.69	56.35	25.71
			RHS	164.31	3.88	100.17	68.03		
Carla 09/09/61	4.12	859	LHS	30.61	2.21	48.47	-15.65	33.24	32.20
			RHS	67.72	3.18	53.31	17.59		
Carla 09/09/61	4.12	715	LHS	35.85	2.40	33.93	4.32	17.03	17.66
			RHS	50.76	2.90	32.31	21.35		
Esther 09/16/61	6.17	477	LHS	52.43	2.15	63.01	-8.42	74.42	40.81
			RHS	129.10	3.14	66.24	66.00		
Dora 09/07/64	1.03	715	LHS	37.23	2.52	32.31	7.43	-6.68	-7.87
			RHS	24.27	2.32	25.85	0.75		

TABLE 23 (Continued)

CYCLONE NAME/DATE	CYCLONE SPEED ($m\ s^{-1}$)	PRESSURE LEVEL (mb)	POSITION OF RADIAL LEG	v^2/r	fv	$\partial\Phi/\partial r$	du/dt	I	I_N
Dora 09/07/64	1.03	667	LHS	28.15	2.44	24.23	6.35	-0.14	-0.18
			RHS	27.83	2.61	24.23	6.21		
Betsy 09/03/65	5.14	667	LHS	28.60	2.32	53.31	-22.40	25.34	27.60
			RHS	56.31	3.18	56.55	2.94		
Debbie 08/18/69	2.57	667	LHS	32.24	2.03	22.62	11.64	22.22	21.18
			RHS	55.21	2.88	24.23	33.86		
Debbie 08/20/69	5.66	667	LHS	30.61	2.29	43.62	-10.72	29.61	29.35
			RHS	62.56	3.18	46.85	18.89		

be expected since at such close-in radii, the effect of the Coriolis force is negligible even though the tangential wind is large. Table 23 also shows that the height gradients between the LHS and RHS, are about the same in almost all the cases, regardless of the strength of the tangential wind. It appears, therefore, that tropical cyclones are fairly symmetrical with respect to their pressure or height field, at least near the RMW. This also suggests that the difference in the radial acceleration (du/dt) between parcels on the LHS and the RHS is basically in the tangential wind. With the exception of two cases, the radial acceleration on the LHS is indeed negative (or very weakly positive), as predicted by the theoretical analysis.

Since the values of I have been 'normalized', it is possible to plot the variation of I_N against the cyclone speed. This is shown in Fig. 34, together with a least-square fit for all the points. The correlation coefficient is 0.90 with the regression equation given by

$$V_c = 1.70 + 0.10\ I_N\ , \qquad (53)$$

where V_c = cyclone speed. As mentioned earlier, the cyclone speed exceeds the environmental wind speed by about the same amount for almost all cyclones. Therefore, one might write

$$c = V_c - k,$$

where k is a constant. Substituting into Eq. 52,

$$\frac{r}{4\bar{v}}\ I = (V_c - k),$$

or

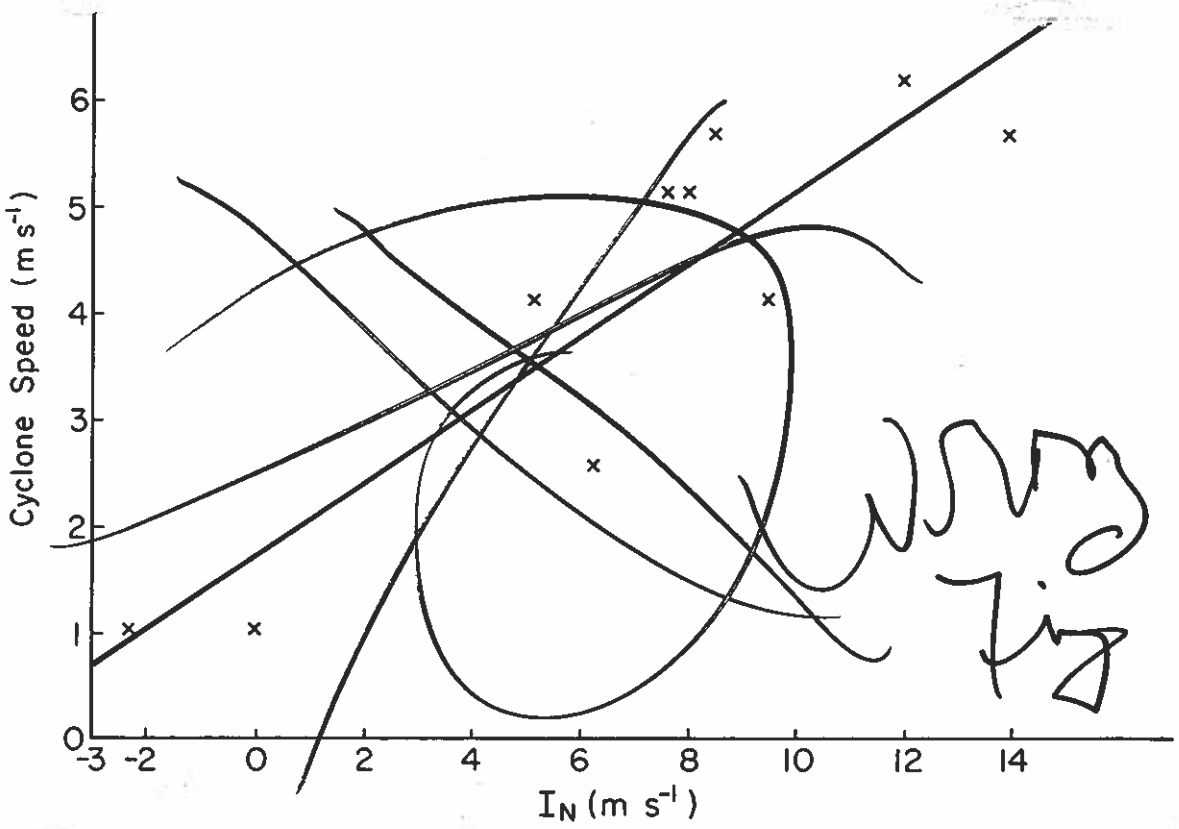

Fig. 34. Plot of the normalized wind-pressure imbalance (I_N) against cyclone speed at the RMW. The straight line is the least-square fit with a correlation coefficient of 0.90.

$$V_c = k + \frac{1}{4} I_N , \tag{54}$$

which is in the same form as Eq. 53, although the actual slope is smaller than that predicted by the theory. The value of k, however, is about the same compared with the observational findings in Chapter 2.

These results demonstrate the approximate validity of the simple theoretical analysis presented in the last section. They point to the importance of the centrifugal force term in determining the radial acceleration of a parcel. As the distance from the cyclone center increases, one would expect the Coriolis force term to be more

significant. How would this affect the validity of the theoretical analysis? The flight data cannot answer this question. It is therefore necessary to use composite rawinsonde data.

5.4 Rawinsonde Composite Data Sets of Cyclone Speed

As mentioned in Chapter 2, rawinsonde data around tropical cyclones are too scarce to allow quantitative studies of the environmental circulation in individual cases. Therefore, composites have to be made. A complete discussion of the composite philosophy has been presented in section 2.2.

Since the wind-pressure imbalance is related to cyclone speed, it is logical to perform calculations on data sets consisting of cyclones that were stratified according to speed. Tables 1 and 2 (section 2.2.1) show that five such data sets are available, three in the northwest Pacific and two in the west Atlantic. Unfortunately, at the time when the Atlantic composites (used by Gray, 1977) were made, no height information was composited with respect to the direction of cyclone movement. Therefore, only the three speed data sets in the northwest Pacific can be used. These are the slow-moving (cyclone speed V_c between 1-3 m s^{-1}, the moderate-speed ($4 \leq V_c \leq 7$ m s^{-1}) and the fast-moving ($V_c > 7$ m s^{-1}) stratifications in Table 1. The height data were composited in the way described in section 2.2.2 for the winds in the coordinate system rotated with respect to cyclone direction (or ROT system).

With these composite data, the centrifugal force and the height gradient terms at various pressure levels can be calculated. The height gradients were computed using a finite difference of 4^o latitude (=444.4 km), except at 2^o latitude radius from the cyclone center where a 2^o

latitude difference (between 4^{o} and 2^{o}) was used. The Coriolis parameter f at any grid point (r, θ) was calculated using the formula

$$f = 2\Omega\sin[\phi_{o} + \frac{r}{R_{E}}\cos(\alpha + \theta)] \qquad (55)$$

where Ω = angular speed of earth's rotation

R_{E} = radius of earth

α = direction of cyclone movement (positive counterclockwise from north) and

ϕ_{o} = mean latitude of all cyclones in the stratification.

Figure 35 shows the vertical variation of wind-pressure imbalance (as defined in Eq. 49) for the three speed stratifications in the northwest Pacific at 2 and 4^{o} latitude radius from the cyclone center. No height data were available at 2^{o} for fast-moving cyclones. A general trend in all the curves is the decrease in the value of I with height. This is reasonable since the value of I calculated this way should depend on the magnitude of the mean tangential wind (see Eq. 52) which in general decreases with height.

The imbalance specified by Eq. 52 deals only with the cyclonic levels. At the anticyclonic levels, a superposition of the environmental flow onto the anticyclonic vortex will produce similar results except now the value of I should increase negatively with increasing wind speed, or correspondingly, cyclone speed. This can be proved easily by deriving similar equations in section 5.2. At 4^{o} latitude radius from the cyclone center, this is indeed the case. That is, fast-moving cyclones have the largest negative imbalance at upper levels.

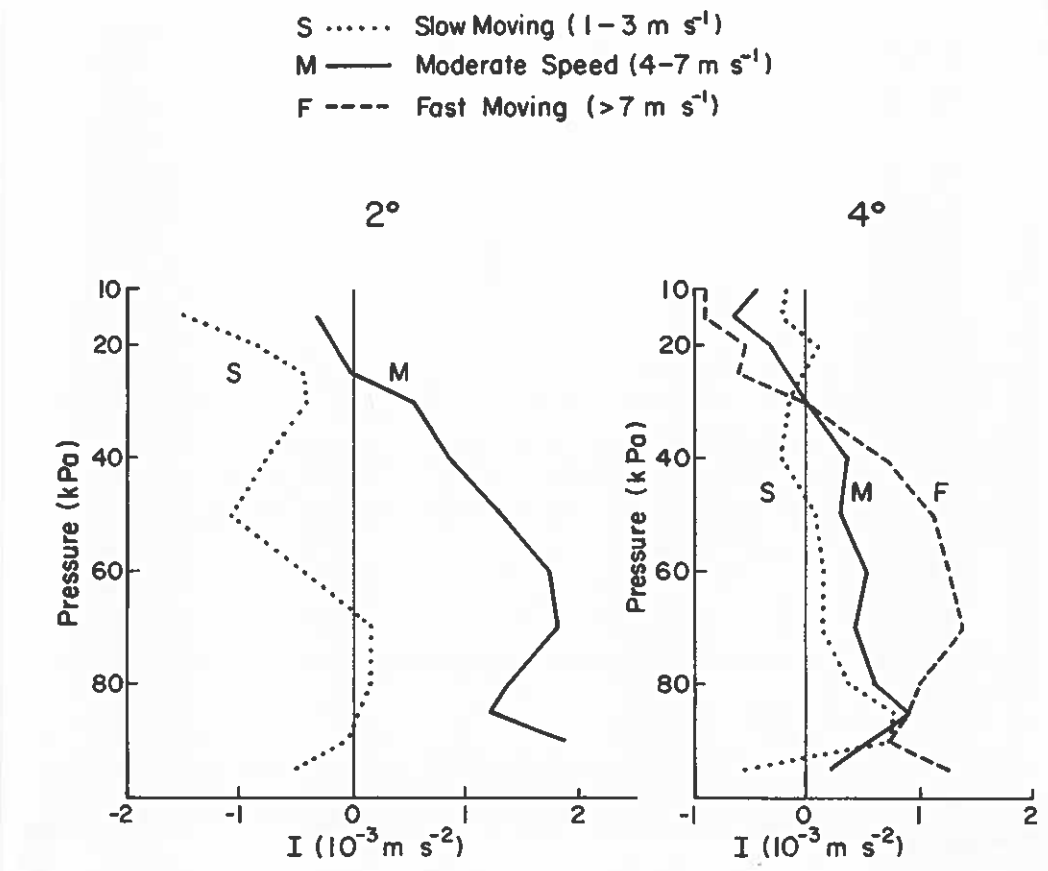

Fig. 35. Vertical variation of the wind–pressure imbalance (I) for speed composite data sets in the northwest Pacific at 2 and 4° latitude radius from the cyclone center. No height data was available at 2° for fast-moving cyclones.

At the cyclonic levels, the difference between the three stratifications at 4° is rather obvious, with the imbalance increasing with cyclone speed. Below 800 mb, little difference is found. This suggests that the middle level flow (which is not strongly influenced by friction and other surface effects) is much more important in determining cyclone speed than the flow at low levels.

At 2°, the moderate-speed stratification has values of I positive at the cyclonic levels and negative at anticyclonic levels, as expected. The slow-moving cyclones, however, behave differently. At low levels, the imbalance is almost zero, probably because of the strong tangential winds and the weak environmental flow. At the middle levels, the

imbalance is negative. An examination of various terms in the balance shows that at these levels, the height gradient on the LHS actually reverses, giving a large positive du_L/dt and hence a negative value of I. Such a height-gradient should correspond to a flow against the direction of cyclone movement. The net effect of this and the flow on the RHS would produce a weak environmental flow. This could be why such cyclones move so slowly.

These results again demonstrate the general validity of the theoretical analysis presented in section 5.2. A basic assumption of this analysis is that the vortex is initially balanced. Assuming this is the case, what would happen if the cyclone subsequently move into a different environmental flow? Would the gradient wind balance be perturbed and new radial accelerations be set up, and subsequently cause the cyclone to adjust to such a perturbation? This will be investigated in the next section.

5.5 Turning Motion Data Sets

Chan et al. (1980) studied the relation between the flow around cyclones undergoing turning motion. They composited rawinsonde data around west Atlantic cyclones that underwent a left or right turn (directional change in 12 h $\geq \pm 20^{\circ}$) or moved relatively straight (directional change in 12 h $< 20^{\circ}$) for a period of at least 36 hours. The composites consist of data sets at turn time and 12, 24 and 36 h before turn time. It is therefore possible to use these data sets to study the wind-pressure balance before and during the turn. A schematic of the tracks for these three classes of cyclones is shown in Fig. 36. For a complete description of the data sets, the reader is referred to their paper.

Put in Johnny Chan's paper 1983

Fig. 36. Schematic of the tracks of the three classes of turning tropical cyclones at turn time T and 12 to 36 h prior to turn (after Chan et al., 1980).

The terms in the radial equation of motion and the resulting wind-pressure imbalance were calculated in the same way as described in the last section. Data sets for all the three stratifications at the turn time T and 12, 24 and 36 h before turn time (T-12, T-24 and T-36 respectively) were studied. Those at T-24 and T-36 do not differ significantly among the three classes of cyclones. However, at T-12 large differences in the environmental flow are present.

Figure 37 shows the vertical variation of the wind-pressure imbalance I at T-12 for the three stratifications at 4° latitude radii from the cyclone center. No height data were available at 2°. For left-turning cyclones, the value of I remains positive and increases with height while right-turning cyclones have negative values of I up to

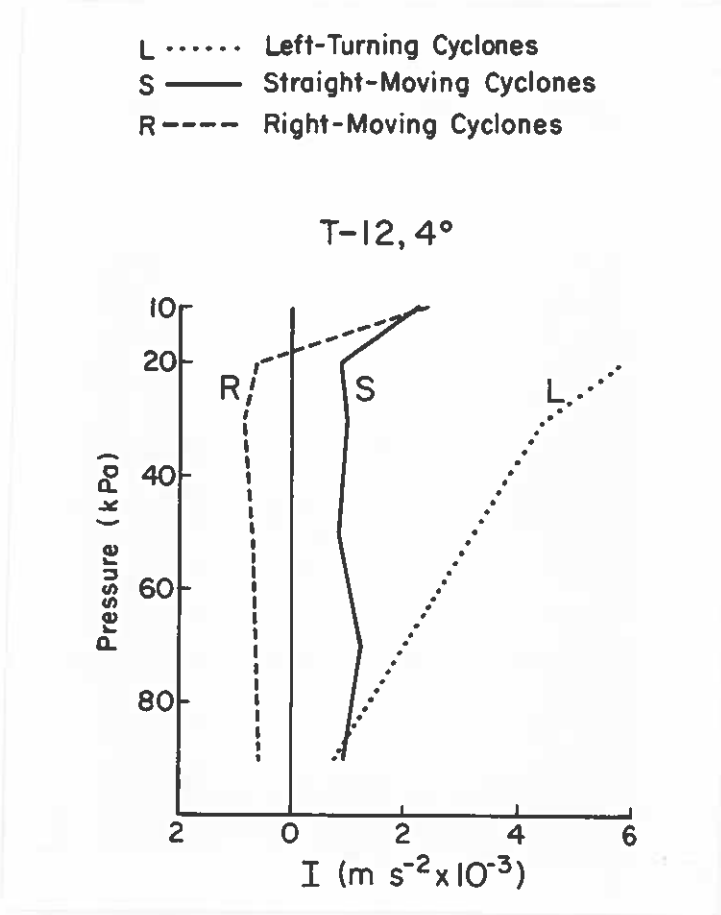

Fig. 37. Vertical variation of the wind-pressure imbalance (I) at T-12 for turning motion data sets in the west Atlantic at 4° latitude radius from the cyclone center.

200 mb. This means that the environmental flow around left-turning cyclones at 4° is relatively strong and increases with height. An examination of the various terms in the radial equation of motion shows this is indeed the case. Moreover, the height gradient force on the RHS is weakly inward but the Coriolis force is relatively strong and outward. At the same time, the reverse occurs on the LHS, with a strong inward height gradient force.

The negative values of I present in right-turning cyclones result from a positive du_L/dt and a negative du_R/dt. On the RHS, the height gradient is stronger than the combination of the centrifugal and Coriolis forces. On the LHS, the opposite occurs. If ones assumes that

the cyclone is in gradient-wind balance at T-24, this result suggests that at T-12, the environment around a right-turning cyclone has a relative height increase on the RHS and a height decrease on the LHS. The latter is probably a result of an approaching trough, a common situation for right-turning cyclones.

These results suggest that if data are available, then by computing the values of I at 4^{o}, it might be possible to predict the future 24 h directional change of a cyclone. The next step is to see if differences among stratifications exist at turn time. This is shown in Fig. 38. No height data were available for left-turning cyclones. Not much difference exists between right-turning and straight-moving cyclones. It appears therefore that wind-pressure imbalance calculations at turn time is not useful in predicting directional change. Perhaps conditions favorable for the turn have already been established by this time. Combining this finding with the results at T-12, one might suggest that the environment conducive to a directional change of a cyclone is present 12 h before turn time.

In section 4.6, it was shown that a cross-wind would change the direction of cyclone movement. This also shows up in the observational study by Chan et al. (1980) on the turning motion of tropical cyclones. Therefore, it should be of interest to study the wind-pressure balance between the front and back of a cyclone under such circumstances. This can be done simply by calculating the radial acceleration in front of (denoted by du_F/dt) and at the back (denoted by du_B/dt) of the cyclone. The front and back areas are defined with respect to the direction of cyclone movement (Octants 1 and 5 respectively in Fig. 4). Then, the

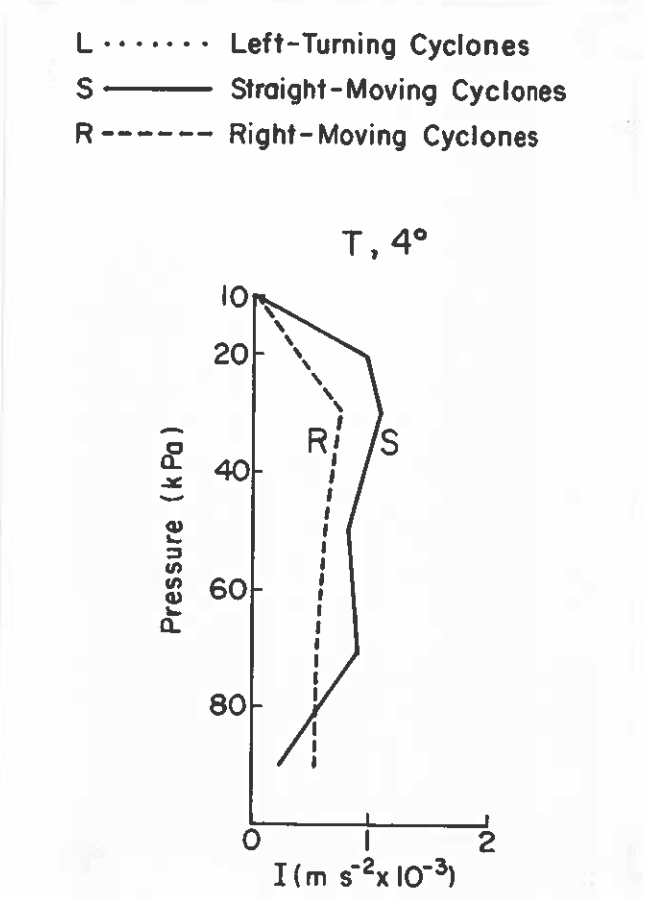

Fig. 38. Same as Fig. 37 except for turn time T. Height data were not available for left-turning cyclones.

wind-pressure imbalance between the front and back, I_{FB}, can be calculated as

$$I_{FB} = \frac{du_F}{dt} - \frac{du_B}{dt} \quad . \tag{56}$$

Again, not much difference exists between the three classes of cyclones at T-24. However, significant differences are present at T-12, as shown in Fig. 39. At 4°, the values of I_{FB} for right-turning cyclones are all negative below 200 mb while left-turning cyclones have values of I_{FB} decreasing with height, changing from strongly positive to strongly negative. This means that for right-turning cyclones, a strong cross current from left to right is present. This is exactly what

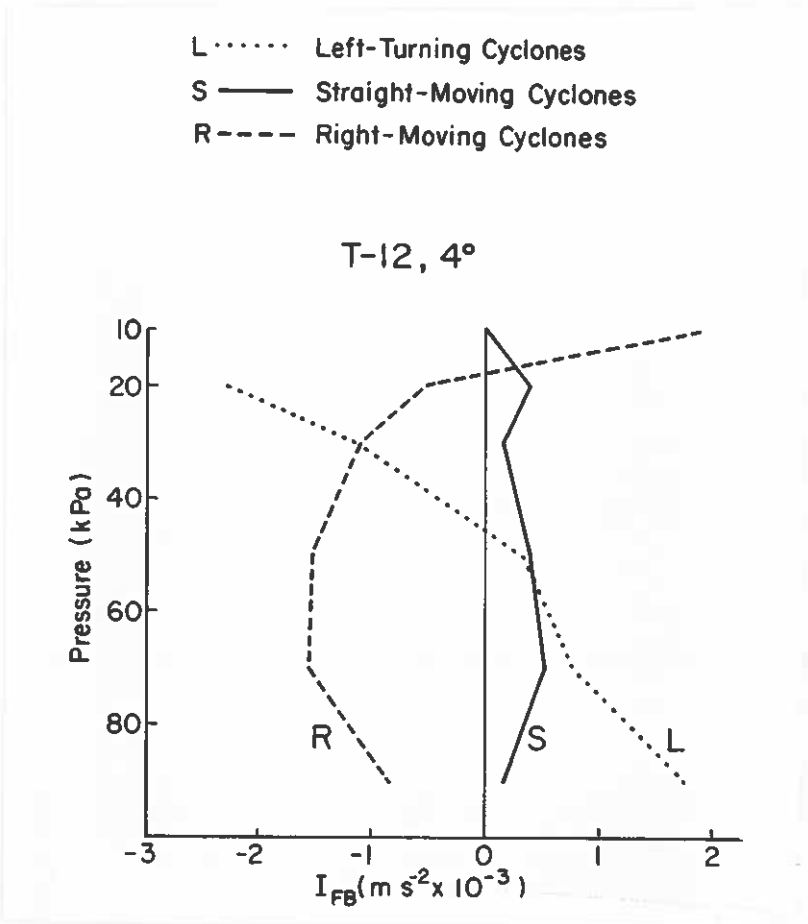

Fig. 39. Same as Fig. 37 except for the front minus back wind-pressure imbalance (I_{FB}) defined in Eq. 56.

happens when a cyclone moves towards a trough and recurves 12 h later. The low to middle level flow is from right to left for left-turning cyclones, thus giving the positive values of I_{FB}. At 300 and 200 mb, the flow in front of the cyclone is actually anticyclonic, producing a negative du_F/dt. Therefore, the value of I_{FB} becomes negative.

At turn time T, 4° front and back height data are only available for straight-moving cyclones. No comparisons between data sets can therefore be made. However, based on the results for the left-right imbalances, one might speculate that the front-back imbalances at turn time might not be very different between data sets.

The main conclusion from these results is that the environmental flow conducive to a directional change of a cyclone is present 12 h before the cyclone actually turns. Such an environment perturbs the wind-pressure balance that is present in the cyclone, not only between the left and right sides but also between the front and back areas of the cyclone. This perturbation then sets up radial accelerations in such a way as to adjust the cyclone to a quasi-balance condition.

From a forecasting point of view, the imbalance created by the environmental flow might be used to predict a 24 h change in the direction of movement of a cyclone. Of course, this has to be verified with many individual cases. However, this would require data in four areas of the cyclone (front, left, back and right, corresponding to Octants 1, 3, 5, and 7 respectively in Fig. 4) at 3 radii. At present, this is hardly possible. It appears, therefore, that some effort should be devoted in acquiring wind and pressure data at these locations. Then, some objective empirical schemes could be developed.

5.6 Summary

This chapter demonstrates, from both a simple theoretical treatment and observations, the presence of a wind-pressure imbalance when the vortex circulation and its surrounding flow are superimposed upon each other. Such an imbalance is found to be related to the speed of the cyclone. Any change in the environmental flow would cause a new imbalance.

In the next chapter, analyses of the vorticity budget of tropical cyclones will be presented. These results, combined with the ones in this chapter, form the basis for establishing a hypothesis of the physical processes responsible for cyclone motion.

CHAPTER 6 - VORTICITY BUDGETS OF TROPICAL CYCLONES

6.1 Introduction

The analytical study of the vorticity budget presented in Chapter 4 indicated the importance of determining the vorticity change in describing cyclone motion. Even though the terms involving vertical motion were neglected, it was possible to use these theoretical results to explain some of the observations presented in Chapter 2. This chapter will present calculations of the vorticity budget using various data sets. These observational results demonstrate the general validity of the analytical results.

Two types of data will be analyzed. The first is the flight data described in Chapter 5. Since only single-level observations of the radial and tangential winds are available, those terms involving vertical motion will again have to be neglected. Nevertheless, the results do point to the significance of the horizontal terms in the vorticity equation in understanding cyclone motion. Equation 9 is used in this part of the calculation.

Composite data sets (described in Chapter 2) that relate to the speed of cyclone movement were also analyzed. Since these include data at all levels in the troposphere, the vertical motion can be calculated kinematically. Therefore, the full vorticity equation (Eq. 8) was used. The results show the relative insignificance of the terms involving vertical motion at radii $> 2^{o}$ latitude from the cyclone center.

Similar calculations were also made using the turning motion data sets used by Chan et al. (1980). Since data are available at more than one time period, the actual time rate of change of vorticity can be computed. Areas of maximum vorticity change can then be compared to the various terms in the vorticity equation to determine the relative importance of each term.

6.2 NHRL Flight Data

This is the same data set used in the last chapter (See section 5.3.1). Calculations of the various terms in the vorticity equation require a very good data coverage because gradients of the winds and vorticity are required. No one single flight has enough azimuthal coverage to allow such computations to be performed. Therefore, composites have to be made.

6.2.1 Method of Compositing

A large variability in the inner core (radius < 200 km) structure of the vortex exists among different cyclones. Therefore, a composite with reference to the cyclone center would not yield very satisfactory results. A better way to composite the data is to use the radius of maximum wind (RMW) as the reference. Observations can then be composited on either side of the RMW. This method has been shown by Shea and Gray (1973) to be far superior to a composite made with respect to the cyclone center.

Therefore, the data were composited using the radius of maximum wind as reference. The composite grid is similar to that in Fig. 4, with eight octants and a radial grid distance of 2.5 n mi. Each radial leg was assigned to one of the eight octants according to its azimuth relative to the direction of cyclone movement. At each pressure level,

radial and tangential winds of all radial legs belonging to the same octant at the RMW and on either side of it (from -15 n mi to +30 n mi) were then averaged. The mean RMW is also calculated. This procedure was repeated for all the eight octants. Because the mean RMW may differ slightly among the octants, and a common reference is necessary in order to calculate the derivatives of radial and tangential winds, the mean RMW of all the eight octants are averaged to give an octant-mean RMW for a particular pressure level.

Because the flights were made at various levels, it is not possible to composite the radial legs at each level. Instead, the data falling within one pressure layer are averaged. These layers are the same as the ones used by Shea and Gray (1973). Figure 40 shows the combination of levels used by them. In this study, only the 5-level storm is used. However, because of the relatively small number of flight legs at 240 mb, the data at this level were not included.

Near the center of the cyclone the curvature vorticity (v/r) is very significant. Since the composites are made with reference to the RMW, rather than absolute radius, the values of relative vorticity, will be meaningful only if cyclones with similar RMW are composited together. To decide on the composite grouping of cyclones based on the RMW, a plot of the distribution of the mean RMW for all flights was made, as shown in Fig. 41. The distribution appears to be tri-modal, with peaks at 12, 22 and 35-40 n mi. The number of cases with RMW $\geq$ 30 n mi is not large enough to produce a meaningful composite. Therefore, two stratifications were made: those with RMW in the range 10-15 n mi (the "small" cyclones) and those in the range 20-25 n mi (the "large" cyclones).

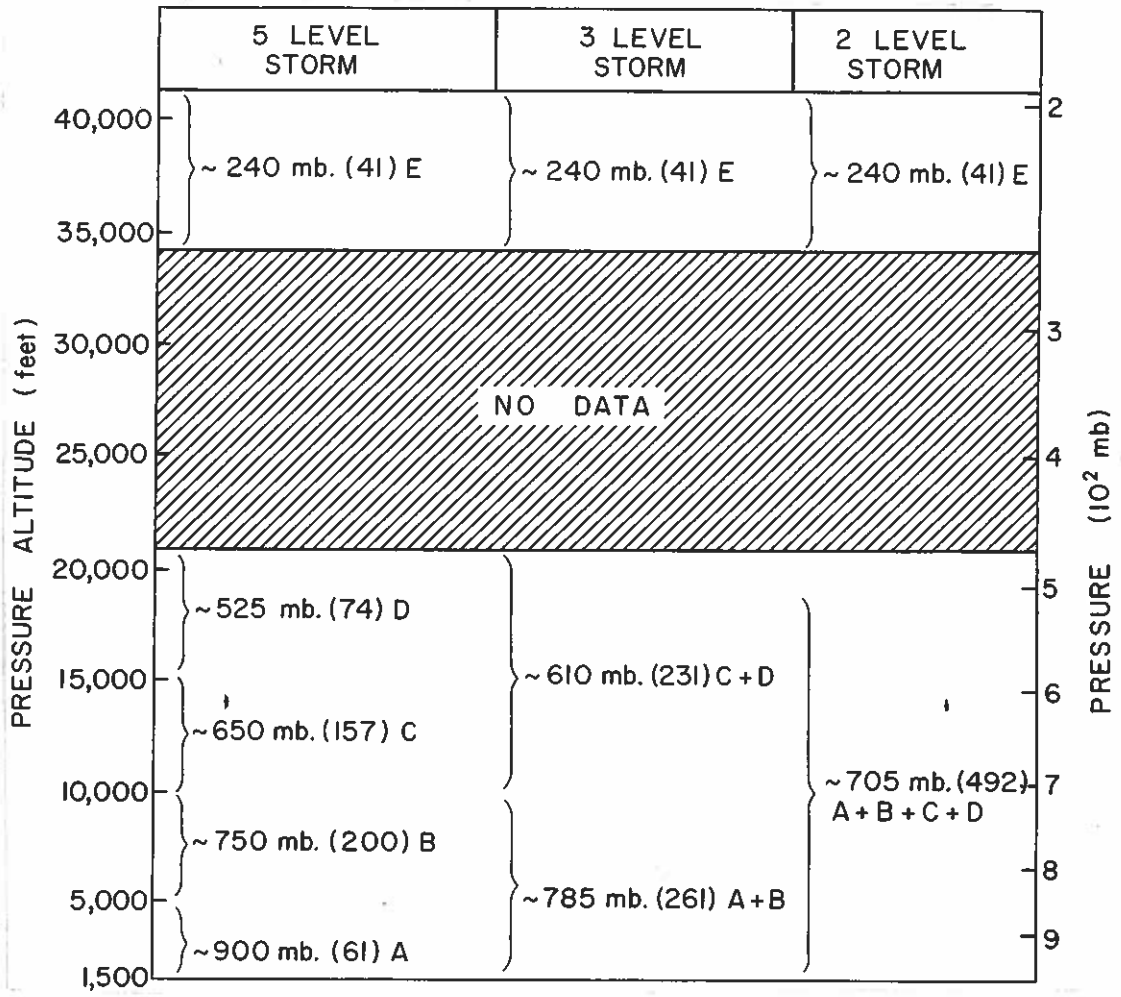

Fig. 40. Distribution of radial leg data in the vertical for five, three and two level mean storms. The number in parentheses is the number of radial legs in each layer average. The pressure level is the level which the data best represents (from Shea and Gray, 1973). In the present study, only the 5-level storm is used.

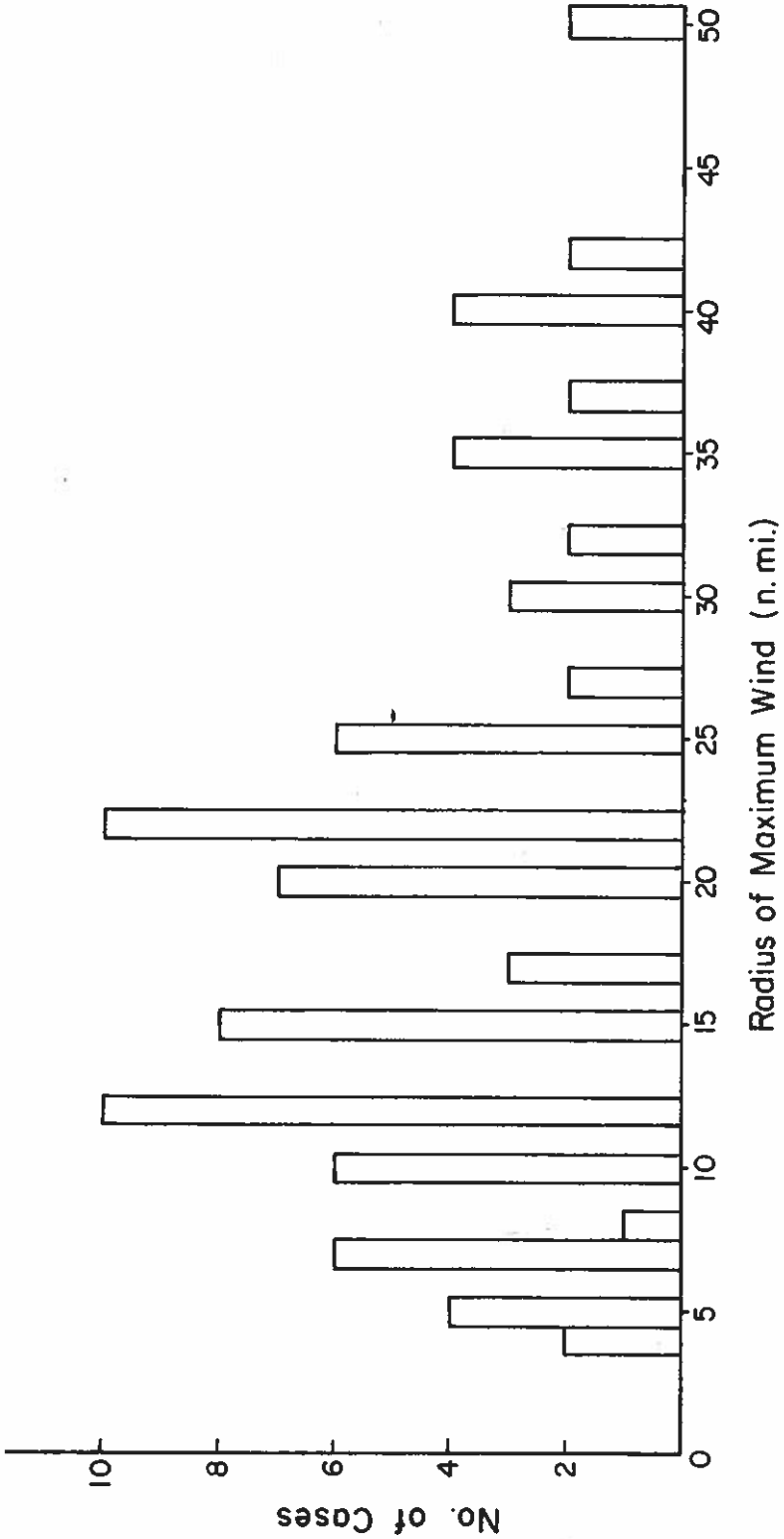

Fig. 41. Distribution of the radius of maximum wind (RMW) for the NHRL flight data. Each case represents one flight mission and the RMW is the mean RMW of all the radial legs on each mission. These data are obtained from Gray and Shea (1976).

6.2.2 Results

The number of radial legs for both stratifications is the largest at 750 mb. Significantly fewer number of cases are available at the other three levels. Therefore, only the data at 750 mb were analyzed.

Figure 42 shows the relative vorticity advection for the two RMW stratifications at 750 mb. Both cases have the area of maximum positive advection in front of the cyclone and near the mean RMW. However, the magnitudes of this vorticity advection in the small cyclone stratification are about 4 times that in the large cyclone group. This is because the vorticity and the vorticity gradient are much larger in the small cyclone group. In addition, the radial winds are more positive in this stratification. The advection by the tangential winds appears to be generally less significant in both stratifications.

The other term in the vorticity equation that was computed is the divergence term $(-(\zeta+f)\nabla\cdot\mathbb{V})$. Results are shown in Fig. 43. In the small cyclone group, because the divergence and the vorticity are both larger than in the other group, the magnitudes of the divergence term are also larger. The divergence term is generally negative in the front in both cases because the radial winds in this area are divergent. However, the sum of this and the relative vorticity advection terms, (which gives an estimate of the local change of relative vorticity) is still positive in front of the cyclone, as can be seen from Fig. 44. This suggests that, indeed, the movement (at least the directional part of it) of a cyclone is related to the local change of relative vorticity.

One could argue about the effect of the vertical advection of vorticity and the tilting terms on the net vorticity change at these

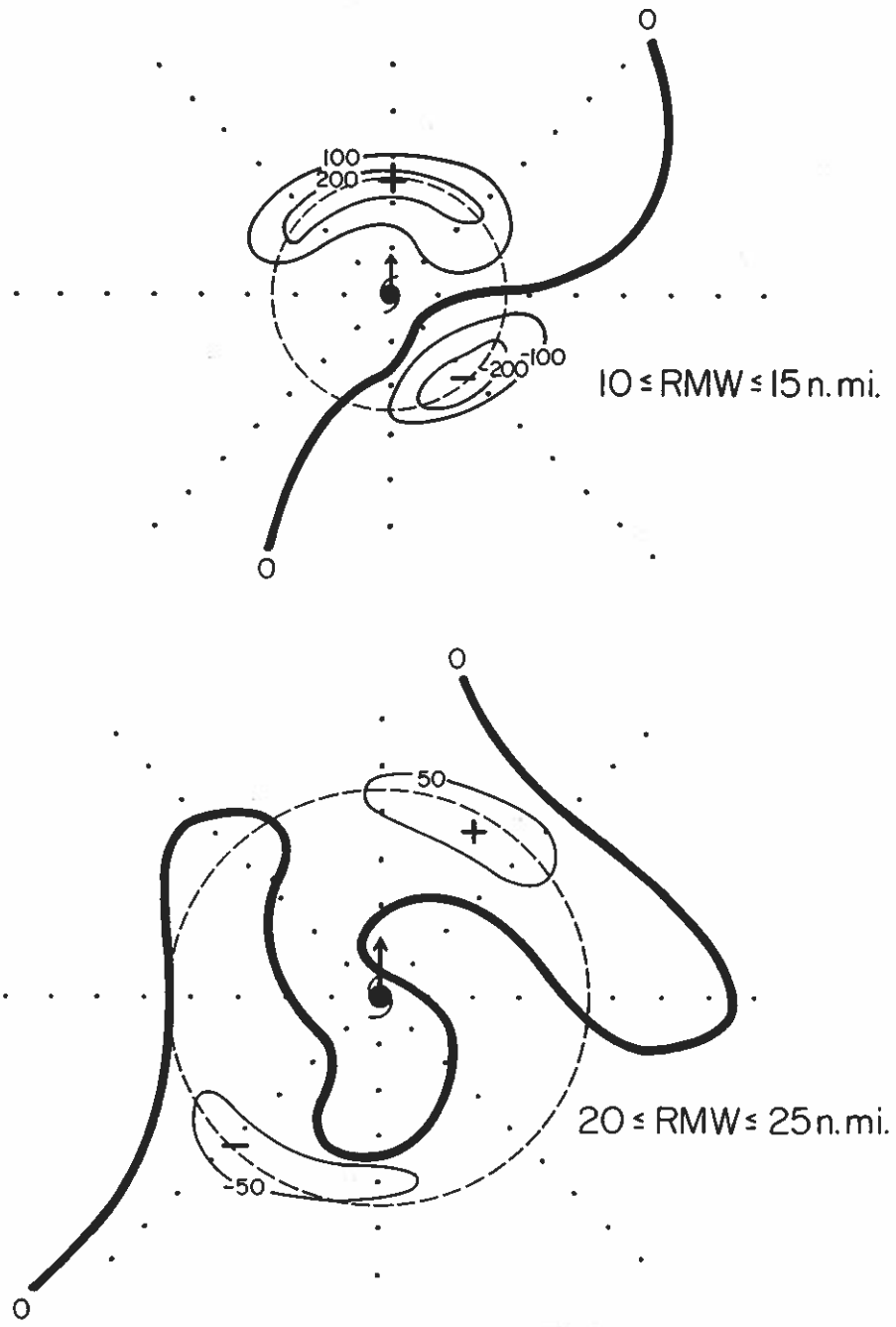

Fig. 42. Horizontal advection of relative vorticity (in units of 10^{-8} s^{-2}) at 750 mb calculated from composite NHRL data for the two RMW stratifications. The dashed circle represents the octant mean RMW. The arrow indicates the instantaneous direction of cyclone motion. The spacing of the grid is 5 n mi.

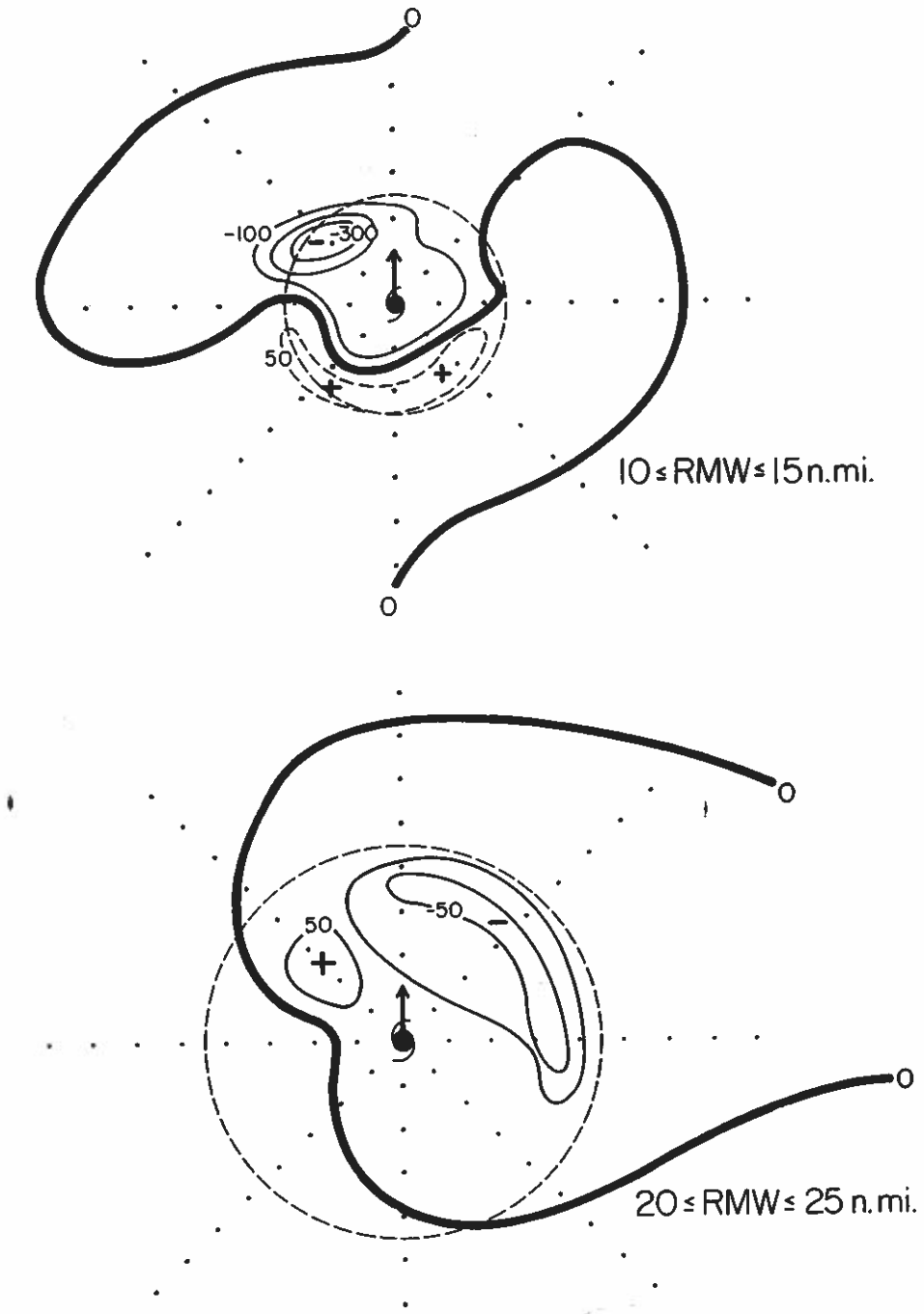

Fig. 43. Same as Fig. 42 except for the divergence term $(-(\zeta+f)\nabla\cdot\mathbf{V})$.

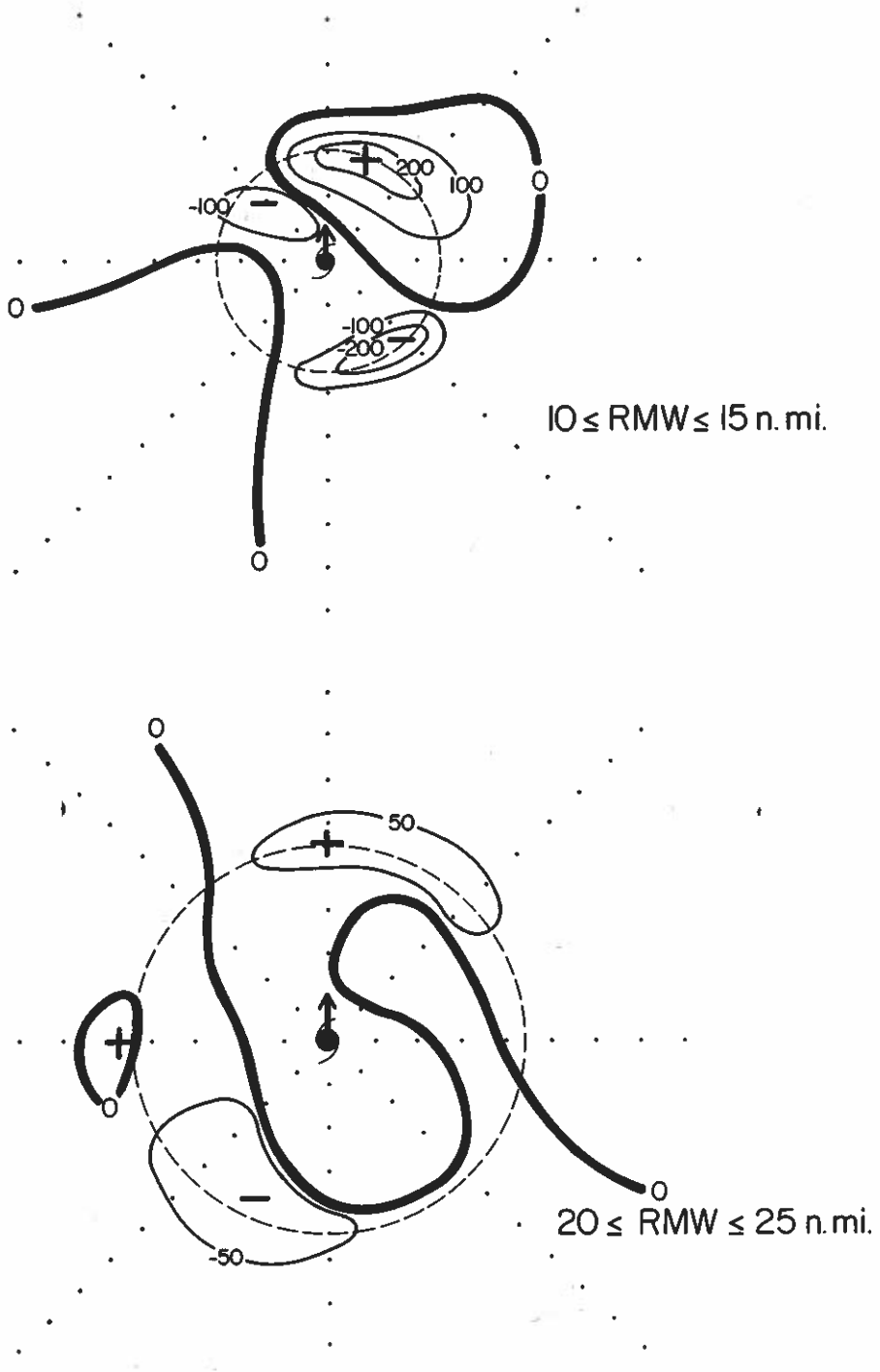

Fig. 44. Same as Fig. 42 except for the sum of the horizontal relative vorticity advection and the divergence terms (that is, $-\mathbb{V}\cdot\nabla\zeta - (\zeta+f)\nabla\cdot\mathbb{V}$).

inner radii. Since the radial and tangential winds are fairly constant with height up to ~ 500 mb around the RMW (Shea and Gray, 1973), the vertical gradients of both these winds and the relative vorticity should be small. Therefore, if the horizontal gradients of vertical motion is not very strong (which is probably true from the scale analysis given in Chapter 4), the terms involving the vertical motion may not have a very significant impact on the net vorticity change. Of course, this assessment has to be justified with actual measurements of vertical motion. Nevertheless, these and later results do point to the importance of computing the local change of relative vorticity in determining cyclone motion.

Rawinsonde composite data available at larger distances ($\geq$ 100 km) from the cyclone center can also be used to study the relation between the vorticity budget and cyclone motion. This type of data provide information at different levels in the atmosphere so that vertical motion and hence the vertical advection and the tilting terms can be calculated. Results from these calculations will be presented in the next two sections.

6.3 Rawinsonde Composite Data Sets of Cyclone Speed

These consist of the fast- ($>$ 3 m s^{-1}) and slow-moving (1-3 m s^{-1}) cyclones in the west Atlantic and the fast ($>$ 7 m s^{-1}), moderate (4-7 m s^{-1}) and slow (1-3 m s^{-1}) speed cyclones in the northwest Pacific studied in Chapter 2 (see Tables 1 and 2). Before the results are presented, the method of calculation will be described.

6.3.1 Data Handling

Although the compositing procedure described in Chapter 2 reduces the amount of noise inherent in the data, calculations of gradients (of

winds and vorticity) require rather smooth data fields especially when the grid points are so widely spaced (see Fig. 4 for the grid size). Therefore, a smoothing routine available from the National Center for Atmospheric Research is applied to the composite radial and tangential wind fields. This routine uses a bicubic spline and fits a smooth surface to a two-dimensional data field. Various degrees of smoothness can be chosen by defining the number of nodes along each axis. Since the purpose here is to reduce the noise in the data further but at the same time retain as much of the 'real' information as possible, the least amount of smoothing is used. This is accomplished by setting the number of nodes along each axis to be 9, the highest number allowed in the routine. From the functional form of the smoothed surface, values of the parameter can be computed at any point within the domain. This will provide estimates of the parameter at grid points where no raw information was available. These estimates are essential in the calculations of gradients when the method of finite-differencing is used. Using this routine, the composite radial and tangential winds at each pressure level are smoothed.

The smoothed radial winds are then mass-balanced. Together with the tangential wind, the horizontal divergence can be calculated. If the vertical motion is zero at the surface and at 100 mb, then the divergence should integrate to zero between the surface and 100 mb. Usually a slight residual remains. This residual is then subtracted from the divergence at each level so that the condition of zero net tropospheric divergence is satisfied. Then, the vertical p-velocity can be calculated from the continuity equation in isobaric coordinates.

With the Coriolis parameter calculated in the way described in section 5.4, all terms in the RHS of the vorticity equation (Eq. 8) can be evaluated using finite differencing. The radial gradient is calculated using a finite difference of 4^{o} latitude ($\pm 2^{o}$), except at 2^{o} latitude where a 2^{o} latitude difference (between 4^{o} and 2^{o}) was used. With the aid of the smoothing routine, values of the radial and tangential winds can be interpolated at points in between the standard 8 octants shown in Fig. 4. In this way, an azimuthal gradient of 45^{o} ($\pm$ 22.5^{o}) can be evaluated. The sum of all the terms on the RHS of Eq. 8 (except for the frictional term Z) will be called the residual R, that is,

$$R = - \mathbb{V}\cdot\nabla(\zeta+f) - (\zeta+f)\nabla\cdot \mathbb{V} - \omega \frac{\partial \zeta}{\partial p} + \left(\frac{\partial u}{\partial p}\frac{\partial \omega}{r\partial \theta} - \frac{\partial v}{\partial p}\frac{\partial \omega}{\partial r}\right) \qquad (57)$$

where the symbols have been defined in section 4.2. The residual R therefore represents the local change of relative vorticity plus all the sources and sinks of vorticity such as friction and sub-grid scale effects. That is,

$$R = \frac{\partial \zeta}{\partial t} + \left[\begin{array}{c}\text{sources and}\\ \text{sinks of vorticity}\end{array}\right] .$$

6.3.2 Calculations of the Residual

An examination of the results from all the five speed composite data sets (two in the west Atlantic and three in the northwest Pacific) show that the largest differences between data sets occur at 2^{o} and 4^{o} latitude radius. Therefore, comparisons will only be made for these radial bands.

Figure 45 shows a pressure-azimuth cross-section of the residual at 2^{o} latitude radius for slow- (1-3 m s^{-1}) and fast-moving (> 3 m s^{-1}) cyclones in the west Atlantic. In both cases, the residual is generally positive in front of the cyclone (azimuth between 335^{o}-45^{o}) and negative behind it (azimuth between 135^{o}-225^{o}) at the levels of cyclonic flow (below ~ 250 mb). At the upper levels, it is generally negative. Comparing the two stratifications, the fast-moving cyclones have a much larger residual (both in front and behind) than those that are slow-moving. Also, the maxima (both positive and negative) are well-defined in the mid-troposphere (500-700 mb) in fast-moving cyclones. In the slow-moving cyclones, the maxima occur in the lower troposphere. Similar, though weaker, differences in the values of the residuals between the two stratifications at 4^{o} radius can be seen in Fig. 46.

In section 4.2, it was mentioned that the speed of a cyclone is related to the ratio of the maximum vorticity change to the radial gradient of relative vorticity (Eq. 20). If these two groups of cyclones have similar intensities, the radial gradients of ζ would be similar and one would expect fast-moving cyclones to have a larger $\partial\zeta/\partial t$. This, in fact, is the case from these results, if the residual is a good representation of $\partial\zeta/\partial t$, which will be shown to be true later. These calculations thus verify that the local change in relative vorticity is very much related to cyclone motion.

Figure 47 shows the residual at 2^{o} for the three speed composite data sets in the northwest Pacific. In general, the faster the cyclone is moving, the larger is the magnitude of the residual. These results are in agreement with those in the west Atlantic. Also, notice that fast-moving cyclones have positive and negative residuals extending

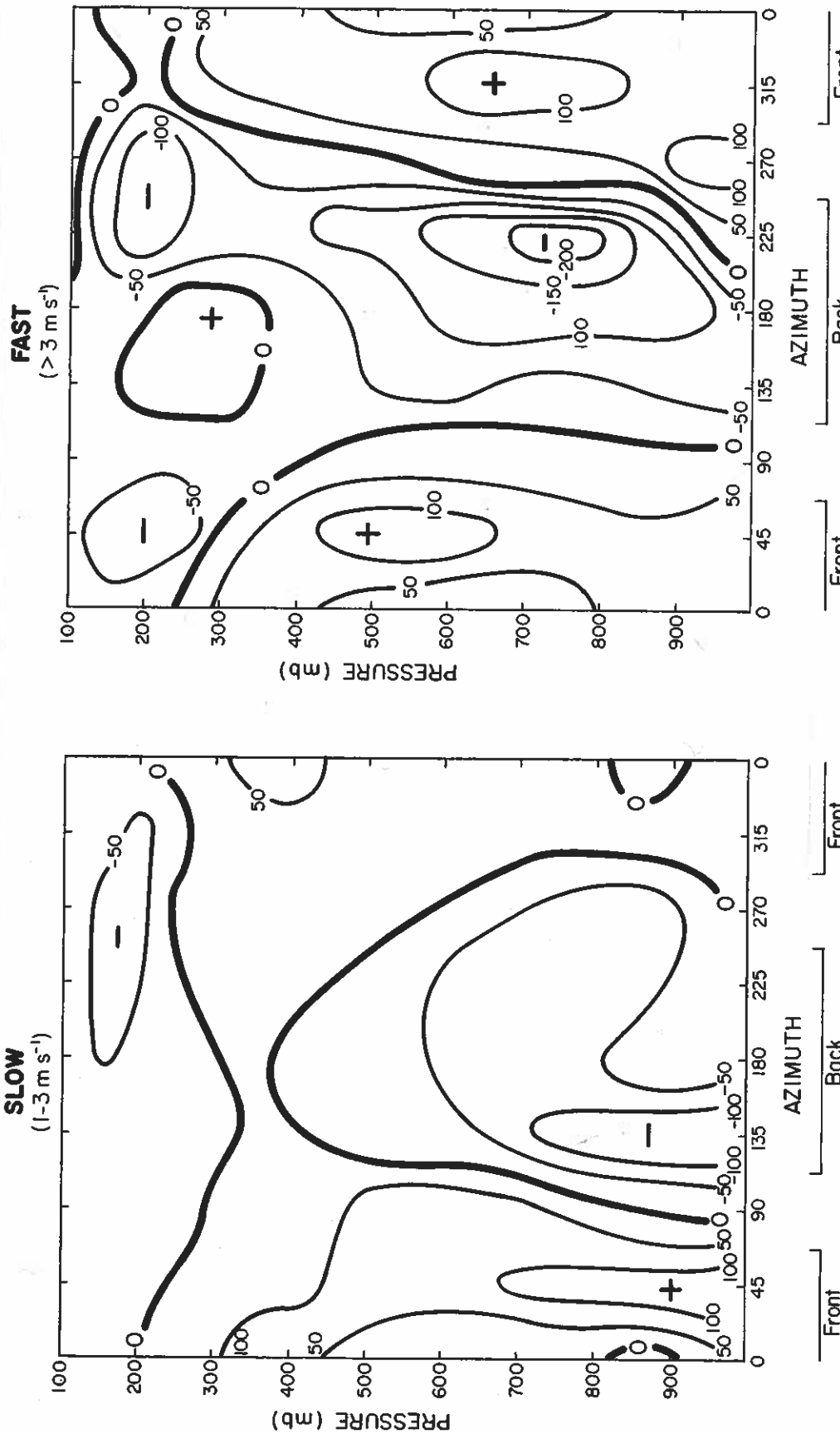

Fig. 45. Pressure-azimuth cross-section of the residual R defined in Eq. 57 (in units of $10^{-6}s^{-1}d^{-1}$) in the vorticity equation at 2° latitude radius for slow- and fast-moving cyclones in the west Atlantic. The azimuth is with respect to direction of cyclone motion, with a value of zero along this direction and increasing counterclockwise.

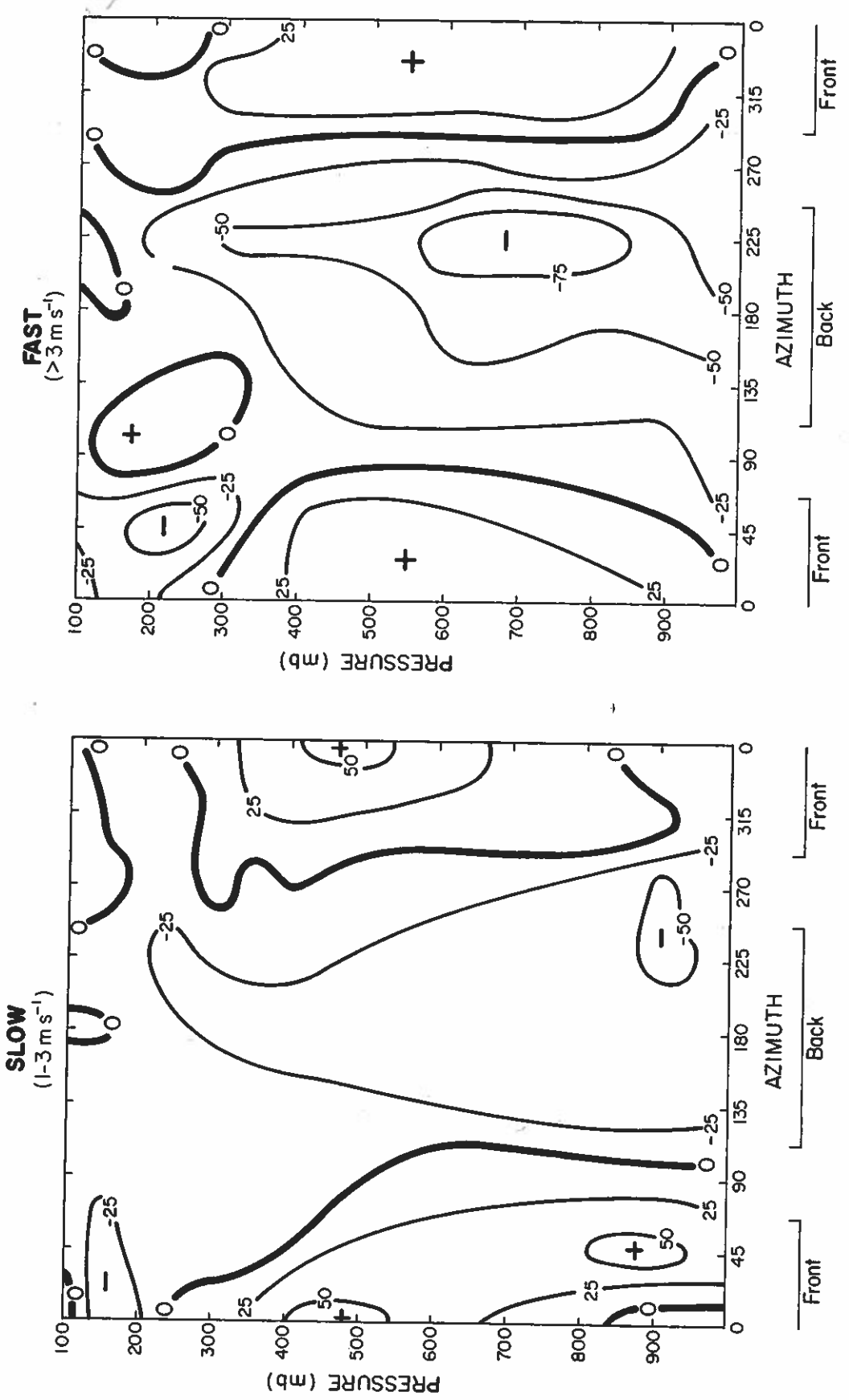

Fig. 46. Same as Fig. 45 except at 4° latitude radius.

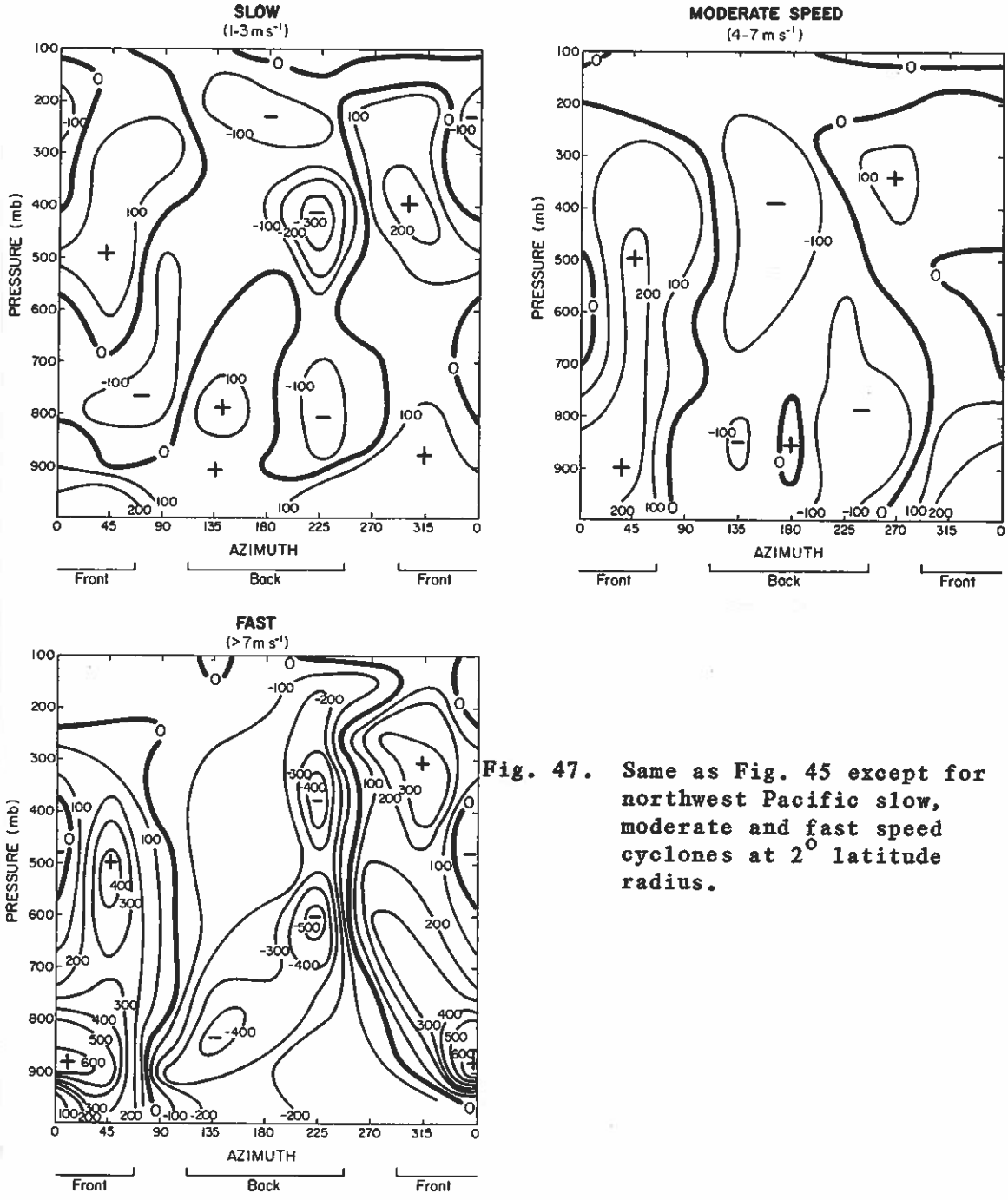

Fig. 47. Same as Fig. 45 except for northwest Pacific slow, moderate and fast speed cyclones at 2° latitude radius.

through a very deep layer of the troposphere. For moderate-speed cyclones this phenomenon is less obvious. For slow-moving cyclones, positive values of the residual are present above negative values in front of the cyclone. Xu and Gray (1982) pointed out that flow fields around slow-moving cyclones are weak and have different directions at different levels in the lower to mid-troposphere. The latter would cause different vorticity advection, and hence different residual, patterns at different levels. On the other hand, fast-moving cyclones have environmental flows that have similar directions at all levels up to the ouflow layer. The areas of maximum vorticity advection would therefore tend to be stacked in the vertical. The results presented here agree very well with their observations.

The residuals at 4^{o} for the three cases of cyclones in the northwest Pacific are depicted in Fig. 48. They show patterns similar to those at 2^{o}. Fast-moving cyclones have the largest residual, while the weakest residuals occur with slow-moving cyclones.

Comparing west Atlantic and northwest Pacific cyclones, the latter have, in general, stronger residuals for the same speed. This is because cyclones in the northwest Pacific are usually stronger in intensity than those in the west Atlantic. Therefore, for the cyclones moving at the same speed, the local change of relative vorticity is larger.

6.3.3 Relative Importance of Various Terms in the Vorticity Equation

The residual R computed using Eq. 57 represents the sum of the local change of relative vorticity $\partial\zeta/\partial t$, the frictional effects Z and any "sub-grid" effects that cannot be resolved by the grid point data used in the calculations. The last two effects are difficult to

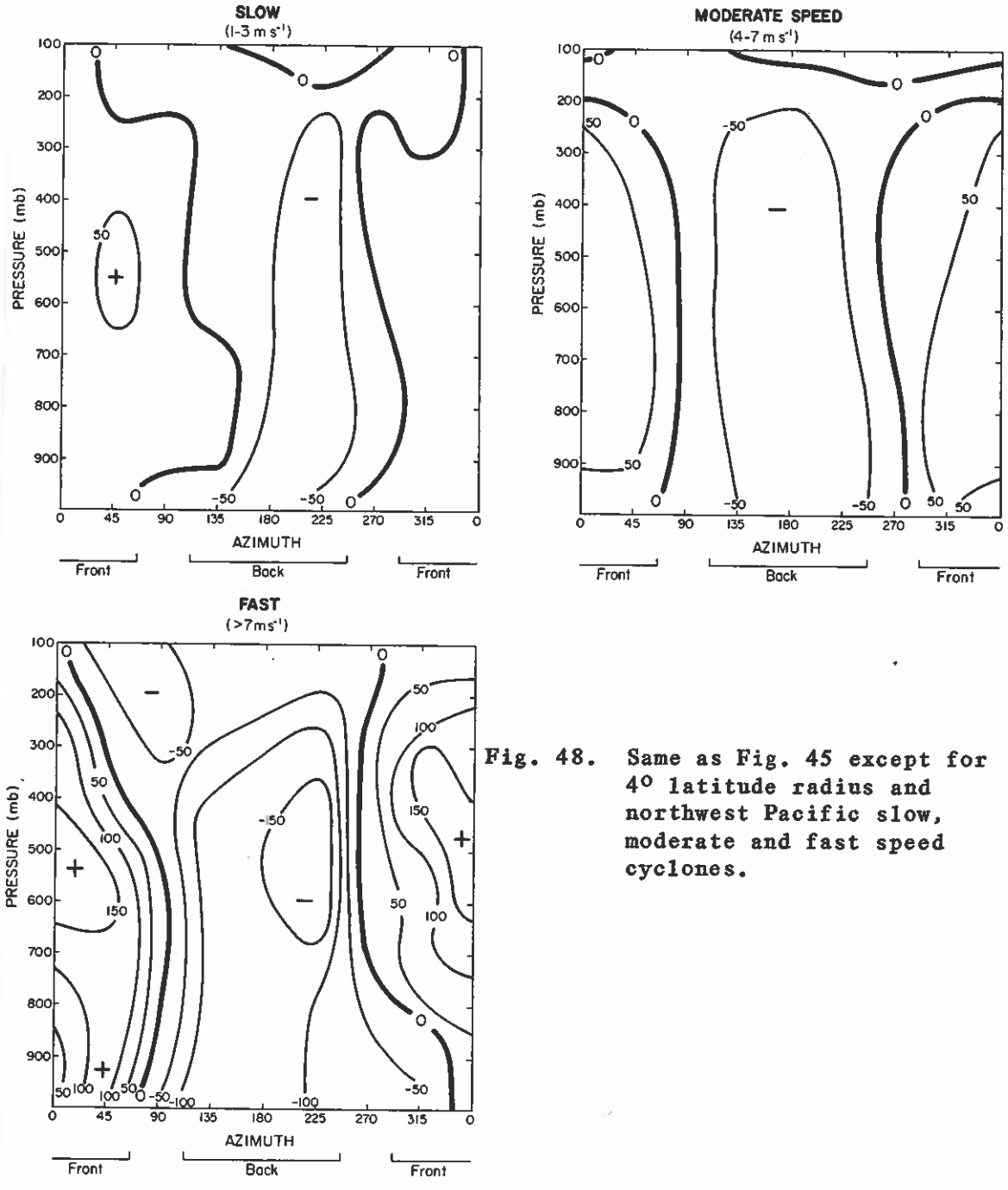

Fig. 48. Same as Fig. 45 except for 4° latitude radius and northwest Pacific slow, moderate and fast speed cyclones.

estimate. However, $\partial\zeta/\partial t$ can be estimated by moving the composite vortex with the mean speed of the composite for a short time and then calculating the change in ζ at each grid point, with the assumption that the intensity of the cyclone is in steady-state. The $\partial\zeta/\partial t$ calculated this way can then be compared with the residual R.

As discussed in Chapter 4, the azimuthal position of maximum $\partial\zeta/\partial t$ varies with the amount of convergence, the presence/absence of a cross-wind, the variation in speeds of the environmental flow, etc. In the speed composite data sets studied here, no consideration was given to these conditions when the cases were selected. Therefore, it would not be meaningful to study the various parameters at one azimuthal location. However, if the values of these parameters are averaged for the three azimuthal locations in front of the cyclone (that is, octants 2, 1 and 8 in Fig. 4), those variations among individual cases mentioned earlier might be averaged out and the comparisons will provide some insight into the importance of the various terms in the vorticity equation.

Figure 49 shows the average between octants 2, 1 and 8 (azimuth between 335^{o}-45^{o}) at 2^{o} latitude radius of all the terms in the vorticity equation, including the estimated local change of relative vorticity at various levels for slow and fast-moving cyclones in the west Atlantic. In general, the tilting and vertical advection terms are relatively small and have opposite signs. They both have maximum values at ~300-400 mb where the mean vertical motion is the strongest. The divergence term appears to be very important in both the upper and lower troposphere. However, in the mid-troposphere, the most dominant term is the horizontal advection of absolute vorticity. The estimated local change in relative vorticity has magnitudes very similar to those of the

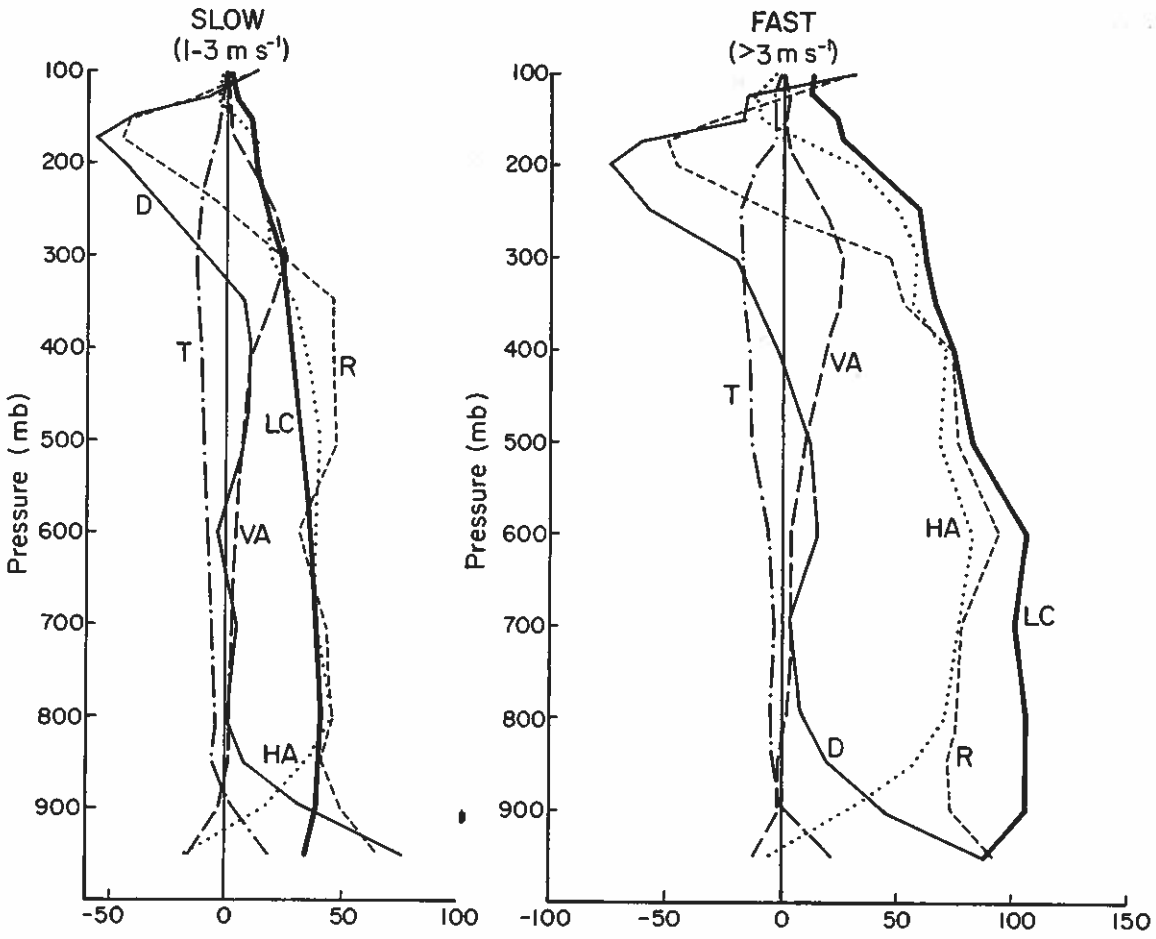

Fig. 49. Vertical variation of parameters in the vorticity equation in front of the cyclone (average between octants 2, 1, and 8 - Fig. 4) at 2° latitude radius for slow- and fast-moving cyclones in the west Atlantic. The labels are LC - local change of relative vorticity, R - residual, HA and VA - horizontal and vertical advection of absolute vorticity respectively, D - divergence term and T - tilting term. The unit is 10^{-6} s^{-1} d^{-1}.

residual in the middle levels. In the upper troposphere, because of the divergence term, the value of R far exceeds that of the estimated local change. This suggests that in the mid-troposphere, the frictional and sub-grid effects are not very important while at the upper levels, they are very significant, acting as an additional vorticity 'source'. This result is in qualitative agreement with Lee's (1982) computations of sub-grid scale effects for tropical cyclones. In general, all the terms in fast-moving cyclones are larger in magnitude than those in slow-moving cyclones.

Similar results are obtained at 4^{o} latitude radius, except that the magnitudes are smaller, as shown in Fig. 50. Notice that in the mid- to lower troposphere, both the tilting and the vertical advection terms are negligible. This, therefore, justifies the dropping of these two terms in the analytical study presented in Chapter 4.

These results clearly demonstrate the relation between the vorticity budget and cyclone motion. By computing the residual using Eq. 57, one can get a very good estimate of the local change of relative vorticity, at least in the mid-troposphere. Here, the most important contribution to the residual is the horizontal advection of absolute vorticity. This, of course, is the basic assumption in barotropic track prediction models (see for example, Sanders and Burpee, 1968; WMO, 1979). These results give a general verification of this assumption. However, forecast models that use a deep tropospheric mean flow might not be as appropriate as the middle level data because the horizontal vorticity advection and the local vorticity change terms differ very much below ~800 mb and above 300 mb.

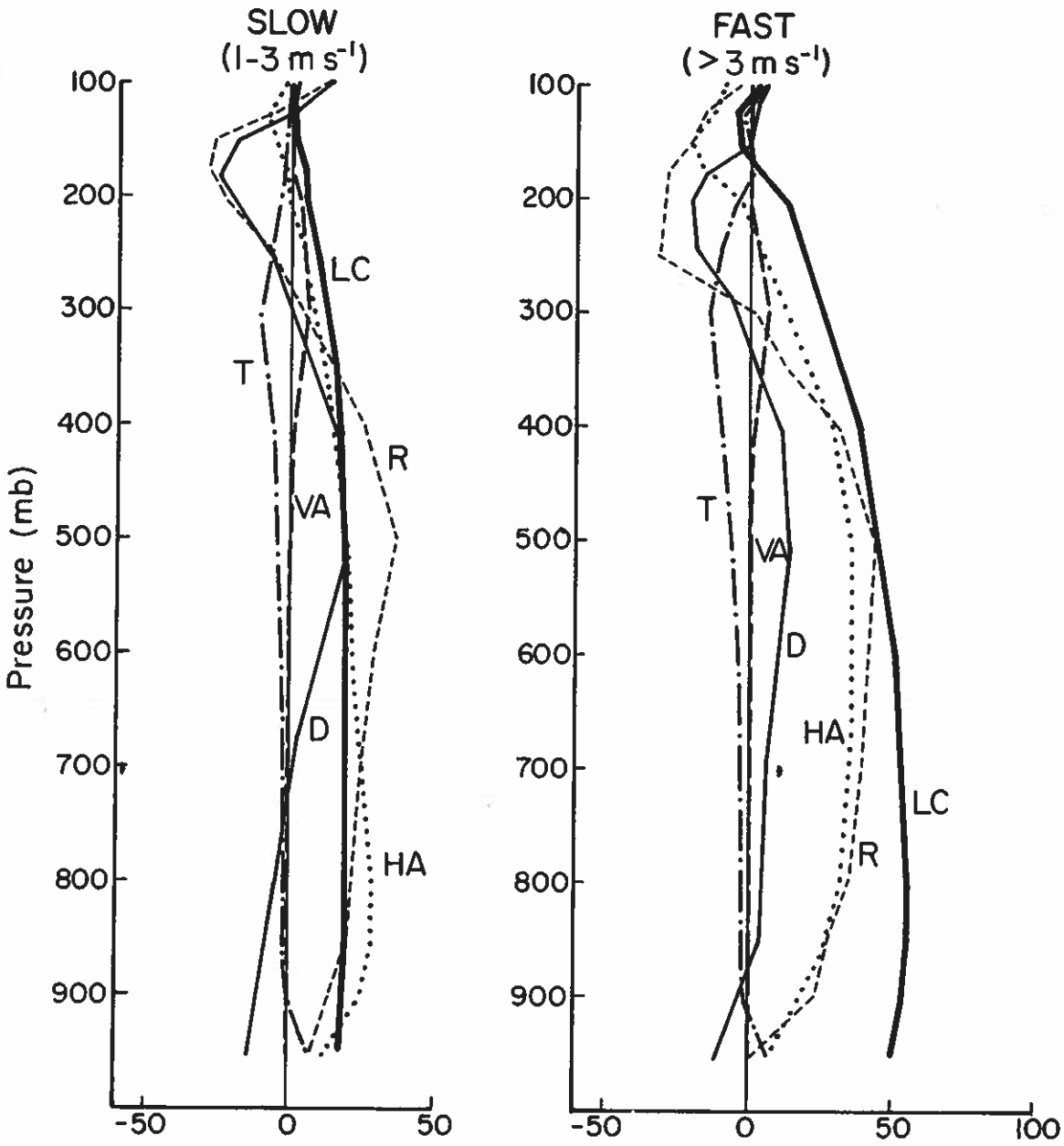

Fig. 50. Same as Fig. 49 except at 4° latitude radius.

The vertical variations of the terms in the vorticity equation for northwest Pacific speed composite cyclones at 2^{o} latitude radius are shown in Fig. 51. In general, all terms have a larger magnitude compared with those for west Atlantic cyclones. The tilting and vertical advection terms are also relatively small. The divergence term for slow-moving cyclones varies considerably in the vertical, contributing to a large variation of the residual. However, the horizontal advection of absolute vorticity still provides a good estimate of the local change of relative vorticity in the mid- to upper troposphere. The moderate and fast speed cyclones have smoother profiles of the divergence term. Nevertheless, the horizontal advection term is still a better estimate of the local change than the residual. The existence of such differences between the local change of relative vorticity and the residual for northwest Pacific cyclones suggests the importance of sub-grid scale effects at this relatively close distance from the cyclone center. The presence of such apparent vorticity sources and sinks are not as obvious in west Atlantic cyclones, except in the upper troposphere. This is probably because northwest Pacific tropical cyclones are, in general, bigger and stronger so that sub-grid scale effects at around 2^{o} latitude radius are important.

At 4^{o} latitude radius, the curves are relatively smoother, as shown in Fig. 52. Now, the residual approximates the local change in relative vorticity very well in the mid-troposphere for all the three cases. This apparently is a result of the diminishing effect of the divergence term. For fast-moving cyclones, a large difference between R and $\partial\zeta/\partial t$ still exists in the lower troposphere.

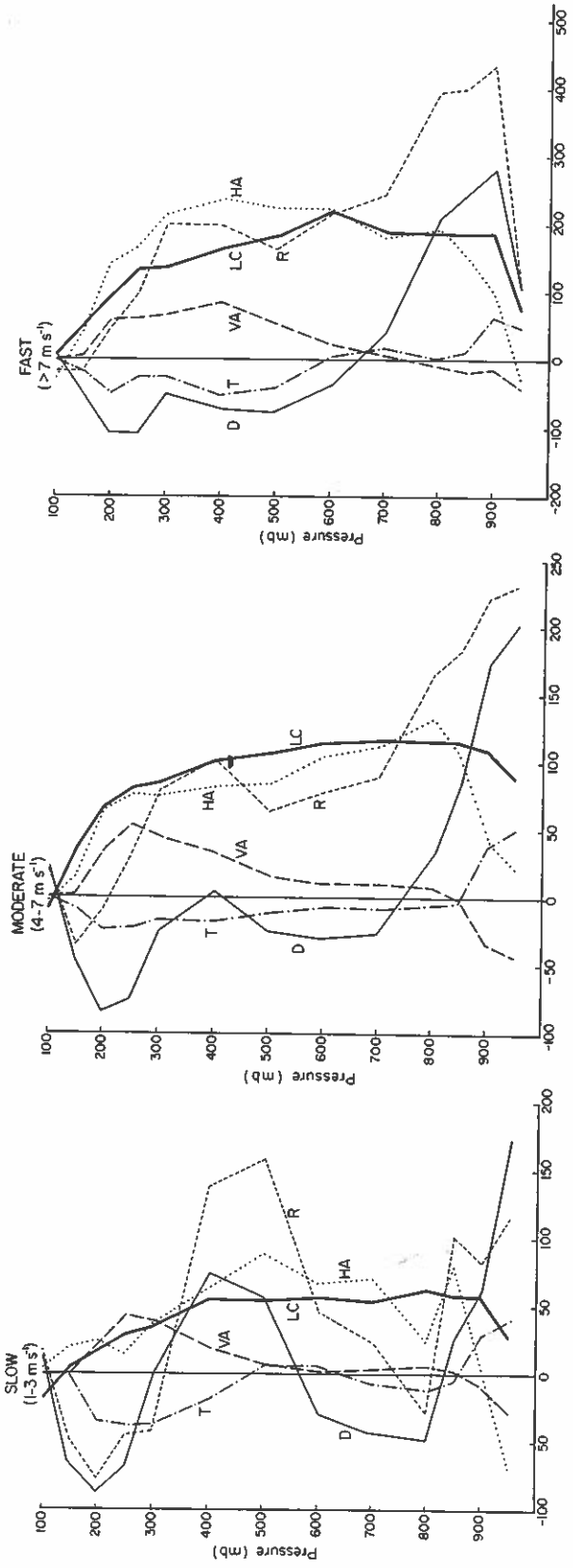

Fig. 51. Same as Fig. 49 except for speed composite data sets in the northwest Pacific at 2° latitude radius. Note the change in scale for the fast-moving data set.

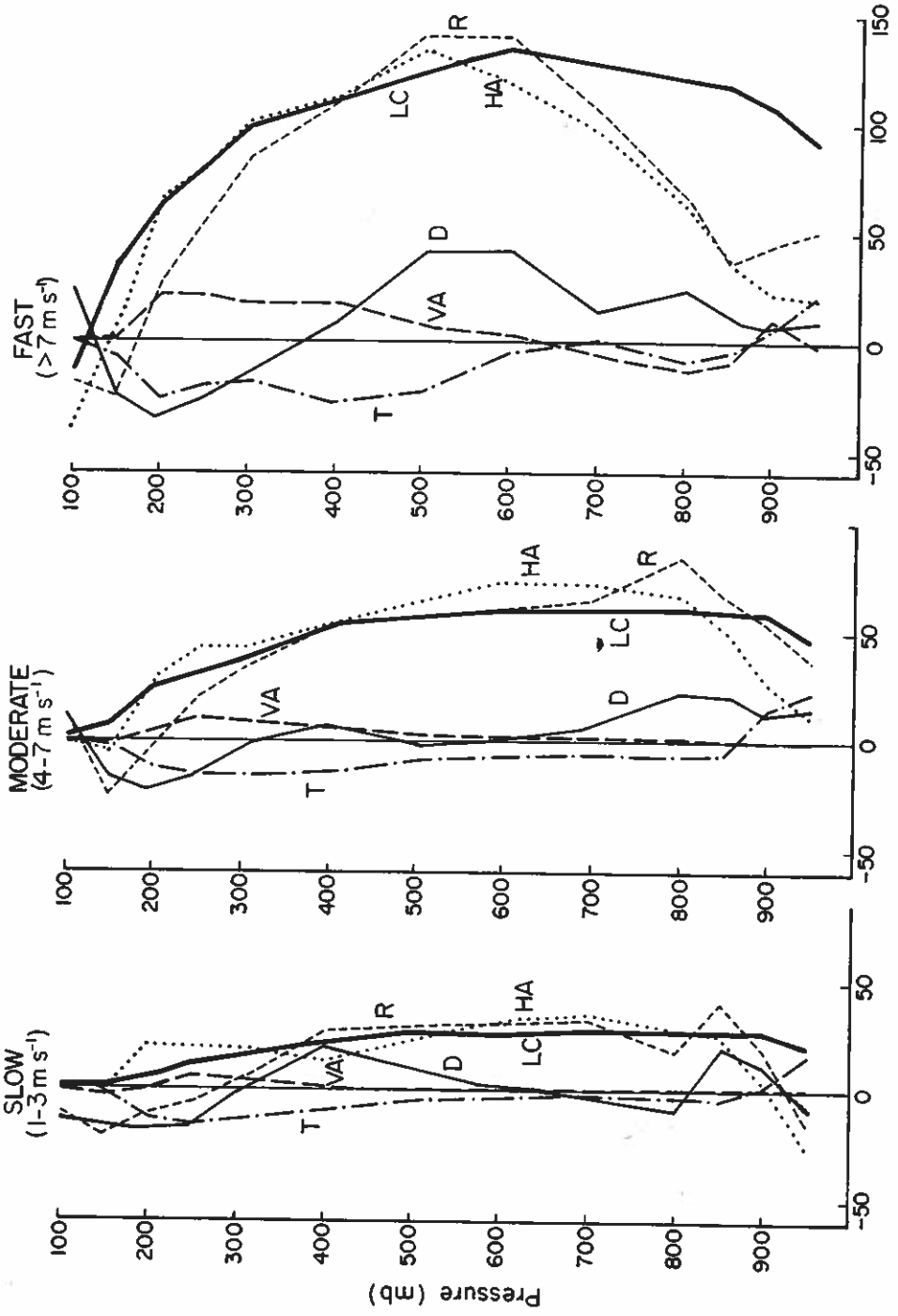

Fig. 52. Same as Fig. 49 except for speed composite data sets in the northwest Pacific and at 4° latitude radius.

The profiles of the various terms in the vorticity equation for speed composite data sets in the two ocean basins are remarkably similar. This lends confidence to the validity of these results. They appear to demonstrate the usefulness of estimating the local change of relative vorticity through the calculations of the residual, at least in the mid-troposphere. These results also point to the predominance of the horizontal advection term in determining the local change in relative vorticity at middle levels. Since the local change of relative vorticity increases with cyclone speed, these calculations suggest the possibility of relating the vorticity tendency to cyclone speed.

As pointed out earlier, it is not possible to study the terms in the vorticity equation at one azimuthal location for these data sets because the cyclone speed is the only criterion used in their selection. However, the turning motion data sets of Chan et al. (1980) have well-defined directional changes. Therefore, it should be possible to analyze the terms in the vorticity equation at different azimuths. Section 4.6 has shown that very significant differences in the local change of relative vorticity between the front left and front right octants exist when different cross-wind profiles are present. The next section will show from observations that this is indeed the case.

6.4 Turning Motion Data Sets

These are the same data sets studied in section 5.5 and by Chan et al. (1980). The results in section 5.5 seem to suggest the presence of conditions in the environment that are conducive to a directional change of a cyclone at 12 h before such a change takes place. It is therefore of great interest to analyze the vorticity budget at this time (T-12) as

well as at the turn time T. The smoothing scheme discussed in section 6.3.1 was also applied to these data sets.

Since the relative vorticity can be calculated at each time period, the local change in relative vorticity ($\partial\zeta/\partial t$) between T-12 and T can be easily derived using the method of graphical subtraction. The level that shows the best correlation between this local change and subsequent cyclone motion is 500 mb. Results are shown in Fig. 53. Two positive maxima of $\partial\zeta/\partial t$ are present near the center of a left-turning cyclone, one situated in front and the other to the left. The largest negative maximum occurs between octants 5 and 6 (rear and right-rear, respectively). For straight-moving cyclones, the positive maximum is in front of the cyclone and slightly to the right of the direction of cyclone movement at time T. Right-turning cyclones clearly have a maximum local change of relative vorticity to the right front of them. These results are consistent with the analysis made in the theoretical study described in section 4.6.

Since the local change in relative vorticity occurs between T-12 and T, the environment must have induced such a change at some intermediate time between these two time periods. To find out which processes are important in producing the local change, one would need to know the flow field at that intermediate time. Since this is not possible, the best alternative is to analyze the flow field at time T. This would tend to overestimate the local change because the $\partial\zeta/\partial t$ derived from the graphical subtraction of the relative vorticity fields can only be considered as the time average during those 12 h while that

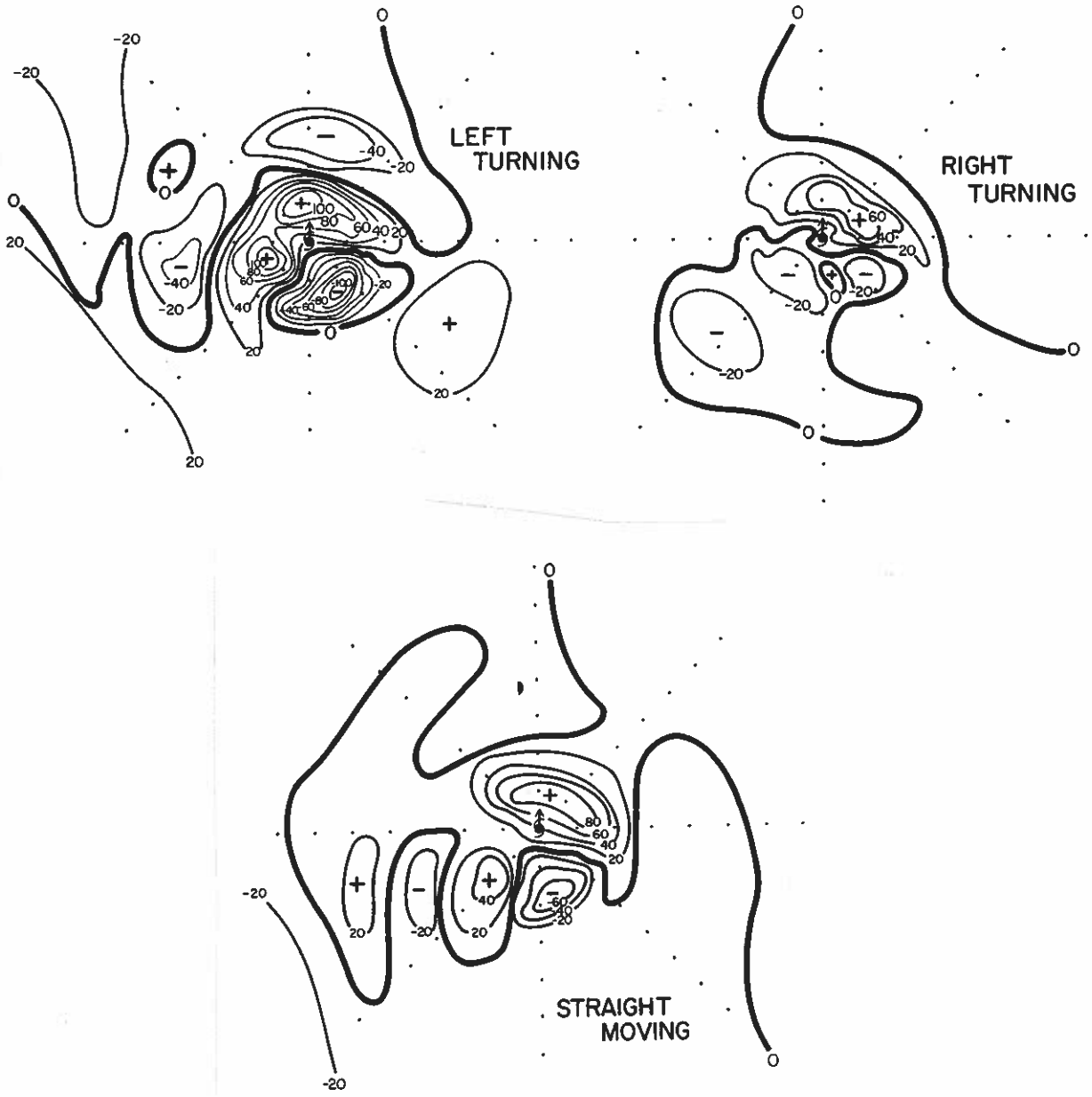

Fig. 53. The 12 h local change in relative vorticity (in units of 10^{-6} s^{-1} d^{-1}) at 500 mb between turn time (T) and 12 h before turn time (T-12) for turning and straight-moving cyclones in the west Atlantic. The arrow indicates the instantaneous direction of cyclone movement. The grid spacing is 2° latitude (222.2 km).

calculated from the flow field at turn time is the instantaneous, and probably maximum, value.

Plan views of the horizontal advection of absolute vorticity at 500 mb and turn time T for the three classes of cyclones are shown in Fig. 54. Inside 4^{o} latitude radius, left-turning cyclones have maximum horizontal vorticity advection to the left front while such a maximum occurs on the right front side for right-turning cyclones. Straight-moving cyclones have two positive maxima, one on each front side of the cyclone as well as a large positive area in front of the cyclone. The positive area in the turning cases is much smaller and more concentrated. The advection of the earth's vorticity is much smaller than that of the relative vorticity at both 2 and 4^{o} latitude radius.

Such vorticity advection patterns are a result of the distribution of relative vorticity, which is shown in Fig. 55. For left-turning cyclones, the maximum relative vorticity is in front of the cyclone. Therefore, a cyclonic tangential wind would tend to advect the vorticity to the region left of the present cyclone direction. In addition, a positive radial wind would also give a maximum advection in this area. Straight-moving and right-turning cyclones both have maximum vorticity at the right hand side. However, the gradient of relative vorticity is a maximum to the right front of right-turning cyclones while the strongest gradient for straight-moving cyclones is in the front. Therefore, radial advection of relative vorticity would result in the observed advection patterns in Fig. 54.

The other term that might contribute significantly to the local change in relative vorticity is the divergence term. Plan views of this at 500 mb are shown in Fig. 56. For left-turning cyclones, this term is

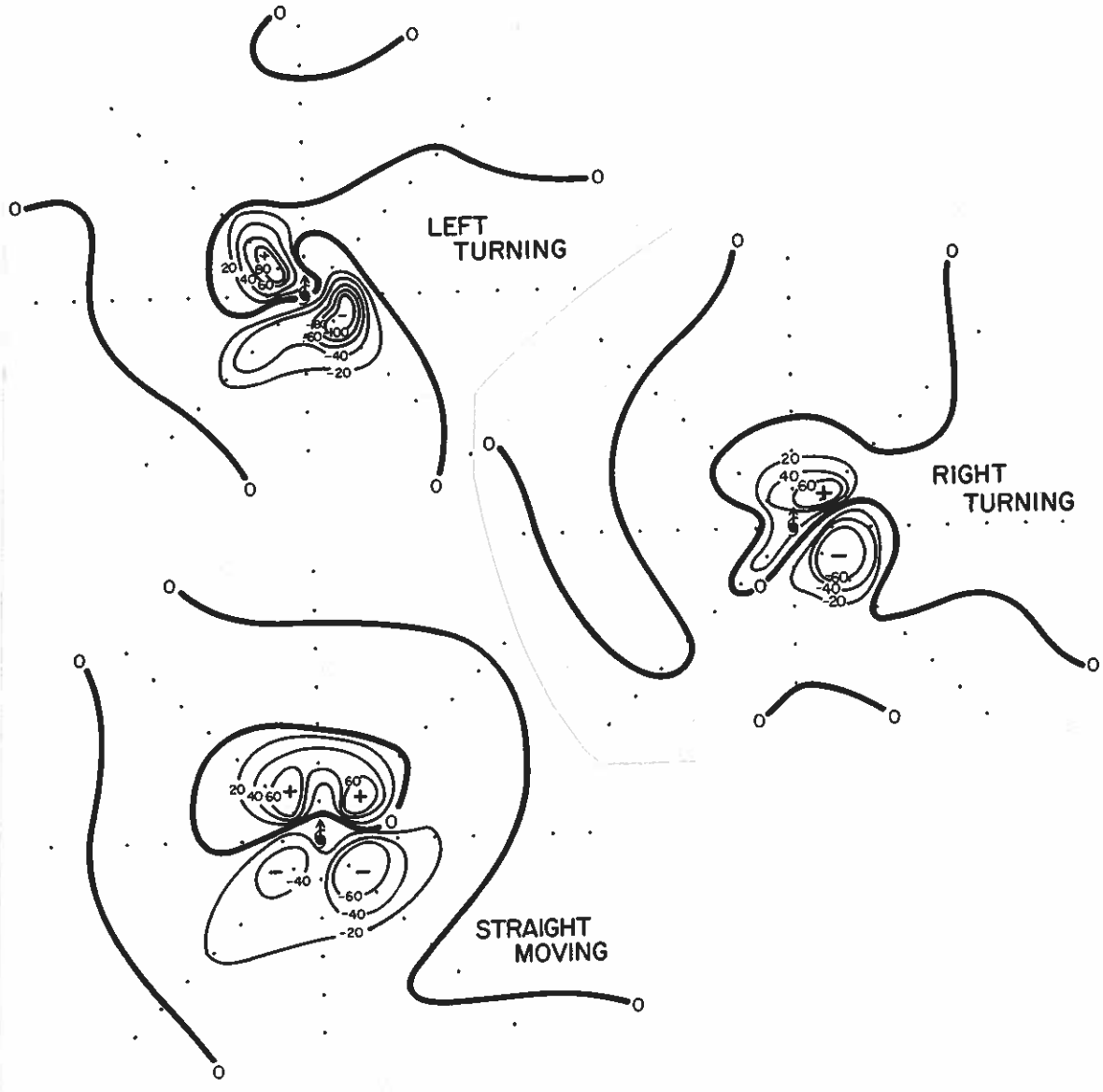

Fig. 54. Horizontal advection of absolute vorticity (in absolute vorticity (in units of 10^{-6} s^{-1} d^{-1}) at 500 mb and turn time (T) for turning and straight-moving cyclones in the west Atlantic. The arrow indicates the instantaneous direction of cyclone movement. The grid spacing is 2° latitude (222.2 km).

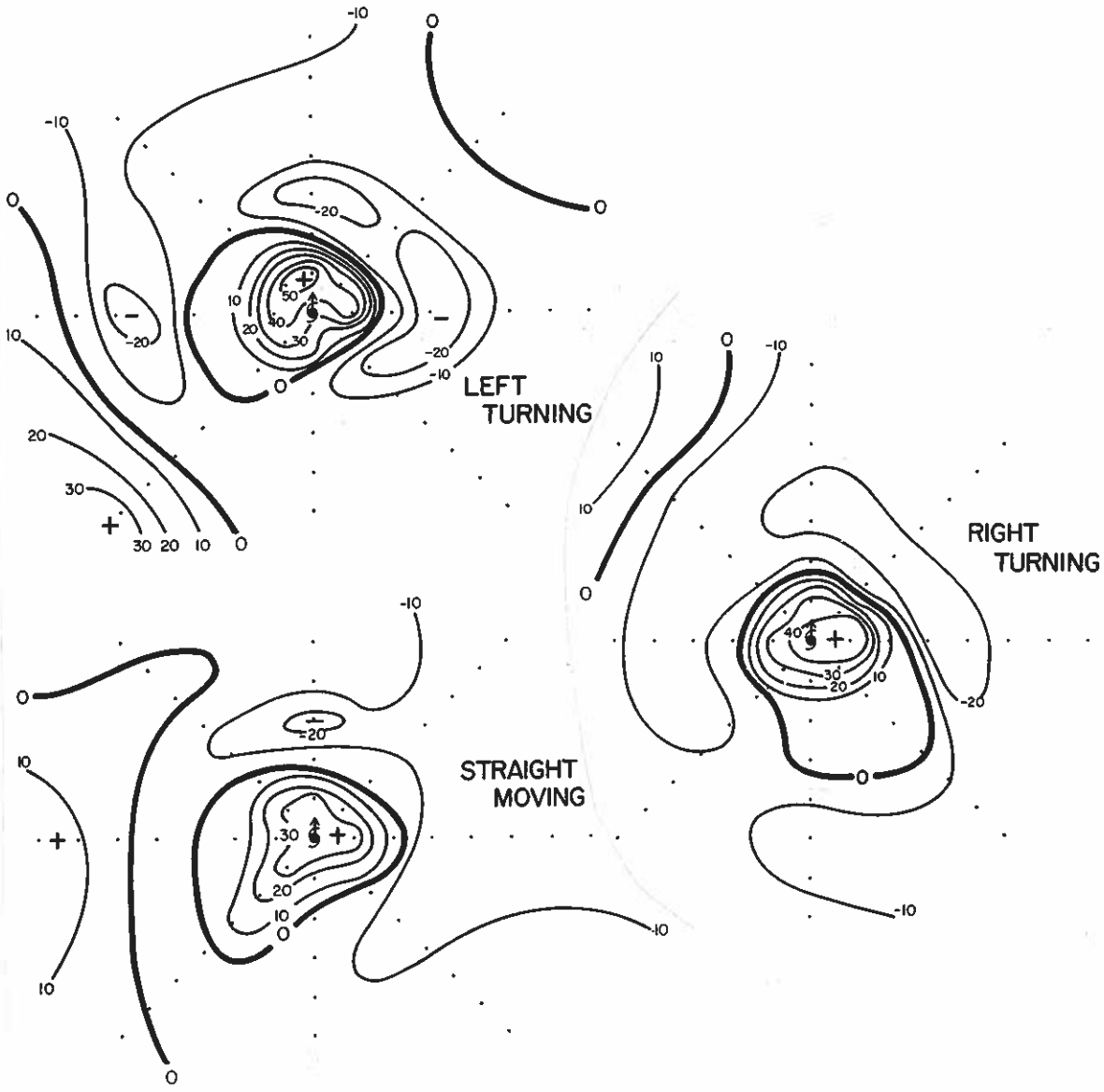

Fig. 55. Same as Fig. 54 except for the relative vorticity (in units of 10^{-6} s^{-1}).

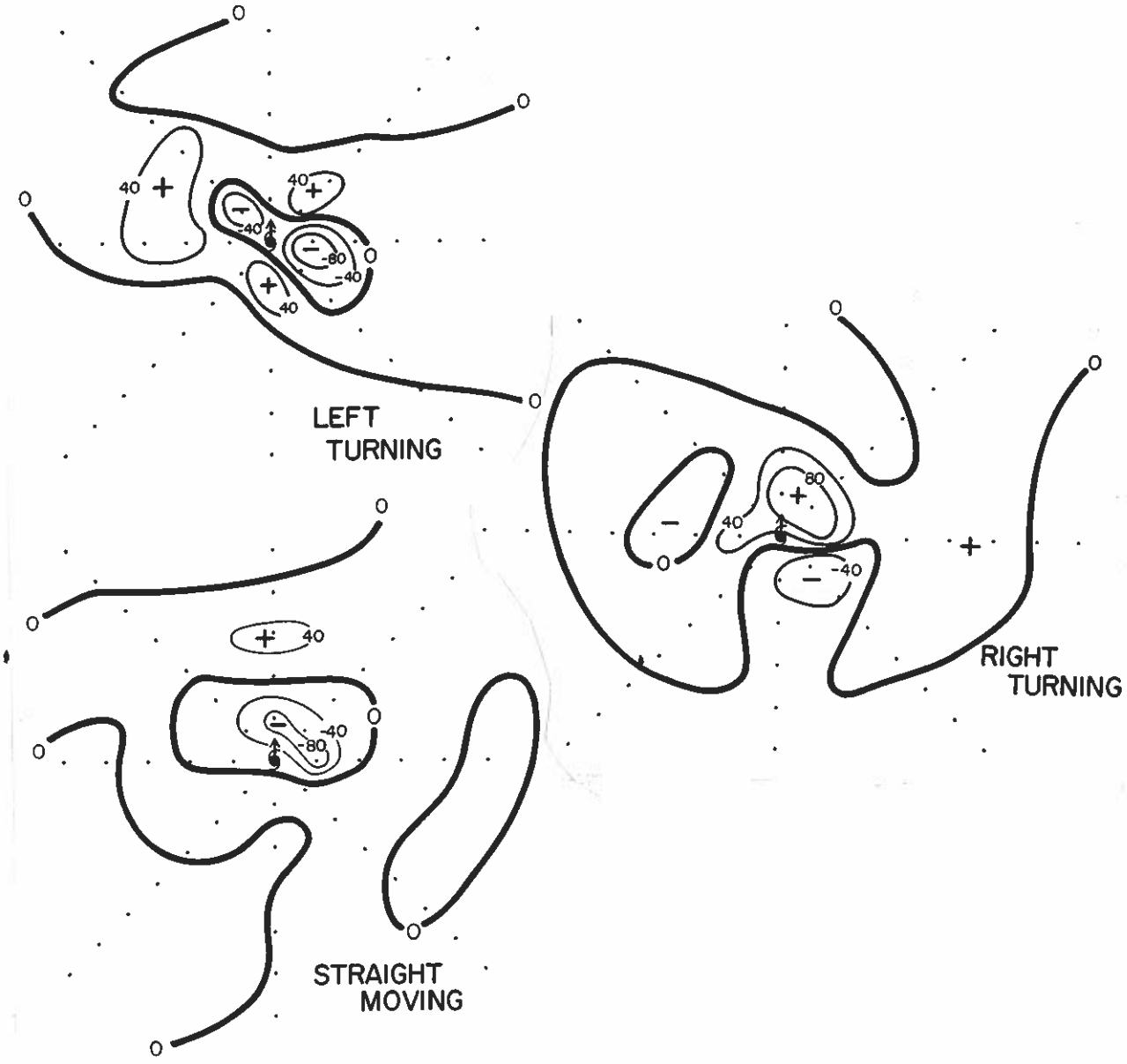

Fig. 56. Same as Fig. 54 except for the divergence term $(-(\zeta+f)\nabla\cdot \mathbf{V})$.

negative to the left-front but is weaker than the advection term. Therefore, the net effect would still be positive, giving the local change pattern in Fig. 53. Right-turning cyclones have positive values to the right front and thus cooperate with the advection term to produce a maximum positive local change in this area. The divergence term is generally negative for straight-moving cyclones. This almost "equalizes" the positive contribution of the advection term. However, at 700 mb, the advection term is much larger than the divergence term, giving a net positive contribution (not shown). Therefore, straight-moving cyclones might actually be affected by the flow at a level lower than that for turning cyclones.

These results clearly suggest the link between local change of relative vorticity and a change in direction of cyclone movement. Again, as in the last section, the horizontal advection of relative vorticity is the main contributor to this local change with the divergence term playing a secondary role. The tilting and vertical advection terms, although not shown here, tend to be small.

6.5 Summary

The results presented in this chapter all point to the importance of calculating the local change of relative vorticity in the determination of tropical cyclone motion. They also suggest that the best way to estimate this local change in the mid-troppposphere is to compute the horizontal advection of relative vorticity. The basic question, however, still remains. That is, how does the cyclone respond to a local change in relative vorticity and move towards the area with a positive maximum? This will be addressed in the next chapter.

CHAPTER 7 - PHYSICAL PROCESSES RESPONSIBLE FOR CYCLONE MOTION

7.1 Review of Previous Results

In Chapter 4, an analytical study of a simplified, divergent, barotropic vorticity equation on a β-plane was presented. The results suggests a possible relationship between the local change of relative vorticity and tropical cyclone motion. These model results also helped explain some of the observational findings in Chapter 2. Vorticity budgets computed from composite flight and rawinsonde data around tropical cyclones (Chapter 6) confirm the link between vorticity tendency and cyclone motion.

Chapter 5 gives a different perspective of cyclone motion. The balance between the centrifugal, the Coriolis and the pressure-gradient forces when an environmental flow is superimposed onto the vortex circulations was investigated. Observations demonstrate the existence of a wind-pressure imbalance that was also predicted from a simple theoretical treatment. Such imbalances appear to be related to cyclone speed as well as changes in cyclone direction.

Since the results obtained from these two approaches (vorticity tendency and wind-pressure imbalances) are both related to cyclone motion, a physical link must exist between them. In the remaining sections of this chapter, such a link will be discussed in terms of a hypothesis of the possible physical processes involved in cyclone motion. This hypothesis will be verified using the turning motion data sets studied in Chapters 5 and 6.

7.2 A Physical Hypothesis

In Chapter 5, it was shown that the wind-pressure imbalance increases with the speed of the cyclone. In Chapter 6, the local change of relative vorticity was also found to increase with cyclone speed. It is hypothesized that these two processes are physically linked in the following way. Air parcels on the right hand side (RHS) of a cyclone with trajectories like the ones portrayed in Fig. 33 will tend to bring the vorticity towards the front of the cyclone. The stronger the imbalance, the farther to the front will these air parcels travel before being forced back. In this way, the increase in vorticity will be at a greater distance and over a larger area in front of the cyclone. Since the speed of a cyclone is given by the ratio of the local increase in vorticity to the radial vorticity gradient, a maximum increase at a location that is farther away from the present position of the cyclone (and hence weaker vorticity) would give a larger ratio and hence a larger vortex speed. Therefore, the superposition of the environmental and vortex flows can be viewed as providing a mechanism for the increase in vorticity in front of the cyclone.

In the case of cyclones that change direction under the influence of a cross-wind, a new wind-pressure imbalance between the front and back of a cyclone was found to be present. The trajectories of air parcels are more complicated. However, they will probably be altered in such a way as to allow an increase in relative vorticity to take place in the future direction of the cyclone in a manner described above.

So far, it has been established that the movement of a cyclone is closely related to the area of positive maximum $\partial\zeta/\partial t$. This local increase can be explained in terms of the trajectories of air parcels as

described above or the different terms in the vorticity equation as discussed in Chapters 4 and 6. The question that still remains is: how does this local change in relative vorticity actually cause the cyclone to move? A physical mechanism will now be proposed.

Because of the increase of relative vorticity, the circulation in this area would tend to spin up (that is, an increase in the tangential wind) more than that in other parts of the cyclone. Since this spin-up occurs over a relatively small area, as evidenced by the results in Chapter 6, the theory of geostrophic adjustment (see for example, Schubert et al., 1980) requires that the mass field adjusts to such a wind perturbation. The most efficient way for the mass field to adjust to this imbalance is through subsidence. The subsiding air then adiabatically warms the air column around the area of maximum spin up. The warming would lower the surface pressure and create a new low pressure center with cyclonic circulation. Therefore, it appears that the center of the cyclone does not move in the physical sense but rather "propagates", with new centers of circulation continually forming in the area of maximum positive $\partial\zeta/\partial t$. In other words, the tropical cyclone does not appear to move like a solid cylinder being "pushed" along by the environmental flow. Rather, the eye wall cloud continually forms around a new center of circulation and dissipates around the 'old' center or eye. Gray and Shea (1973) also speculated the formation of the eye of a tropical cyclone as a continual process of ventilation of air within the eye and the subsequent sinking and warming of air in the direction of the cyclone motion.

The forced subsidence suggested in this hypothesis would imply divergence (convergence) in the lower (upper) troposphere. This would

lead to a spin-down (spin-up) in the lower (upper) troposphere from the vorticity equation, an unfavorable condition for maintaining the tropical cyclone. Therefore, the horizontal advection of absolute vorticity must be able to overcompensate this loss (gain) in relative vorticity due to the stretching process. In view of this 'complication', the chain of events that lead to the eventual propagation of a tropical cyclone may be like the one described below and schematically portrayed in Fig. 57.

The superposition of the vortex and environmental flows, and the effect of the differential in the Coriolis parameter across the cyclone cause an increase in relative vorticity in one area of the cyclone as a result of the advection of absolute vorticity. This vorticity advection can be viewed from the kinematic trajectory perspective or from the dynamic perspective of the 'coupling' of the wind and the absolute vorticity gradient. In either case, the increase in relative vorticity would lead to an imbalance between the wind and pressure fields. The atmosphere tries to restore balance through subsidence. This forced subsidence gives rise to two processes: 1) it adiabatically warms the air column and lowers the surface pressure, and 2) the divergence associated with it spins down the vortex in the lower troposphere. This second process would reduce the increase in relative vorticity due to the advection of absolute vorticity. However, the advective term is usually greater than the divergence term (see the discussion in section 6.4) and therefore the result is still a net increase in relative vorticity. This net spin up creates the new wind center and the lowering of the surface pressure caused by process (1) described above

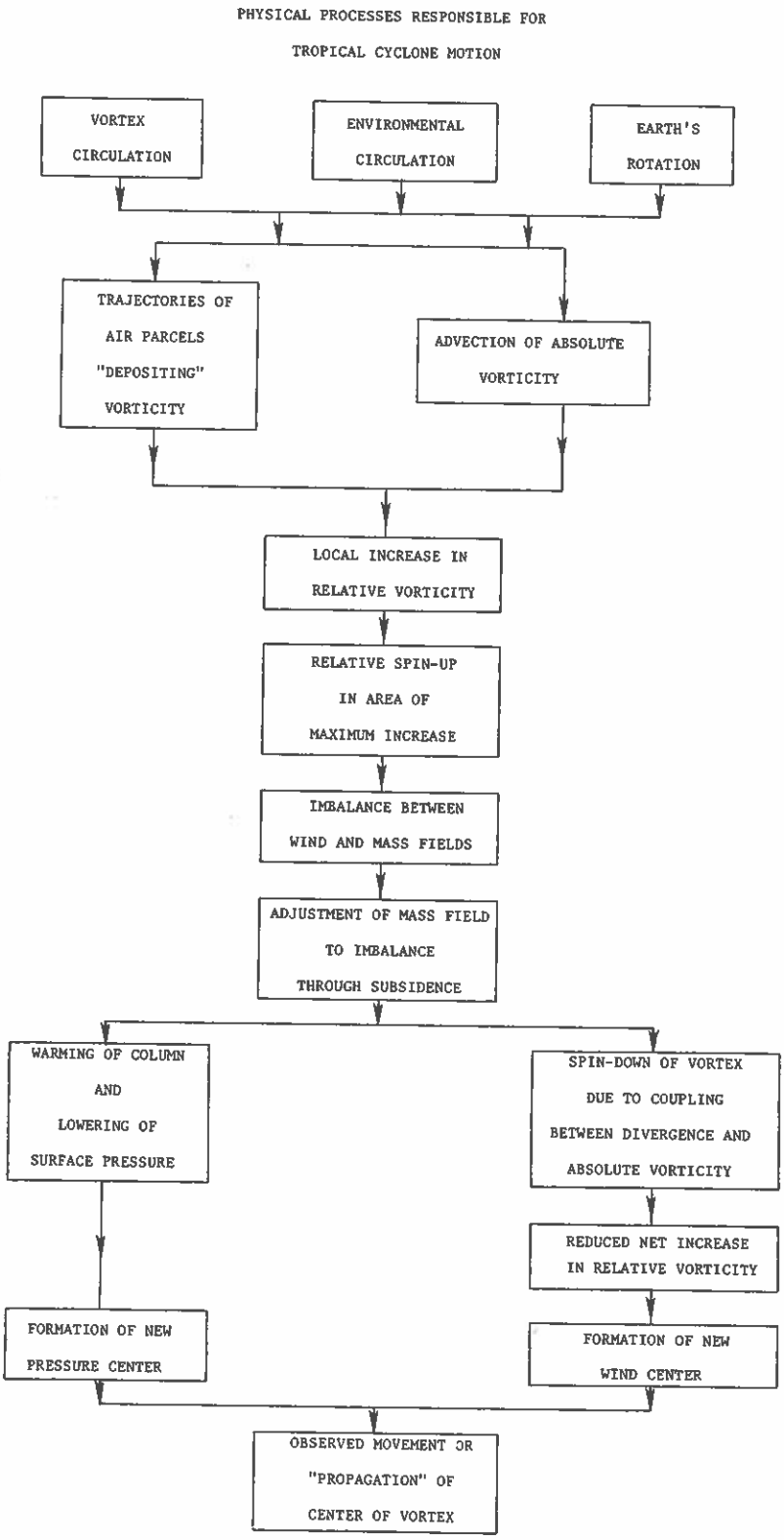

Fig. 57. Flow diagram of the proposed physical processes responsible for tropical cyclone motion.

produces the new pressure center. Thus, the vortex is seen to have moved when in fact it has 'propagated'.

The best way to demonstrate the validity of this hypothesis is to study the vertical motion patterns as a function of time and compare them with the time variation of the direction and speed of a cyclone. This is, of course, impossible at this stage because of the lack of observations of vertical motion. The next alternative is to analyze the composite data. However, one has to be very careful with such an analysis. This is because cyclones move in a myriad of directions and speeds. A composite that might be able to resolve this type of physical processes has to consist of cyclones having very similar track characteristics. The best data set available is that relating to turning motion which has been extensively studied in Chapters 5 and 6. Although cyclones in each class might not be traveling at exactly the same speed, the difference in speed is not very large. More importantly, they all had a significant change in direction. This should enhance differences in vertical motion fields between the data sets.

7.3 The Physics of Turning Motion

In section 6.4, it was shown that the maximum local change of relative vorticity is to the left-front for left-turning cyclones and right-front for right-turning cyclones. Therefore, the vertical motion profiles in these two areas (octants 2 and 8 respectively, see Fig. 4) will be compared.

These profiles at turn time at 2 and 4^{o} latitude radius are shown in Fig. 58. In octant 2 (left-front), both left-turning and straight-moving cyclones have downward vertical motion while right-turning

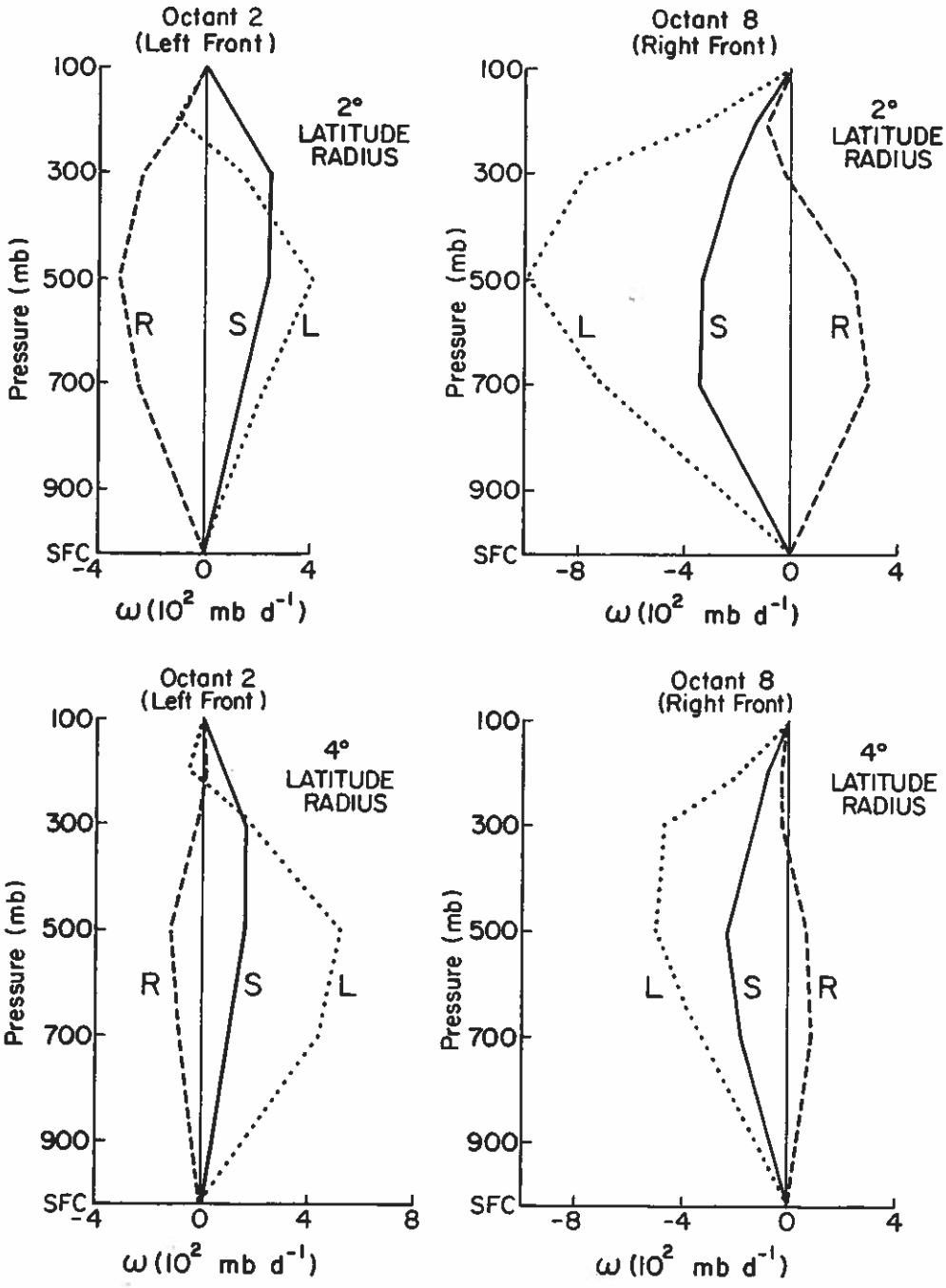

Fig. 58. Vertical motion (p-velocity) profiles of left-turning (L), straight-moving (S) and right-turning (R) cyclones at turn time and 2 and 4° latitude radius in octants 2 (left-front) and 8 (right-front). The unit is 10^2 mb d^{-1}. Positive values indicate downward motion.

cyclones have rising motion. The opposite is true in octant 8 (right-front). The profiles are very similar at 2 and 4^{o} latitude radii, with the ones at 4^{o} having smaller magnitudes. These profiles correspond to what the present physical hypothesis would suggest. Straight-moving cyclones appear to have a tendency to move leftward of the present direction, since their vertical motion profiles are similar to those of left-turning cyclones.

These results also bring up another interesting point. On the side which the cyclone is not turning into, upward motion exists. This implies convection is probably more prevalent in this area. On the other hand, the side into which the cyclone is turning has subsidence, suggesting a reduction in convective cloudiness. Therefore, a comparison of the amount of convection between the left and right sides of a cyclone might provide some clues as to the future direction of movement of the cyclone. This, in fact, has been proposed by Lajoie (1976) from analyses of satellite pictures.

As discussed in the last section, the vertical motion profiles in Fig. 58 must be accompanied by different divergence profiles. These are shown in Fig. 59. In general, divergence (convergence) exists at lower (upper) levels in the area which the cyclone is turning into (octant 2 for left-turning and octant 8 for right-turning) while in the other area, the reverse is true. The divergence in the lower troposphere in the area which the cyclone is turning into would produce a spin down. Such a spin down is compensated by the advection term so that the net effect is still a spin up of the region. This has been discussed in the last section.

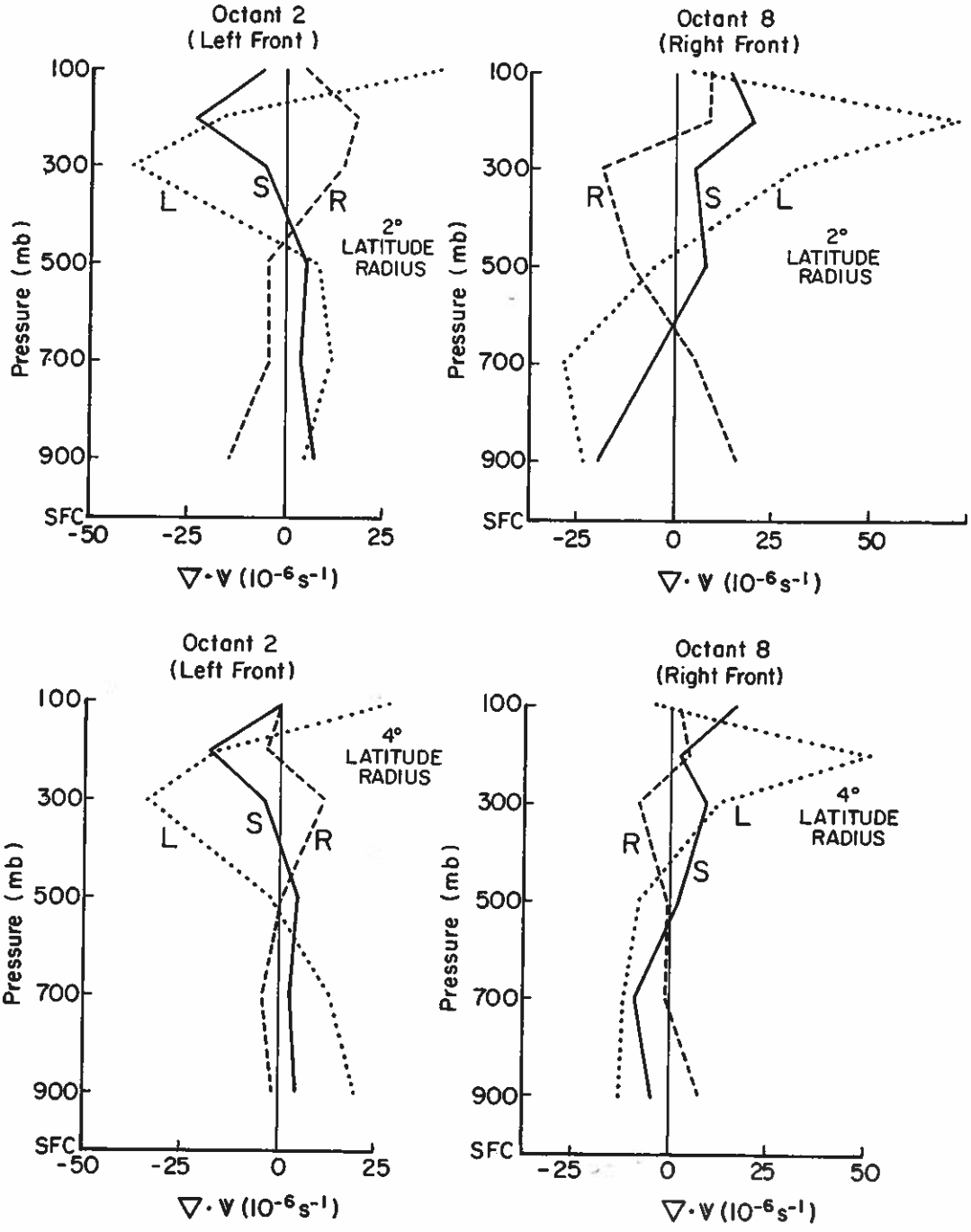

Fig. 59. Same as Fig. 58 except for divergence (in units of 10^{-6} s^{-1}).

These results appear to demonstrate the validity of the hypothesis proposed in the last section. They also provide the basis for a model to explain the physical processes involved with changes in the direction of cyclone motion. At 12 h before any such changes occur, the cyclone moves into an environment which has a cross-wind component. This modifies the trajectories of air parcels and the vorticity advection patterns, resulting in the maximum vorticity tendency in the next 12 h to be at an angle to the present direction of cyclone movement. Such a vorticity change perturbs the wind field, forcing the mass field to adjust through subsidence. The subsequent warming then lowers the surface pressure and eventually forms a new circulation center. The tropical cyclone will therefore be observed as "turning" while in fact the center starts to propagate in a new direction.

CHAPTER 8 - CONCLUSION

8.1 Summary

This study is an attempt to understand, from both observational and theoretical approaches, the physical processes responsible for tropical cyclone motion. To provide an observational basis for such a study, the relation between the synoptic-scale flow around tropical cyclones and cyclone movement was first established. It was found that in the Northern Hemisphere, cyclones generally move to the left of and faster than their surrounding flow while cyclones in the Southern Hemisphere tend to move more to the right of this flow. These general results are in agreement with previous steering flow studies (George and Gray, 1976; Gray, 1977; Brand et al., 1981; etc.). Cyclones having a large zonal component of motion, however, behave somewhat differently. Westward-moving cyclones in the Northern Hemisphere move more to the right of their environmental flow than an average cyclone does. Eastward-moving cyclones, on the other hand, move more to the left of their environmental flow than an average cyclone does. The opposite is true for cyclones in the Southern Hemisphere.

A review of previous theoretical and numerical studies suggests the potential significance of the vorticity budget in determining cyclone movement. These studies also point to the importance of the latitudinal variation of the earth's vorticity in cyclone motion. To investigate further the contribution of each term in the vorticity equation to the vorticity tendency, an analytical study of the vorticity budget was

made. Starting with simple cases, the importance in tropical cyclone motion of the differential in the earth's vorticity across the cyclone was established. This observation was first made by Rossby (1948) although the physical processes he suggested appear to be incorrect. Other researchers also arrived at the same conclusion (for example, Adem and Lezama, 1960; Kasahara, 1957; Anthes and Hoke, 1975; Holland, 1982; etc.) based on the more physically reasonable explanation of the advection of earth's vorticity by the vortex flow. The coupling between the convergence/divergence of the vortex and the earth's vorticity differential was also found to be responsible for deflecting the cyclone away from the direction of its environmental flow and moving it faster than the speed of the mean flow. At the same time, the environmental flow is instrumental in moving the cyclone along the direction of the flow by advecting the vorticity of the vortex along. A combination of these two effects produces a maximum local change of relative vorticity at a location which corresponds to the generally observed cyclone movement, assuming that the cyclone would move towards this maximum. This result was also obtained by Holland (1982) using a slightly different approach. This physical idea is capable of explaining some of the observed relationships (presented in Chapter 2) between cyclone motion and its surrounding flow.

More complicated environmental flows were then superimposed onto the vortex. The resultant local changes of relative vorticity could be used in explaining a drastic change in direction or speed of a cyclone. These vorticity changes are again brought about by the interaction between the vortex and the environmental flows with their associated vorticity and divergence.

The interaction between the environmental and the vortex flows was further examined by computing the wind-pressure balance in the combined flow. A simple theoretical analysis suggests the existence of a wind-pressure "imbalance". Such an imbalance would produce radial accelerations of air parcels (on the left and right hand sides of the vortex) that can be explained in terms of the trajectories of the air parcels. In addition, the magnitude of this imbalance was found to be proportional to the environmental wind speed. This theoretical result was tested using both aircraft data and rawinsonde composites. The observed and predicted imbalances generally agree with each other. This study was then extended to analyze possible changes in the wind-pressure balance associated with sudden changes in the environmental flow using a data set which dealt with the turning motion of tropical cyclones. The results show the presence of an additional imbalance between the front and back sides of the cyclone. This additional imbalance appears ~12 h before the cyclone actually changes direction.

Before these results are linked to the vorticity changes, analyses of the vorticity budget were made on various rawinsonde composite data sets. The results generally verify the validity of the analytical study described earlier. They show that the main contributors to the local change in relative vorticity are the horizontal advection of absolute vorticity and the divergence terms in the vorticity equation. In the mid-troposphere, the advection term is usually much more predominant. The tilting and vertical advection terms are generally much smaller. The sum of all these terms appear to give a very good estimate of the local change in relative vorticity in the mid-troposphere. This

estimated local change relates very well to the speed and change in direction of tropical cyclones.

Results of these observational analyses and the analytical study establish a definite link between the local change in relative vorticity with tropical cyclone movement. Combining this with the study of the wind-pressure balance, the following hypothesis is advanced to describe the possible physical processes involved in cyclone motion.

The basic movement of a cyclone is a result of the interaction/superposition of the environmental and the vortex flows. This interaction produces trajectories of air parcels in such a way as to increase the vorticity in front of the cyclone. A different perspective of the interaction suggests that the environmental flow advects vortex vorticity to the front. Either process would produce a net increase of relative vorticity in front of the cyclone and at an angle to the direction of the environmental flow. The magnitude of this local change depends on the speed of the environmental flow, the convergence and vorticity present in the combined flow. The increase in relative vorticity will cause the air in this area to spin up, forcing the mass field to adjust through subsidence. The warming resulting from the subsidence lowers the surface pressure and a new pressure center forms. At the same time, the subsidence spins down the vortex and reduces the increase in relative vorticity. However, the advection term overcompensates such a spin down and the net result is still an inrease in relative vorticity. This then leads to the formation of a new wind center. The tropical cyclone therefore "propagates" into this position. Eye wall clouds continually form around the new eye and dissipates around the 'old' center. The measurements of vertical motion

and the proposed ventilation associated with it, as suggested by Gray and Shear (1973), support this propagation view of cyclone motion.

A special case of this is the turning motion of tropical cyclones. Observational evidence supports the above proposed hypothesis. At 12 h before a change in cyclone direction, the environmental flow changes (in fact, the cyclone moves into a region with a different flow pattern). Such changes create new wind–pressure imbalances and produce a different vorticity advection pattern. This results in a shift in the azimuthal location of maximum increase in relative vorticity. The mass to wind adjustment process as a response to this vorticity increase then occurs in the way described above.

Therefore, by combining observational and analytical results, a hypothesis has been proposed to describe the possible physical processes responsible for tropical cyclone motion. This hypothesis was tested with the special case of turning cyclones and found to be valid. The present study has thus provided a comprehensive evaluation of the steering flow problem and the physics of tropical cyclone motion. It points out that although the long-standing steering-flow concept is approximately valid in describing cyclone motion, it is not sufficient in explaining the physical processes involved. The study of the physics of cyclone motion had virtually stopped in the 1960's when emphasis was shifted to the development of track forecast schemes. This paper can therefore be considered as a new attempt towards a more complete understanding of tropical cyclone motion.

8.2 Possible Future Research

8.2.1 Individual Case Study

One major disadvantage of the present study is the lack of availability of data around tropical cyclones. With the exception of the aircraft data, this entire study is based almost exclusively on composite rawinsonde data. Although this is inevitable due to the sparseness of observations around tropical cyclones, limitations do exist in the interpretation of the results derived from the composites. The question of how representative the composite data are in individual cases often arises. The fact that results from different ocean basins agree with one another and appear to be physically reasonable lends some confidence to these individual rawinsonde composites. In addition, these results are consistent with those predicted from theoretical studies. Nevertheless, efforts should still be made to verify the proposed hypothesis using individual cases. Attempts along this line should be possible with the data obtained from the proposal by R. Burpee of the National Hurricane Research Laboratory (AMS, 1982) to fly research aircrafts around the periphery of individual cyclones and obtain dropwindsonde measurements at closely-spaced intervals. Data from these flights and the dropwindsondes will make it possible to perform computations for individual cyclones. Results can then be compared with those from the composites.

The data from these future flights might also be tested for forecasting potential. Results in Chapters 5 and 6 suggest the presence of an environment conducive to a directional change of a cyclone 12 h before such a change takes place. Such an environment produces a wind-pressure imbalance between the front and back sides of the cyclone. The

new dropwindsonde data might also be used to compute the radial accelerations present in a cyclone which could then be compared with the directional change of the cyclone. This might eventually provide another aid in determining the future track of the cyclone.

8.2.2 Relation of Cyclone Motion to Flows of Other Scales

The study in this paper deals with tropical cyclone motion on a synoptic scale. No consideration has been given to the small scale motions such as the trochoidal movement that is so often observed. The results in this paper may provide some insight for a furture study of these small scale motion features. This could be accomplished through the use of radar observations and inner-core flight data with more frequent 'eye-fixes'. Such data are available from recent flights made by the National Hurricane Research Laboratory. An understanding of the physical processes involved in these small scale motions might then lead to a better short-term forecast which is often critical in landfall situations.

The sub-synoptic scale flow that interacts with the cyclone must 'originate' from a circulation that is larger in scale. Xu and Gray (1982) found significant relationships between the planetary scale circulation and cyclone movement. Through what physical processes do these two types of flows "communicate"? This problem can be studied using synoptic-scale rawinsonde data.

8.2.3 Numerical Modeling

The hypothesis proposed in the present study could also be tested with various types of numerical models. By imposing different environmental flows, the time evolution of the vorticity budget and other dynamic parameters can be studied.

To conclude, although this study provides some new insights into the problem of tropical cyclone motion, it has left a number of questions unanswered. Speculations proposed in this study also need to be verified. In addition, the problem of track forecasting still has to be addressed. Therefore, the present study should only be considered as a beginning and more research is essential in the understanding and forecasting of tropical cyclone motion.

ACKNOWLEDGEMENTS

The material in this report represents the work of the author as a Ph.D. student. I would therefore like to express my deepest gratitude to my advisor, Professor William M. Gray, for his continuous guidance, encouragement and support throughout this work. I also appreciate the helpful comments on the manuscript from my committee members, Professors W. H. Schubert, R. H. Johnson and P. W. Mielke. In addition, I would like to thank Mr. Greg Holland for his many enlightening discussions on the theoretical aspects of this work. I have also benefited from discussions with Mr. Bob Merrill and Mr. Cliff Matsumoto. Mr. C. S. Lee has kindly allowed me to adapt his smoothing routine in the vorticity budget analyses of the rawinsonde composite data.

I especially would like to thank Ms. Barbara Brumit for her highly professional help in manuscript preparation, and Ms. Cindy Schrandt and Mrs. Judy Sorbie for drafting the figures. Programming assistance from Mr. Edwin Buzzell and Mr. Grant Burton is also appreciated.

This research is sponsored by the National Science Foundation Grant No. ATM-7923591-02, NOAA/CIRA Grant No. NA81RA-H-00001 and Naval Environmental Prediction Research Facility Grant No. N00228-81-C-H620.

Lastly, and above all, thanks to my mother for understanding.

REFERENCES

Adem, J. and P. Lezama, 1960: On the motion of a cyclone embedded in a uniform flow. Tellus, 12, 255-258.

American Meteorological Society, 1982: Announcements, Bull. Amer. Meteor. Soc., 62, 1678.

Anthes, R. A., 1982: Tropical cyclones: their evolution, structure and effects. Meteor. Monographs, Vol. 19, No. 41, Amer. Meteor. Soc., Boston, MA, 208 pp.

Anthes, R. A. and J. A. Hoke, 1975: The effect of horizontal divergence and the latitudinal variation of the Coriolis parameter on the drift of a model hurricane. Mon. Wea. Rev., 103, 757-763.

Bell, G. J., 1980: Some aspects of tropical cyclone movement and forecasting. Symp. on Typhoons, Shanghai, China, Oct. 6-11, World Meteorological Organization, Geneva, Switzerland, 104-109.

Bell, G. J. and C. Y. Lam, 1980: Departures of tropical cyclone movement from geostrophic steering. WMO Symp. on Typhoons, Shanghai, China, Oct. 6-11, World Meteorological Organization, Geneva, Switzerland, 110-115.

Birchfield, G. E., 1960: Numerical prediction of hurricane movement with the use of a fine grid. J. Meteor., 17, 406-414.

Birchfield, G. E., 1961: Numerical prediction of hurricane movement with the equivalent-barotropic model. J. Meteor., 18, 402-409.

Brand, S., C. A. Buenafe and H. D. Hamilton, 1981: Comparison of tropical cyclone motion and environmental steering. Mon. Wea. Rev., 109, 908-909.

Chan, J. C. L. and W. M. Gray, 1982a: Tropical cyclone movement and surrounding flow relationships. Atmos. Sci. Paper No. 343, Colo. State Univ., Ft. Collins, CO, 68 pp.

Chan, J. C. L. and W. M. Gray, 1982b: Tropical cyclone movement and surrounding flow relationships. Mon. Wea. Rev., 110, 1354-1374.

Chan, J. C. L., W. M. Gray and S. Q. Kidder, 1980: Forecasting tropical cyclone turning motion from surrounding wind and temperature fields. Mon. Wea. Rev., 108, 778-792.

Frank, W. M., 1977: The structure and energetics of the tropical cyclone, I: Storm structure. Mon. Wea. Rev., 105, 1119-1135.

REFERENCES (cont'd)

George, J. E. and W. M. Gray, 1976: Tropical cyclone motion and surrounding parameter relationships. J. Appl. Meteor., 15, 1252-1264.

Gray, W. M., 1977: Tropical cyclone motion and steering flow relationships in the western Atlantic and in the western Pacific. Preprints, 11th Tech. Conf. on Hurricanes and Tropical Meteorology, Dec. 13-16, Miami Beach, FL, 472-477.

Gray, W. M., 1981: Recent advances in tropical cyclone research from rawinsonde composite analysis. WMO Programme on Research in Tropical Meteorology, World Meteorological Organization, Geneva, Switzerland, 407 pp.

Gray, W. M. and D. J. Shea, 1973: The hurricane's inner core region, II: Thermal stability and dynamic characteristics. J. Atmos. Sci., 30, 1565-1576.

Gray, W. M. and D. J. Shea, 1976: Data summary of NOAA's hurricane inner-core radial leg penetrations 1957-1967, 1969. Atmos. Sci. Paper No. 257, Colo. State Univ., Ft. Collins, CO, 219 pp.

Harrison, E. J., Jr., 1981: Initial results from the Navy two-way interactive nested tropical cyclone model. Mon. Wea. Rev., 109, 173-177.

Holland G. J., 1982: Tropical cyclone motion: environmental interaction plus a beta-effect. Submitted to J. Atmos. Sci.

Hubert, L. F., 1959: An operational test of a numerical prediction method for hurricanes. Mon. Wea. Rev., 87, 222-230.

Huschke, R. E., (Ed.), 1959: Glossary of Meteorology. American Meteor. Society, Boston, MA, 638 pp.

Jones, R. W., 1961: The tracking of hurricane Audrey, 1957 by numerical prediction. J. Meteor., 18, 127-138.

Jones. R. W., 1977a: The potential of hurricane modification for causing a systematic predictable change in a hurricane track as a result of the Rossby acceleration. NOAA Tech. Memo. ERL WMPO-42, 1-18.

Jones, R. W., 1977b: Vortex motion in a tropical cyclone model. J. Atmos. Sci., 34, 1518-1527.

Jordan, E. S., 1952: An observational study of the upper wind circulation around tropical storms. J. Meteor., 9, 340-346.

Kasahara, A., 1957: The numerical prediction of hurricane movement with the barotropic model. J. Meteor., 14, 386-402.

REFERENCES (cont'd)

Kasahara, A., 1959: A comparison between geostrophic and non-geostrophic numerical forecasts of hurricane movement with the barotropic steering model. J. Meteor., 16, 371-384.

Kasahara, A., 1960: The numerical prediction of hurricane movement with a two-level baroclinic model. J. Meteor., 17, 357-370.

Kasahara, A. and G. W. Platzman, 1963: Interaction of a hurricane with the steering flow and its effect upon the hurricane trajectory. Tellus, 15, 321-335.

Kuo, H.-L., 1950: The motion of atmospheric vortices and the general circulation. J. Meteor., 7, 247-258.

Kuo, H.-L., 1969: Motions of vortices and circulating cylinder in shear flow with friction. J. Atmos. Sci., 26, 390-398.

Kitade, T., 1980: Numerical experiments of tropical cyclones on a plane with variable Coriolis parameter. J. Meteor. Soc. Japan, 58, 471-488.

Kitade, T., 1981: A numerical study of the vortex motion with barotropic models. J. Meteor. Soc. Japan, 59, 801-807.

Lajoie, F. A., 1976: On the direction of movement of tropical cyclones. Aust. Met. Mag., 24, 95-104.

Lee, C.-S., 1982: Cumulus momentum transports in tropical cyclones. Atmos. Sci. Paper No. 341, Colo. State Univ., Ft. Collins, CO, 78 pp.

Madala, R. V. and A. A. Piacsek, 1975: Numerical simulation of asymmetric hurricane on a β-plane with vertical shear. Tellus, 27, 453-468.

Mathur, M. B., 1974: A multiple-grid primitive equation model to simulate the development of an asymmetric hurricane (Isbell, 1964). J. Atmos. Sci., 31, 371-393.

Merrill, R. T., 1982: A comparison of large and small tropical cyclones. Dept. of Atmos. Sci. Paper No. 352, Colo. State Univ., Ft. Collins, CO, 75 pp.

Miller, B. I., 1958: The use of mean layer winds as a hurricane steering mechanism. Nat'l Hurricane Res. Proj. Rept., No. 18, 24 pp. (Available from Natinal Hurricane Research Lab., Coral Gables, FL.)

Miller, B. I. and P. L. Moore, 1960: A comparison of hurricane steering levels. Bull. Amer. Meteor. Soc., 41, 59-63.

REFERENCES (cont'd)

Nitta, T., 1980: Preliminary results of track prediction by a JMA three-dimensional model with use of the moving multi-nested grid. WMO Symp. on Typhoons, Shanghai, China, Oct. 6-11, 132-140.

Pettersen, S., 1956: Weather analysis and forecasting. Vol 1, 2nd Edition, McGraw-Hill Book Co., 428 pp.

Neumann, C. J. and J. M. Pelissier, 1981: Models for the prediction of tropical cyclone motion over the north Atlantic: An operational evaluation. Mon. Wea. Rev., 109, 522-538.

Rao, G. V., 1969: Role of differential friction and asymmetry of the total flow on hurricane movement. Mon. Wea. Rev., 97, 502-509.

Rao, G. V., 1970: An analytical study of the differential frictional effect on vortex movement. Mon. Wea. Rev., 98, 132-135.

Renard, R. J., S. G. Colgan, M. J. Daley and S. K. Rinard, 1973: Forecasting the motion of North Atlantic tropical cyclones by the objective MOHATT scheme. Mon. Wea. Rev., 101, 206-214.

Riehl, H. and R. J. Shafer, 1944: The recurvature of tropical storms. J. Meteor., 1, 42-54.

Riehl, H. and N. H. Burgner, 1950: Further studies of the movement and formation of hurricanes and their forecasting. Bull. Amer. Meteor. Soc., 31, 244-253.

Rossby, C. G., 1939: Relation between variations in the intensity of the zonal circulation of the atmosphere and the displacements of the semi-permanent centers of action. J. Marine Res., 2, 38-55.

Rossby, C. G., 1948: On displacements and intensity change of atmospheric vortices. J. Marine Res., 7, 175-187.

Sanders, F. and R. H. Burpee, 1968: Experiments in barotropic hurricane track forecasting. J. Appl. Meteor., 7, 313-323.

Sanders, F., A. C. Pike and J. P. Gaertner, 1975: A barotropic model for operational prediction of tracks of tropical storms. J. Appl. Meteor., 14, 265-280.

Schubert, W. H., J. J. Hack, P. L. Silva Dias and S. R. Fulton, 1980: Geostrophic adjustment in an axisymmetric vortex. J. Atmos. Sci., 37, 1464-1484.

Shea, D. J. and W. M. Gray, 1973: The hurricanes inner-core region, I: Symmetric and asymmetric structure. J. Atmos. Sci., 30, 1544-1564.

REFERENCES (cont'd)

Tse, S. Y. W., 1966: A new method for the prediction of tyhoon movement using the 700 mb chart. Quart. J. Roy. Meteor. Soc., 92, 239-254.

Williams, K. T. and W. M. Gray, 1973: Statistical analysis of satellite-observed trade wind cloud clusters in the western North Pacific. Tellus, 25, 313-336.

World Meteorological Organization, 1979: Operational techniques for forecasting tropical cyclone intensity and movement. WMO-528, Geneva, Switzerland, 138 pp.

Xu, J. M. and W. M. Gray, 1982: Environmental circulations associated with tropical cyclones experiencing fast, slow and looping motion. Atmos. Sci. Paper No. 341, Colo. State Univ., Ft. Collins, CO, 273 pp.

Yeh, T.-C., 1950: The motion of tropical storms under the influence of a superimposed southerly current. J. Meteor., 7, 108-113.